National Library of Canada
Bibliothèque nationale du Canada

Canadian Theses Service
Service des thèses canadiennes

Ottawa, Canada
K1A 0N4

NOTICE

The quality of this microform is heavily dependent upon the quality of the original thesis submitted for microfilming. Every effort has been made to ensure the highest quality of reproduction possible.

If pages are missing, contact the university which granted the degree.

Some pages may have indistinct print especially if the original pages were typed with a poor typewriter ribbon or if the university sent us an inferior photocopy.

Reproduction in full or in part of this microform is governed by the Canadian Copyright Act, R.S.C. 1970, c. C-30, and subsequent amendments.

AVIS

La qualité de cette microforme dépend grandement de la qualité de la thèse soumise au microfilmage. Nous avons tout fait pour assurer une qualité supérieure de reproduction.

S'il manque des pages, veuillez communiquer avec l'université qui a conféré le grade.

La qualité d'impression de certaines pages peut laisser à désirer, surtout si les pages originales ont été dactylographiées à l'aide d'un ruban usé ou si l'université nous a fait parvenir une photocopie de qualité inférieure.

La reproduction, même partielle, de cette microforme est soumise à la Loi canadienne sur le droit d'auteur, SRC 1970, c. C-30, et ses amendements subséquents.

NL-339 (r. 88/04) c

Canada

UNIVERSITY OF ALBERTA

COLLECTION AND TRANSMISSION OF SUNLIGHT VIA FIBER OPTIC CABLES FOR HORTICULTURAL CROP PRODUCTION

BY

DENNIS R. ST. GEORGE

A THESIS
SUBMITTED TO THE FACULTY OF GRADUATE STUDIES AND RESEARCH
IN PARTIAL FULFILLMENT OF THE REQUIREMENTS FOR THE DEGREE
OF MASTER OF SCIENCE

DEPARTMENT OF AGRICULTURAL ENGINEERING

EDMONTON, ALBERTA

FALL 1990

National Library of Canada
Bibliothèque nationale du Canada

Canadian Theses Service
Service des thèses canadiennes

Ottawa, Canada
K1A 0N4

The author has granted an irrevocable non-exclusive licence allowing the National Library of Canada to reproduce, loan, distribute or sell copies of his/her thesis by any means and in any form or format, making this thesis available to interested persons.

L'auteur a accordé une licence irrévocable et non exclusive permettant à la Bibliothèque nationale du Canada de reproduire, prêter, distribuer ou vendre des copies de sa thèse de quelque manière et sous quelque forme que ce soit pour mettre des exemplaires de cette thèse à la disposition des personnes intéressées.

The author retains ownership of the copyright in his/her thesis. Neither the thesis nor substantial extracts from it may be printed or otherwise reproduced without his/her permission.

L'auteur conserve la propriété du droit d'auteur qui protège sa thèse. Ni la thèse ni des extraits substantiels de celle-ci ne doivent être imprimés ou autrement reproduits sans son autorisation.

ISBN 0-315-65053-2

UNIVERSITY OF ALBERTA

RELEASE FORM

NAME OF AUTHOR: Dennis R. St. George

TITLE OF THESIS: Collection And Transmission Of Sunlight Via Fiber Optic Cables For Horticultural Crop Production

DEGREE: Master Of Science

YEAR THIS DEGREE GRANTED: 1990

PERMISSION IS HEREBY GRANTED TO THE UNIVERSITY OF ALBERTA LIBRARY TO REPRODUCE SINGLE COPIES OF THIS THESIS AND TO LEND OR SELL SUCH COPIES FOR PRIVATE, SCHOLARLY OR SCIENTIFIC RESEARCH PURPOSES ONLY.

THE AUTHOR RESERVES OTHER PUBLICATION RIGHTS, AND NEITHER THE THESIS NOR EXTENSIVE EXTRACTS FROM IT MAY BE PRINTED OR OTHERWISE REPRODUCED WITHOUT THE AUTHOR'S WRITTEN PERMISSION.

Dennis R. St. George

Dennis R. St. George

Box 6, Group 5, RR #1
Dugald, Manitoba, R0E 0K0

Date: June 28, 1990

UNIVERSITY OF ALBERTA

FACULTY OF GRADUATE STUDIES AND RESEARCH

THE UNDERSIGNED CERTIFY THEY HAVE READ, AND RECOMMEND TO THE FACULTY OF GRADUATE STUDIES AND RESEARCH FOR ACCEPTANCE, A THESIS ENTITLED COLLECTION AND TRANSMISSION OF SUNLIGHT VIA FIBER OPTIC CABLES FOR HORTICULTURAL CROP PRODUCTION SUBMITTED BY DENNIS R. ST. GEORGE IN PARTIAL FULFILMENT OF THE REQUIREMENTS FOR THE DEGREE OF MASTER OF SCIENCE IN AGRICULTURAL ENGINEERING.

John Feddes
Dr. J.J.R. Feddes

Dr. J.J. Leonard

Gerald W. Sadler
Dr. G.W. Sadler

M. Mohyuddin
Mr. M. Mohyuddin

Date: June 12, 1990

ABSTRACT

A prototype light collection and transmission device was developed to evaluate the potential of irradiating horticultural crops grown in an opaque, insulated structure with sunlight supplied via fiber optic cables. The objective of the research was to develop an energy efficient method for producing horticultural crops in Northern Canada.

The prototype device functioned by concentrating solar energy into 600 μm core-diameter, plastic-clad silica fiber optic cables with 63.5 mm-diameter, acrylic fresnel lenses. A total of 96 fiber optic cable and fresnel lens sets were assembled within two collector panels. An azimuth-elevation solar tracker mount, which incorporated a shadow band sensor and microprocessor-based controller, positioned the collector panels perpendicular to the sun's incoming rays. The effective collection surface area was 0.30 m^2 and the length of the fiber optic cables attached to the prototype device was 5.00 m. The opaque, insulated structure consisted of a growth cabinet with an internal volume of 0.28 m^3. The fiber optic cables were mounted in a panel at the top of the growth cabinet, such that the distance between the ends of the fiber optic cables and the bottom of the growth cabinet was 40 cm.

The prototype device was tested for a total of eleven days at the University of Alberta in Edmonton, Alberta during the Fall of 1989 and the Winter of 1990. Direct solar radiation, photon flux, spectral photon flux, and temperature were measured in order to evaluate the prototype device. The prototype device was operated under clear and sunny, partly overcast,

and overcast sky conditions. The results indicated that the concept of transmitting photosynthetic and photomorphogenic radiation from the sun via fiber optic cables was viable. The prototype device accurately tracked the sun under a variety of sky conditions and produced a photon flux of 130 $\mu mol/s/m^2$ (400-700 nm) near the bottom of the growth cabinet when the direct solar radiation was 800 W/m^2 (300-2500 nm) outside. The efficiency of the prototype device for collecting and transmitting daylight in the blue and red regions of the spectrum was 5% and 30%, respectively. The overall collection and transmission efficiency for photosynthetically active radiation was 19.2%. The infra-red component of the transmitted irradiation was minimal.

In conclusion, the prototype device was capable of supplying suitable irradiation for plant growth. However, the quantity and duration of the irradiation was dependent upon the availability of direct solar radiation.

ACKNOWLEDGEMENTS

I wish to acknowledge the support and assistance provided by several organizations, departments, and persons involved with my Master of Science Degree in Agricultural Engineering.

First, I wish to thank the Natural Science and Engineering Research Council of Canada, the University of Alberta, and the Department of Agricultural Engineering for the personal financial support in the form of scholarships, fellowships, and teaching assistantships during my studies. Also, I wish to thank the Department of Economic Development and Tourism of the Government of the Northwest Territories for the research project's financial support.

Secondly, I wish to thank Dr. Jerry Leonard for proposing a "crazy" idea, the Librarians for identifying some "incredible" literature, Mr. Eugene Hachey for investing the "necessary" dollars, Dr. John Feddes for backing a "bizarre" project, Mr. Pierre Tremblay and the Alberta Telecommunications Research Center for providing some "crucial" facilities, and the Agricultural Engineering Staff for supplying "terrific" support.

Thirdly, I wish to thank all my friends for making my stay in Edmonton a most enjoyable experience.

TABLE OF CONTENTS

1. INTRODUCTION 1

1.1 OBJECTIVE 1
1.2 PROBLEM 1
1.3 SOLUTION 2
1.4 SCOPE 2

2. REVIEW OF LITERATURE 4

2.1 CONTROLLED ENVIRONMENTAL AGRICULTURE IN NORTHERN REGIONS 5

2.1.1 Horticultural Crop Production In Greenhouses 5
2.1.2 Horticultural Crop Production In Growth Chambers 6

2.2 RADIANT ENERGY AND PLANT GROWTH 7

2.2.1 Radiant Energy 8
2.2.2 Quantity 9
2.2.3 Quality 10
2.2.4 Direction 11
2.2.5 Periodicity 11
2.2.6 Sources 12

2.3 METHODS OF COLLECTING AND TRANSMITTING RADIANT ENERGY 14

2.3.1 Light Beams 15
2.3.2 Light Conductors 15
2.3.3 Light Pipes 16
2.3.4 Problems With Systems Cited 17
2.3.5 Himawari System 17

2.4 COLLECTING SOLAR RADIATION 19

2.4.1 Concentrating Solar Energy 19
2.4.2 Parabolic Concentrating Collectors 20
2.4.3 Fresnel Lenses 21

2.5 TRANSMISSION OF SOLAR ENERGY BY FIBER OPTIC CABLES . . 22

2.5.1 Attenuation 23
2.5.2 Numerical Aperture And Size 24

2.6 SOLAR TRACKING 24

2.6.1 Types Of Solar Tracking Systems 25
2.6.2 Solar Tracking Errors 26
2.6.3 Solar Tracking Control Strategies 26

2.7 SUMMARY 28

3. DESIGN THEORY FOR COLLECTION AND TRANSMISSION OF SUNLIGHT . 29

3.1 GEOMETRICAL OPTICS 29

3.1.1 Rectilinear Propagation 29
3.1.2 Reflection 29
3.1.3 Refraction 30

3.2 FRESNEL LENSES 30

3.2.1 Solar Energy Concentration 30
3.2.2 Chromatic Aberration 32

3.3 FIBER OPTIC CABLES 33

3.3.1 Acceptance Angle 33
3.3.2 Core Diameter 34
3.3.3 Attenuation 35

3.4 SUMMARY 35

4. DESIGN OF PROTOTYPE DEVICE 36

4.1 GENERAL DESCRIPTION 37

4.2 PRIMARY COMPONENTS 41

4.2.1 Fresnel Lens 41
4.2.2 Fiber Optic Cable 43
4.2.3 Solar Tracking Kit 45
4.2.4 Gearmotors And Gearboxes 47

4.3 SECONDARY COMPONENTS 48

4.3.1 Collector Panel 48
4.3.2 Module Assembly 50
4.3.3 Connector Assembly 51
4.3.4 Rib Plate 55
4.3.5 Tracker Mount Frame 56
4.3.6 Additional Electric Circuits 57

4.4 SUMMARY 58

5. EVALUATION PROCEDURE 59

5.1 PROTOTYPE DEVICE SETUP 59

5.1.1 Alignment Of The Sets 60
5.1.2 Alignment Of Fresnel Lenses To Shadow Band Sensor 62
5.1.3 Alignment Of Shadow Band Sensor To The Sun . . . 63
5.1.4 Limit Switch Setup 64

5.2 INSTRUMENTATION 65

5.2.1 Photon Flux 65
5.2.2 Spectral Photon Flux 66
5.2.3 Direct Solar Radiation 66
5.2.4 Temperature 67
5.2.5 Data Acquisition System 68

5.3 EXPERIMENTAL SETUP 68

5.3.1 Location Of Testing 69
5.3.2 Opaque, Insulated Structure 69
5.3.3 Orientation Of The Fiber Optic Cables 71
5.3.4 Orientation Of Instruments 72
5.3.5 Measurement Technique 74

6. TESTING AND RESULTS 75

6.1 FALL 1989 TESTING 76

6.1.1 November 29, 1989 77
6.1.2 December 3, 1989 81
6.1.3 December 4, 1989 83

6.2 WINTER 1990 TESTING 85

6.2.1 February 28, 1990 85
6.2.2 March 1, 1990 88
6.2.3 March 2, 1990 90
6.2.4 March 13, 1990 92
6.2.5 March 14, 1990 96
6.2.6 March 15, 1990 98
6.2.7 March 16, 1990 100
6.2.8 March 21, 1990 102

6.3 SUMMARY 105

7. DISCUSSION 106

7.1 DESIGN 106

7.2 EVALUATION 107

7.2.1 Solar Tracking Accuracy 108
7.2.2 Efficiency 113
7.2.3 Quantity 114
7.2.4 Quality 115
7.2.5 Duration 116

7.3 SUMMARY 117

8. CONCLUSIONS 118

9. RECOMMENDATIONS 120

REFERENCES 121

APPENDIX A 124

APPENDIX B 125

APPENDIX C 127

APPENDIX D 132

APPENDIX E 134

APPENDIX F 150

CURRICULUM VITAE 152

LIST OF TABLES

Table 6.1 Summary Of Testing On The Prototype Device 76

Table 6.2 Photon Flux Near Bottom Of Growth Cabinet 95

Table 6.3 Results Calculated From Measurements 105

Table 7.1 Assessment Of Solar Tracking Accuracy 110

LIST OF FIGURES

Figure 4.1 Frontal View Of Prototype Device 38

Figure 4.2 Side View Of Prototype Device 39

Figure 4.3 Cross Sectional Views Of Module Assembly 52

Figure 6.1a Direct Solar Radiation (1989-11-29) 79

Figure 6.1b Photon Flux Inside Cabinet (1989-11-29) 79

Figure 6.1c Temperature Inside Cabinet (1989-11-29) 79

Figure 6.2a Spectral Photon Flux (1989-11-29) 80

Figure 6.2b Spectral Photon Flux With Greater Resolution (1989-11-29) 80

Figure 6.3a Direct Solar Radiation (1989-12-03) 82

Figure 6.3b Photon Flux Inside Cabinet (1989-12-03) 82

Figure 6.3c Temperature Inside And Outside Cabinet (1989-12-03) 82

Figure 6.4a Direct Solar Radiation (1989-12-04) 84

Figure 6.4b Photon Flux Inside Cabinet (1989-12-04) 84

Figure 6.4c Temperature Inside And Outside Cabinet (1989-12-04) 84

Figure 6.5a Direct Solar Radiation (1990-02-28) 87

Figure 6.5b Photon Flux Inside Cabinet (1990-02-28) 87

Figure 6.5c Temperature Inside And Outside Cabinet (1990-02-28) 87

Figure 6.6a Direct Solar Radiation (1990-03-01) 89

Figure 6.6b Photon Flux Inside Cabinet (1990-03-01) 89

Figure 6.6c Temperature Inside And Outside Cabinet (1990-03-01) 89

Figure 6.7a Direct Solar Radiation (1990-03-02) 91

Figure 6.7b Photon Flux Inside Cabinet (1990-03-02) 91

Figure 6.7c Temperature Inside And Outside Cabinet (1990-03-02) 91

Figure 6.8a Direct Solar Radiation (1990-03-13) 93

Figure 6.8b Photon Flux Inside Cabinet (1990-03-13) 93

Figure 6.8c Temperature Inside Cabinet (1990-03-13) 93

Figure 6.9a Spectral Photon Flux (1990-03-13) 94

Figure 6.9b Spectral Photon Flux With Greater Resolution (1990-03-13) 94

Figure 6.10 Location Of Photon Flux Measurements 95

Figure 6.11a Direct Solar Radiation (1990-03-14) 97

Figure 6.11b Photon Flux Inside Cabinet (1990-03-14) 97

Figure 6.11c Temperature Inside Both Cabinets (1990-03-14) . . . 97

Figure 6.12a Direct Solar Radiation (1990-03-15) 99

Figure 6.12b Photon Flux Inside Cabinet (1990-03-15) 99

Figure 6.12c Temperature Inside Both Cabinets (1990-03-15) . . . 99

Figure 6.13a Direct Solar Radiation (1990-03-16) 101

Figure 6.13b Photon Flux Inside Cabinet (1990-03-16) 101

Figure 6.13c Temperature Inside Cabinet (1990-03-16) 101

Figure 6.14a Direct Solar Radiation (1990-03-21) 103

Figure 6.14b Photon Flux Inside Cabinet (1990-03-21) 103

Figure 6.14c Temperature Inside Cabinet (1990-03-21) 103

Figure 6.15a Spectral Photon Flux (1990-03-21) 104

Figure 6.15b Spectral Photon Flux With Greater Resolution (1990-03-21) 104

Figure 7.1 Linear Regression Analysis (1990-02-28) 111

Figure 7.2 Linear Regression Analysis (1990-03-01) 111

Figure 7.3 Linear Regression Analysis (1990-03-02) 112

Figure 7.4 Efficiency Of Prototype Device (1990-03-13) 114

LIST OF PLATES

Plate 5.1 Front View Of Prototype Device 70

Plate 5.2 Back View Of Prototype Device 70

Plate 5.3 Orientation Of Fiber Optic Cables 71

Plate 5.4 Instruments Inside Growth Cabinet 73

Plate 5.5 Pyrheliometer 73

LIST OF SYMBOLS

α	attenuation factor	(dB/km)
β	half angle of circular object at infinity	
δ	half angle of convergence	
θ	angle of incidence	
θ'	angle of refraction	
θ''	angle of reflection	
θ_c	critical angle	
λ	wavelength	(nm)
σ	half angle of acceptance	
C	concentration ratio	
D	direct solar radiation	(W/m^2)
f	focal length	
n	index of refraction	
n'	index of refraction	
n_0	index of refraction for core	
n_1	index of refraction for cladding	
n_L	index of refraction for lens	
$n_{\lambda 1}$	index of refraction for λ_1	
$n_{\lambda 2}$	index of refraction for λ_2	
NA	numerical aperture	
P	voltage output signal	(V)
P_i	input power	(W)
P_o	output power	(W)
PF	photon flux	($\mu mol/s/m^2$)
r	radius of lens	

R radius of curvature or resistance

RS range setting

S voltage output signal

S' distance of image between λ_1 and λ_2 or voltage signal

T temperature

T' temperature

x length of fiber optic cable

X distance between chromatic images at λ_1 and λ_2

1. INTRODUCTION

The successful operation of any plant growth structure is dependent upon providing a suitable environment for the plants, while still being able to maintain an environment on an economical basis. This is especially important when producing horticultural crops in adverse environments, such as found in Northern Canada.

1.1 OBJECTIVE

The overall objective of this research is to develop an energy efficient method for producing horticultural crops in Northern Canada.

1.2 PROBLEM

The problem under examination is energy efficient horticultural crop production in Northern Canada. At present, fresh vegetables from Southern Canada and the United States are supplied to Northern communities via air transport. As a result, fresh vegetables are expensive, of poor quality, or not available in many communities. The alternative to the present situation is to grow the vegetables locally. However, harsh environment, limited growing season, and high priced energy inhibit production of horticultural crops with conventional methods, such as greenhouses and growth chambers. The heating and lighting systems consume the largest quantities of energy for greenhouse and growth chamber horticultural crop production, respectively. In the North, the heating requirement combined

with insufficient daylight during the winter are limitations to the use of greenhouses. On the other hand, the high cost of electricity combined with a large requirement for electrical energy to generate radiant energy for photosynthesis prohibits the use of growth chambers in the North.

1.3 SOLUTION

The solution proposed is to produce horticultural crops in an opaque, insulated structure equipped with a unique lighting system. The opaque, insulated structure would protect the crop, provide growing space, and would reduce the energy requirement for heating in comparison to a greenhouse. The unique lighting system, based upon a device capable of collecting and transmitting sunlight via fiber optic cables, would reduce the energy requirement for lighting in comparison to a growth chamber. When sunlight is not available, irradiation would be supplied by a backup electrical lighting system.

1.4 SCOPE

The scope of the research was to design and evaluate a prototype device capable of collecting and transmitting sunlight via fiber optic cables to plants grown in an opaque, insulated structure. The prototype device featured a small lens design to maximize the collection and transmission of solar energy. The effective collector surface area of the prototype device was 0.30 m^2 and the length of the fiber optic cables attached to the prototype device was 5.00 m. The prototype device

functioned by concentrating solar energy into fiber optic cables with an array of fresnel lenses. An azimuth-elevation solar tracker was used to position the fresnel lenses perpendicular to the sun's incoming rays. The prototype device was operated for a total of eleven days on two separate occasions. The primary variables measured were the direct solar radiation available to the prototype device, the photon flux emitted from the fiber optic cables inside an opaque, insulated structure, and the temperature in the opaque, insulated structure. In addition, spectral photon flux measurements were made inside the opaque, insulated structure and outside near the prototype device. The prototype device was operated on clear and sunny, partly overcast, and overcast days. Overall, the prototype device performed as designed.

2. REVIEW OF LITERATURE

Prince et al. (1982) state that very little imagination has gone into combining plant growth structures, energy utilization, and environmental control systems in the past.

To date, the majority of projects dealing with horticultural crop production in northern regions, Lewis et al. (1978), Poole (1985), Loomis (1987), Burdett-Moulton et al. (1988), have only focused on the use of conventional greenhouse and growth chamber technology. The authors cited draw attention to the fact that greenhouses and growth chambers are not adapted for efficient use of energy in northern regions.

Bickford and Dunn (1972) indicate that the design of a system for irradiating plants must consider the photosynthetic and photomorphogenic responses of a plant. The key requirements of the irradiating system are the quantity, quality, direction, and periodicity of radiant energy supplied.

The concept of producing horticultural crops in an opaque, insulated structure with radiant energy supplied via fiber optic cables bridges the gap between plant growth structures, energy utilization, and environmental control systems.

2.1 CONTROLLED ENVIRONMENTAL AGRICULTURE IN NORTHERN REGIONS

A controlled environment is neccessary to produce horticultural crops in northern regions for extended periods of the year. The systems commercially available for controlling a horticultural crop's environment are greenhouses and growth chambers. However, limitations exist to the operation of greenhouses and growth chambers in northern regions.

2.1.1 Horticultural Crop Production In Greenhouses

A greenhouse is a plant growth structure employing translucent or transparent coverings to allow the plants within to be irradiated by daylight. The ambient temperature within a greenhouse is controlled with heating, ventilating, and/or cooling systems. ASHRAE (1981) indicates that the heating system compensates for heat loss during low ambient temperature periods, while the ventilating and/or cooling systems compensate for heat gain during sunny or high ambient temperature periods.

A computer model developed by St. George and Feddes (1988) identified the heating and ventilating requirements of a greenhouse in a sub-arctic region. The computer model predicted the heat losses and gains within a 9 m^2 by 15 m^2, quonset style, double polyethylene covered, greenhouse in Norman Wells, N.W.T. (65° North latitude). The results indicate, that beyond September 15 and prior to May 1, increasing amounts of supplemental energy are required to maintain a suitable temperature for plant growth in the greenhouse.

An actual greenhouse evaluation project conducted by Poole (1985) at Pond Inlet, N.W.T. for the Toonoonik-Sahoonik Cooperative identified similar limitations for operating a greenhouse in an arctic environment.

In addition to the energy requirements, the cosine effect is a concern for greenhouses in northern regions. The amount of radiant energy entering a greenhouse in a northern region is influenced by the low elevation of the sun. Stine and Harrigan (1985) indicate that, over a twelve month period, the cosine effect can reduce the irradiation received upon a horizontal surface by 74% at 80° North latitude.

2.1.2 Horticultural Crop Production In Growth Chambers

According to ASHRAE (1981), a growth chamber provides environmental control with the use of heating, ventilating, air conditioning, and lighting systems. As a result, a growth chamber is an energy-intensive means for producing horticultural crops. In addition, electrical costs in northern regions are high (Loomis 1987). Therefore, the economics of operating growth chambers in northern regions are questionable.

A report prepared by Lewis et al. (1978), relating to the Kenai Native Association Project, identifies the problem of operating growth chambers in northern regions. The Kenai Project studied the technical and economic aspects of Controlled Environment Agriculture (CEA) or growth

chambers in Alaska. The following statement is taken from the Kenai Project's final report (Lewis et al. 1978);

> *" The energy issue is also critical. Even in a remote Alaskan location, if a cheap and abundant energy source is not available, CEA production is possible only if the consumer of the produce is prepared to pay a substantial price for the commodity. The high energy requirements of CEA relative to any other type of commercial plant growing system must be a major consideration in the planning of a CEA facility."*

In conclusion, high energy costs coupled with high energy demands are a concern for producing horticultural crops within growth chambers in northern regions.

2.2 RADIANT ENERGY AND PLANT GROWTH

Hart (1988) states that radiant energy is utilized by plants in two distinct ways, first as a source of energy and secondly as a source of information. Sager et al. (1982) concur by stating that the responses of a plant to radiant energy are categorized as photosynthetic or photomorphogenic. According to Bickford and Dunn (1972), photosynthesis is the autotrophic synthesis of organic materials in which the source of energy is visible radiation, while photomorphogenesis is the non-photosynthetic influence of radiant energy on germination, growth, development, and reproduction. Hart (1988) indicates that the quantity,

quality, direction, and periodicity of radiant energy have an effect on both the photosynthetic and photomorphogenic responses of a plant.

2.2.1 Radiant Energy

Radiation is the emission and propagation of electromagnetic waves and/or photons through space or matter. Radiant energy is the transfer of energy by radiation. Hart (1988) states that radiant energy with wavelengths between 300 and 1000 nm is biologically useful for plant growth. Radiation of wavelengths greater than 1000 nm contain insufficient energy to initiate a photochemical reaction, whereas, wavelengths less than 300 nm contain sufficient energy to break chemical bonds.

ASAE (1989) defines photosynthetically active radiation as the total radiation in the wavelength range 400 to 700 nm contributing to photosynthetic productivity in relation to the relative photosynthetic quantum efficiency of the radiation. The relative photosynthetic quantum efficiency relates the quantity of molecules that are excited to the quantity of photons available. Furthermore, ASAE (1989) defines photomorphogenic radiation as the radiation with wavelengths approximately ranging between 380 and 800 nm contributing to photomorphogenic responses in relation to the relative quantum efficiency of the spectral quality of the radiation in discrete spectral regions.

The term radiant energy is frequently interchanged with the term light throughout the published literature. Discretion is required to avoid

confusing light for plant growth with light for a visual response by the human eye. ASAE (1989) defines light to be visually evaluated radiant energy, with wavelengths approximately ranging between 380 and 770 nm. Cathey and Campbell (1980) indicate light for plant growth is measured with radiometric and/or quantum sensors, whereas, light for visual responses is measured with photometric sensors. Hart (1988) states that photometric methods are totally inappropriate for investigating the effects of radiant energy on plants, since plants respond to energy rather than luminosity. Hart's statement is confirmed when equal luminosities at different wavelengths are considered. For instance, one lumen at a wavelength of 562 nm contains 1.49 mW of energy, whereas, one lumen at a wavelength of 430 nm contains 126.7 mW of energy. Holms et al. (1985) indicate that the use of photometric terms, when discussing the plant sciences, is regressive.

2.2.2 Quantity

ASAE (1989) indicate that the rate of radiant energy flow per unit plane surface area is referred to as irradiance, energy flux, or photon flux. Bickford and Dunn (1972) point out that photosynthesis increases in a linear manner with increasing irradiance up to a saturation plateau. The irradiance required for saturation differs for different types of plants and varies with the age of a plant. In contrast, Bickford and Dunn (1972) indicate the process of photomorphogenesis is initiated by very low irradiances. The units of photon flux are $\mu mol/s/m^2$ or W/m^2.

Cathey and Campbell (1980) indicate that 9 W/m^2 (400-850 nm) can maintain plant growth, while plants exposed to 18 W/m^2 (400-850 nm) exhibit rapid growth. Furthermore, 24 to 50 W/m^2 (400-850 nm) provides prompt development of leaves, branches, and flower initiation. ASHRAE (1981) recommend 50 W/m^2 (400-850 nm) for producing plants in commercial growth chambers. Cathey and Campbell (1980) indicate the irradiance required to initiate photomorphogenic response is approximately 0.9 W/m^2.

2.2.3 Quality

ASAE (1989) indicate the photon flux per unit wavelength interval at a specific wavelength is referred to as spectral photon flux. Hart (1988) specifies that for radiant energy to trigger a photoreceptor, the radiant energy must be within a specific region of the electromagnetic spectrum known as the action spectrum. In other words, the radiant energy must possess a specific spectral photon flux or quality to have a biological effect. The units for spectral photon flux are $\mu mol/s/m^2/nm$ or $W/m^2/nm$.

Hart (1988) indicates that plants can obtain energy to some extent from the entire visible spectrum (380-770 nm), while information is obtained particularly from the blue, red and far red regions of the electromagnetic spectrum. According to Hart (1988), the photosystems responsible for initiating photosynthesis are chlorophyll and carotenoid pigments, while the photosystems responsible for monitoring photomorphogenesis are phytochrome and the blue light photoreceptors. The

irradiance and periodicity of the red and far red regions of the spectrum are significant parameters for phytochrome, while the irradiance, spectral photon flux, direction, and periodicity of the blue region of the spectrum initiate responses by the blue light photoreceptors.

2.2.4 Direction

Hart (1988) states that the direction of radiant energy has an influence upon the orientation of a plant in space. A plant's response to the direction of radiant energy is classified as either phototaxic, photokinetic, or phototropic. Phototaxis is the movement of a plant or parts of a plant in relation to the direction of the incoming radiant energy. If the rate of movement is affected by the direction of the incoming radiant energy, then the phenomenon is called photokinesis. Phototropism, on the other hand, is a directional growth movement of a plant in response to the direction of irradiation. Phototropism is most apparent in young, rapidly growing tissues.

2.2.5 Periodicity

Hart (1988) indicates that radiant energy influences both the daily and yearly temporal behavior of a plant. Daily temporal responses include functions such as stomatal opening/closing and nyctinastic movements. On the other hand, yearly temporal responses or photoperiodic responses are the non-directional developmental responses to the periodic stimulus of

daylength. Photoperiodism influences flowering, bud development, stolon and runner production, and the formation of perennating organs.

In relation to photoperiodic responses, Hart (1988) indicates that plants are classified by three daylength requirements (short day, long day, and day neutral) and two control types (obligate and facultative). The distinction between short day plants and long day plants is a response to changes in daylength. Obligative control indicates that a specific photoperiod is required to initiate a response. Facultative control indicates that a specific photoperiod will initiate a response sooner, however, the response would occur anyway. Also, a plant species can be day neutral with respect to flowering, yet photoperiodically responsive in other respects. For instance, Hart (1988) indicates that day neutral tomato plants are bushy under short day and tall under long day photoperiods.

2.2.6 Sources

The sources of radiant energy for growing plants are electrical lamps and the sun. According to Sager et al. (1982), the best source of radiant energy for plant growth combines the greatest photosynthetic utilization efficiency for radiant to chemical energy and the desired photomorphogenic effects to produce the desired plant development. Hart (1988) indicates the important features of a radiant energy source are irradiance and spectral photon flux.

Electrical lamps produce radiant energy by either thermal emission or electrical discharge. Lamps operating on thermal emission are classified as incandescent, while lamps operating on electrical discharge are classified as luminescent or fluorescent. Incandescent sources of radiant energy are characterized by continuous spectra, low efficiency, low energy flux, and short life spans. Hart (1988) states that incandescent lamps are biologically poor sources of radiant energy. Luminescent sources of radiant energy are characterized by wavelength specific spectral distributions, high efficiency, high energy flux, and longer life. Hart (1988) states luminescent and fluorescent lamps provide high rates of photosynthesis, however the photomorphogenic responses are not normal in comparison to plants grown under daylight. According to Bickford and Dunn (1972) the uniformity of light distribution from an electrical lamp is affected by the type of lamp, type of reflector, lamp spacing, and the reflectivity of the surfaces in the plant growth structure.

The sun is the most important source of biologically significant natural radiant energy. The sun produces radiant energy by thermal emission from a nuclear fusion reaction. The irradiance and spectral photon flux received at the earth's outer atmosphere are constant but, vary at the earth's surface. The radiant energy received at the earth's surface, referred to as total radiation, is composed of direct radiation transmitted from the sun's disc and diffuse radiation transmitted from the sky. The proportions of direct and diffuse radiation are dependent upon the atmospheric conditions and the elevation of the sun in the sky.

According to Stine and Harrigan (1985), direct radiation can constitute 80% or 90% of total radiation under clear skies, while diffuse radiation can constitute 100% of total radiation under completely overcast skies or when the sun is below the horizon. According to Hart (1988), direct radiation possesses a spectral distribution similar to the sun's extraterrestrial radiation, whereas, diffuse radiation possesses a spectral distribution enriched in the blue region. According to Cathey and Campbell (1980), radiant energy from the sun is available in optimal levels for plant growth, however, the radiant energy is not sustained due to varying daylength and atmospheric conditions. The earth's rotation about its polar axis, the tilt of the axis relative to the ecliptic plane, and the elliptical orbit around the sun alters the position of the sun in the sky and, hence, the direction and periodicity of direct radiation. Stine and Harrigan (1985) indicate that the changes in daylength are most pronounced at northern latitudes.

2.3 METHODS OF COLLECTING AND TRANSMITTING RADIANT ENERGY

A variety of systems have been proposed for collecting and transmitting sunlight into opaque, insulated structures. Each system incorporates similar functions for tracking, collecting, transmitting, and distributing solar radiant energy. However, only one system is well suited for irradiating horticultural crops grown in an opaque, insulated structure with sunlight in northern regions.

2.3.1 Light Beams

Duguay and Edgar (1977) proposed a dual axis heliostat to reflect, concentrate, and direct a beam of sunlight through a hole in the roof of a building. Once inside, the beam of sunlight is relayed and dispersed throughout the building by means of mirrors and lenses. The beam of sunlight is produced by reflecting sunlight off a flat mirror mounted on the heliostat onto a fixed converging mirror. The visible and infra-red portions of the solar spectrum are separated with optical filters. The system is intended to provide room lighting.

2.3.2 Light Conductors

Fraas et al. (1983) promoted a light guide to convey sunlight into buildings. The light guide consists of a 5.5 cm diameter, solid acrylic rod with an index of refraction of 1.5 surrounded by a teflon layer with an index of refraction of 1.4. A 2.4 m^2 plastic fresnel lens and a light beam splitter mounted on a polar axis solar tracker are used to focus visible sunlight upon the end of the acrylic rod. The fresnel lens concentrates the sunlight upon the beam splitter which separates the visible and infra-red components and reflects the visible component onto the end of the acrylic rod. The rod conveys the visible sunlight via total internal reflection to a remote location for dispersal.

2.3.3 Light Pipes

Whitehead et al. (1982) described a prism light guide, called a light pipe, for the transmission of light to remote locations. The light pipe employs the principles of total internal reflection and the low attenuation of air to transmit radiant energy. The light pipe is a square cross section, transparent acrylic tube with a 1.5 index of refraction possessing prism shaped facets on the tube's outer surfaces. Light is transmitted down the tube by a combination of reflection at the inner surface of the tube and total internal reflection at the outer surface of the tube. Bulley and Phillips (1984) evaluated the use of a light pipe for distributing radiant energy from high intensity discharge lamps to plants. Bulley and Phillips (1984) concluded that a light pipe provides an efficient method of transferring light from high intensity discharge lamps into confined spaces. However, the light distribution was not uniform and, hence, was not well suited for horticultural production. SESCI (1986) describes the heliostat tracker used for delivering solar energy to the light pipe. A dual-axis tracking heliostat relied on preprogrammed instructions to position a flat mirror which reflected solar energy onto a fixed, converging mirror. In turn, the fixed mirror directed light through a hole in the roof of the building into the light pipe.

2.3.4 Problems With Systems Cited

The three systems cited are not well suited for irradiating horticultural crops grown in an opaque, insulated structure with sunlight for northern regions. The three systems use either stationary mirrors and lenses, rigid light conductors, or rigid light pipes to transmit the solar energy. As a result, heliostat-type trackers are required to reflect solar energy into the apertures of the transmission systems. Stine and Harrigan (1985) indicate the cosine efficiency of a heliostat system depends upon the position of the sun and the location of the heliostat. Since the sun's position varies greatly over the period of a year at northern latitudes, a large number of heliostats would be required to maintain a high cosine efficiency. In addition, uniform distribution of the solar energy to the plants would be difficult, since the spacing of the transmission systems cannot be easily adjusted.

2.3.5 Himawari System

A method that appears to be well suited for collecting and transmitting solar energy into opaque, insulated structures in northern regions utilizes flexible fiber optic cables to transfer radiant energy. Since the flexible fiber optic cables can move with the solar tracker, a simple and more efficient system is obtained. As well, a uniform distribution of the solar energy to the plants is possible, since the spacing of the fiber optic cables can be adjusted easily.

Mori (1987) has patented a device that incorporates flexible fiber optic cables to collect and transmit solar energy to remote locations. The device, referred to as a Himawari, employs an azimuth-elevation (az-el) solar tracker, fresnel lenses, and flexible fiber optic cable bundles. The azimuth elevation tracker positions an array of fresnel lenses perpendicular to the incoming rays of the sun. The fresnel lenses concentrate an image of the sun upon the end of a flexible fiber optic cable bundle. The solar energy is transmitted along the fiber optic cables by total internal reflection to the remote location for distribution. Cariou et al. (1982) proposed a similar system, except parabolic dishes were used to concentrate an image of the sun upon individual fiber optic cables.

Mori (1985) indicated that fiber optic cables can be used to transmit radiant energy for photosynthetic production. Mori (1985) experimented with a system that transmits radiant energy from the sun and/or electrical lamps via fiber optic cables to irradiate a photoautotrophic bioreactor. This method of irradiation, in combination with a bioreactor provided higher algea growth rates in comparison to algea grown in shallow pools irradiated with sunlight and/or electrically-generated light. Specifications provided by the manufacturer of the Himawari (La Foret Engineering and Information Systems, Tokyo, Japan) indicated that a Himawari with 5 m long cables has an overall efficiency for collecting and transmitting solar energy of 35 percent.

The published literature also deals with an analogous concept, the use of fiber optic cables to transmit radiant energy from the sun into spacecraft. Mori et al. (1984) proposed that sunlight be transmitted via fiber optic cables into a space station to irradiate plants. In addition, Olson et al. (1988) speculated that the use of fiber optic cables may reduce the energy required to irradiate plants for NASA's Controlled Ecological Life Support System (CELSS). Similarly, Langhans and Dreesen (1988) promoted fiber optic cables to transmit sunlight for the irradiation of plants in spacecraft.

2.4 COLLECTING SOLAR RADIATION

In order to minimize the size of the opening in an opaque, insulated structure, the solar energy transported through the opening must be concentrated. As a result, some means of concentrating the available solar radiation is required. Mori (1987) employed fresnel lenses to concentrate solar energy, while Cariou et al. (1982) preferred reflective parabolic dishes to concentrate solar energy.

2.4.1 Concentrating Solar Radiation

Welford and Winston (1978) indicate that a solar concentrator increases the energy flux upon a receiver. Normally, solar energy is concentrated to improve the performance of thermal and photovoltaic collection systems. However, solar energy must also be concentrated to focus an image of the sun upon the end of a fiber optic cable or a fiber

optic cable bundle. In terms of geometrical optics, the sun represents an object at infinity.

Three factors limit a concentrating collector's ability to concentrate solar energy. First, as Stine and Harrigan (1985) indicate, diffuse radiation cannot be concentrated. Therefore, when diffuse radiation is the significant portion of total radiation, the performance of a concentrating collector suffers. Second, as Welford and Winston (1978) observe, that reflective/refractive surfaces are not 100% reflective/anti-reflective and are not perfect in shape. Thirdly, as Stine and Harrigan (1985) indicate, a concentrator must be continually repositioned normal to the sun's rays to maintain an image of the sun on a receiver.

2.4.2 Parabolic Concentrating Collectors

Reflecting concentrators employing both spherical and parabolic geometries are used for concentrating solar energy. However, parabolic geometries dominate. Stine and Harrigan (1985) indicate that a parabolic concentrator must track the motion of the sun to maintain the concentrator's axis or plane of symmetry parallel to the incident rays of the sun. Line-focusing troughs and point-focusing dishes are the two types of parabolic geometries used for concentrating solar energy. Cariou et al. (1982) used silver and aluminum coated parabolic dishes that were 6.7 cm in diameter with a 10 cm focal length to concentrate solar energy.

Mori et al. (1984) stated that chromatic aberration is not a consequence of reflective concentrators. As a result, beam splitters or filters are required, in association with reflecting concentrators, to separate the ultraviolet and infra-red components from the solar spectrum.

2.4.3 Fresnel Lenses

Kritchman et al. (1979) point out that refracting concentrators, such as fresnel lenses, are efficient solar energy concentrators which are capable of high concentration ratios. A fresnel lens is a flat lens that approximates the curvature of a convex lens by employing canted facets on the lens's surface. The advantages of fresnel lenses, according to Kritchman et al. (1979), are the thin lens profile and lower amount of material required for manufacture. The thin profile reduces transmission loss and the lower amount of material reduces manufacturing costs. Harmon (1977) and Oshida (1961) promote the use of fresnel lenses for concentrating solar energy. Furthermore, Mori (1985) used a fresnel lens to concentrate sunlight upon the end of a fiber optic cable bundle. As with parabolic reflectors, a fresnel lens must track the sun in order to focus an image of the sun upon a receiver fixed with respect to the fresnel lens. Linear and point focusing fresnel lenses are the two types of fresnel lenses available for concentrating solar energy. Mori et al. (1984) recommended 4.0 to 12.5 cm diameter point focusing fresnel lenses with diameter-to-focal length ratios of 1.0 to 1.15 to concentrate solar energy.

A phenomenon associated with refractive concentration of solar energy is chromatic aberration. Klein and Furtak (1986) indicate that chromatic aberrations are caused by the variation in the index of refraction of a transparent material with the wavelength of the radiant energy. In effect, chromatic aberrations cause different wavelengths of radiant energy to be focused at different points along a fresnel lens's optical axis. Mori (1984) used the chromatic aberration phenomenon of fresnel lenses to eliminate the ultraviolet and reduce, by 60%, the infra-red components of the solar spectrum. The ultraviolet and infra-red wavelengths are focused beyond the numerical aperture of the fiber optic cable by positioning the end of the fiber optic cable bundle at a focal point corresponding to a wavelength of 550 nm. Thus, a fresnel lens performs the dual functions of concentrating solar energy and reducing and/or eliminating the ultraviolet and infra-red components of the solar spectrum, respectively. Mori (1985) promoted irradiating plants with solar energy devoid of ultraviolet and infra-red wavelengths to reduce harmful effects on the plants.

2.5 TRANSMISSION OF SOLAR ENERGY BY FIBER OPTIC CABLES

A fiber optic cable is a single slender strand of a highly transparent material, the core, surrounded by a thin coating of material, the cladding. The differences in the indices of refraction of the core and the cladding materials cause total internal reflection of light within the fiber optic cable. Prior research has determined that fiber optic cables can transmit solar energy. For instance, Kato and Nakamura (1976)

concluded that silica core fiber optic cables can transmit solar energy effectively over distances of about 40 m. Furthermore, experiments conducted by Cariou et al. (1982) indicate that 2.0 W of solar energy can be transmitted via one, 10 m long, 1.0 mm core-diameter, plastic clad silica fiber optic cable with an efficiency of 70%. As previously mentioned, Mori (1984) successfully used fiber optic cables to transmit photosynthetically active radiation from the sun and electric lamps to algae.

2.5.1 Attenuation

Attenuation of radiant energy in a fiber optic cable is caused by absorption, scattering, microbending, and end loss reflections. Seippel (1984) indicates that fiber optic cables used for telecommunications possess wavelength-optimized regions with low attenuation. Fiber optic cables used for transmitting the visible portion of the solar spectrum must possess a broad wavelength region with low attenuation. Izawa and Sudo (1987) indicated that silica oxide glass (SiO_2), poly-methyl methacrylic (PMMA), and quartz crystal are highly transparent materials in the visible region. Izawa and Sudo (1987) indicated that SiO_2 and PMMA are suitable materials for manufacturing fiber optic cables, whereas, quartz crystal is a difficult material to manufacture fiber optic cables. Mori et al. (1984) used fiber optic cables with a quartz crystal core to transmit solar energy. Both Kato and Nakamura (1976) and Cariou et al. (1982) use silica core fiber optic cables to transmit solar energy.

2.5.2 Numerical Aperture And Size

According to Cariou et al. (1982), large core diameter fiber optic cables with large numerical apertures are best suited for transporting solar energy. Mori (1987) substituted bundles of small fiber optic cables for a single, large core diameter fiber optic cable. Cariou et al. (1982) pointed out that packing individual fibers into a bundle produces dead spaces on the end of the bundle. Concentrated solar energy received between the cores of the individual fiber optic cables is lost and burns the cladding material. As a result, Cariou et al. (1982) recommend associating one fiber optic cable with one concentrator. Cariou et al. (1982) use 0.6 and 1.0 mm core-diameter fiber optic cables with a numerical aperture of 0.4 to transmit solar energy. Mori et al. (1984) also suggested the use of individual fiber optic cables with a core diameter of 0.5 to 1.8 mm and a numerical aperture of 0.4.

2.6 SOLAR TRACKING

Hughes (1980) indicated that the fundamental requirement of a point-focusing solar collector is to maintain the energy flux into the receiver's aperture so as to maximize useful output. In order to achieve the fundamental requirement, a dual axis solar tracker with minimal pointing error is required. A dual axis solar tracker eliminates the cosine effect by orienting an attached collector perpendicular to the sun's rays. In addition, Mori et al. (1984) indicated that the error should be minimized for proper functioning of the chromatic aberration

filtering of ultraviolet and infra-red wavelengths between the fresnel lenses and the end of the fiber optic cable.

2.6.1 Types Of Solar Tracking Systems

Point-focusing parabolic dishes and fresnel lenses require solar tracking about two axes. Stine and Harrigan (1985) indicate that there are two types of dual-axis solar trackers, azimuth-elevation (az-el) and polar trackers. An az-el tracker rotates a collector about a zenith axis and an axis parallel with the surface of the earth (elevation axis). The slew rates about the azimuth and elevation axes vary due to geographical location, time of day, and season. A polar tracker rotates a collector about an axis aligned parallel to the earth's rotational pole and an axis perpendicular to the polar axis. Since the slew rate about the polar axis is constant at 15°/h and the slew rate about the perpendicular axis is very slow, a continuous rotation of the polar axis and a daily, incremental manual adjustment of the perpendicular axis are feasible.

2.6.2 Solar Tracking Errors

According to Hughes (1980), pointing error is defined as the angular difference between the aperture center and the flux distribution center. The causes of pointing errors can be classified as constant or time-varying. Constant errors are the result of misalignments and sag, while time varying errors are created by wind loads and the control scheme employed. Misalignments can be minimized by quality construction of the collector and solar tracker mount. Sagging and wind load effects are reduced by designing a collector and solar tracking mount with sufficient rigidity. Lastly, an accurate and stable control scheme reduces time-varying errors due to solar tracking and wind loading. Hughes (1980) indicated that point-focusing concentrators have the most stringent pointing accuracy requirements. In addition, Hughes (1980) indicated that pointing errors can be reduced to within ±1 min of arc with current, state-of-the-art controllers.

2.6.3 Solar Tracking Control Strategies

A common element with solar trackers is a control algorithm that commands the required motion in the articulation axes. Hughes (1979) indicated that a control algorithm can be either open-loop or closed-loop. An open-loop control algorithm relies on precomputed motion commands to position a collector perpendicular to the sun's incoming rays, while a closed-loop control algorithm relies on measurements of the desired

output to generate motion commands for positioning a collector perpendicular to the sun's incoming rays.

D'Azzo and Houpis (1981) indicate that a polar tracker with a clock-actuated drive on the polar axis is an example of an open loop control system. Hughes (1979) indicates that closed loop control systems are most common for solar trackers aiming point-focusing solar concentrators. Hughes (1979) describes an on-off or "bang-bang" control algorithm which employs threshold sensing to effect the required motion. The drawbacks associated with the on-off control algorithm are pointing inaccuracy and possible instability. An optimal control scheme proposed by Hughes (1979) converts the tracking problem into a regulator problem with a sun rate input. The optimal control scheme would provide an almost zero steady state tracking error even in windy conditions. However, Hughes (1979) rejected the actual implementation of the optimal control scheme due to the associated high cost and complexity.

2.7 SUMMARY

Previous research indicates that a device which collects and transmits photosynthetically active radiation from the sun via fiber optic cables to plants grown in an opaque, insulated structure is technically feasible. However, to be effective, the device must provide the plants with the proper quantity, quality, direction, and periodicity of radiant energy for photosynthetic and photomorphogenic responses. The three essential components of the device are the solar concentrator, the fiber optic cable, and the solar tracker. Fresnel lenses are the best solar energy concentrator for the application due to the chromatic aberration phenomenon. One fiber optic cable oriented with one fresnel lens is the most efficient setup for transmitting solar energy. A fiber optic cable with a silica oxide glass or poly-methyl methacrylic core provides the lowest attenuation over the visible region of the spectrum. Large core-diameter fiber optic cables with large numerical apertures are best suited for transmitting solar energy. An on-off control algorithm is suitable for commanding the motion of a sun-following tracker.

3. DESIGN THEORY FOR TRANSMISSION AND COLLECTION OF SUNLIGHT

The theory required to develop a mechanism capable of collecting and transmitting solar radiant energy via fiber optic cables involves geometrical optics. Fresnel lenses and fiber optic cables function according to the laws of geometrical optics.

3.1 GEOMETRICAL OPTICS

Geometrical optics is the basic tool for designing most optical systems. The three principle laws of geometrical optics are rectilinear propagation, reflection, and refraction.

3.1.1 Rectilinear Propagation

The law of rectilinear propagation states that in a homogeneous media, light travels in straight lines. The law of rectilinear propagation enables ray tracing for the design and analysis of optical components.

3.1.2 Reflection

The law of reflection states that a reflected ray and an incident ray lie in the plane of incidence and that the angle of reflection (θ'') equals the angle of incidence (θ).

3.1.3 Refraction

The law of refraction states that the sine of the angle of incidence (θ) bears a constant ratio (n/n') to the sine of the angle of refraction (θ'). The law of refraction or Snell's law is described by Equation 3.1.

$$n \sin(\theta) = n' \sin(\theta') \quad \ldots\ldots\ldots\ldots\ldots\ldots \quad (3.1)$$

where; n = First Medium Index of Refraction and
n' = Second Medium Index of Refraction.

3.2 FRESNEL LENSES

A lens operates on the principle of refraction. Properly oriented, a lens is capable of concentrating the incoming rays from the sun in order to increase the power density of the solar radiation. A fresnel lens is a flat lens that approximates the curvature of a convex lens by employing canted facets on the lens surface.

3.2.1 Solar Energy Concentration

An optical system designed to concentrate solar energy normally consists of an entrance aperture and an exit aperture which are referred to as the concentrator and the receiver, respectively. The image-forming properties of the concentrator and the image-acceptance properties of the receiver determine how efficiently the optical system handles solar energy. The following discussion is limited to lenses as concentrators.

The geometrical concentration ratio (C) of a concentrating optical system is defined as the area of the concentrator divided by the area of the receiver. The theoretical maximum concentration of a circular object at infinity (C_{max}) subtending a half angle, β, is described by Equation 3.2.

$$C_{max} = (\sin\beta)^{-2} \quad \ldots\ldots\ldots\ldots\ldots\ldots\ldots \quad (3.2)$$

The diameter of an image produced by a lens with a focal length, f, from a circular object at infinity subtending a half angle, β, is limited to $2f\beta$. The consequence is that the focal length of a lens determines the concentrating capability of an optical system. If the diameter of the concentrated image is greater than the diameter of the receiver, then a portion of the solar energy is lost. Also, the diameter of a lens (2r) influences the efficiency of an optical system, since the lens diameter and the focal length determine the angle of convergence for the concentrated image. If the angle of convergence for the lens is beyond the angle of acceptance for the receiver, then a portion of the concentrated image is lost. The angle of convergence for a lens (δ) is calculated with Equation 3.3.

$$\delta = \mathrm{Sin}^{-1}(r/f) \quad \ldots\ldots\ldots\ldots\ldots\ldots\ldots \quad (3.3)$$

In summary, the efficiency of a concentrating optical system is dependent upon the geometrical concentration ratio, the concentrator's image forming properties, and the receiver's angle of acceptance.

3.2.2 Chromatic Aberration

Paraxial or Gaussian optics describe the ideal situation where all parallel light rays passing through a lens converge to a single point. In reality, the ideal paraxial optics situation does not occur due to the theoretical maximum concentration and lens aberrations. Several different types of lens aberrations alter the image forming capabilities of an optical system. However, a lens aberration that is benefical for the application under consideration is chromatic aberration. Chromatic aberration aids in eliminating and/or reducing the ultraviolet and infra-red wavelengths received at the end of the fiber optic cable. When chromatic aberration is present, the paraxial image point of a lens depends upon the wavelength of the radiant energy. As a result, chromatic aberration causes blue light and red light to form separate images along a paraxial axis. Chromatic aberrations are due to the variation in the index of refraction of a transparent material with the wavelength of the radiant energy. The longitudinal chromatic aberration (X) between two different wavelengths as produced by a single refracting surface is calculated with Equation 3.4.

$$X = S'^2 \{ [n_{w2} - n_{w1}]/ n_l \} \{ 1/R - 1/S' \} \quad \ldots\ldots\ldots \quad (3.4)$$

where; S' = image distance between two λ's,
R = radius of curvature for lens,
n_l = index of refraction for lens,
n_{w1} = lens index of refraction λ_1, and
n_{w2} = lens index of refraction λ_2,
such that, $n_{w2} > n_{w1}$.

3.3 FIBER OPTIC CABLES

A fiber optic cable is a single slender strand of a highly transparent material, the core, surrounded by a thin coating of material, the cladding. The differences in the indices of refraction of the core and cladding materials causes light within the cable to undergo the phenomenon of total internal reflection. Total internal reflection occurs when a light ray travels from a medium with a high index of refraction (n_0) toward a medium with a low index of refraction (n_1) and the sine of the angle of incidence (θ) of the light ray is equal to or greater than the critical angle (θ_c).

3.3.1 Acceptance Angle

Light is admitted into and transmitted along a fiber optic cable via refraction at the end and total internal reflection at the core/cladding interfaces, respectively. Therefore, an incoming light ray must be within the acceptance angle of the fiber optic cable. The acceptance angle specifies the angular range within which the incident light rays must travel to be admitted into the fiber optic cable. Light rays beyond the acceptance angle are either reflected from the end or refracted into the cladding of the fiber optic cable. Half the acceptance angle (σ) is calculated from the fiber optic cable's numerical aperture (NA) and the index of refraction of the outside medium (n_o) with Equation 3.5.

$$\sigma = \mathrm{Sin}^{-1}(NA)/n_o \quad \ldots\ldots\ldots\ldots\ldots\ldots \quad (3.5)$$

The numerical aperture relates the acceptance cone of a fiber optic cable to the outside medium. Normally, the outside medium is air which has an index of refraction of 1.0. Therefore, Equation 3.5 can be simplified to Equation 3.6.

$$\sigma = \text{Sin}^{-1}(NA) \quad \ldots\ldots\ldots\ldots\ldots\ldots \quad (3.6)$$

The numerical aperture is calculated from the indices of refraction of the core (n_0) and cladding (n_1) materials by Equation 3.7.

$$NA = (n_0^2 - n_1^2)^{\frac{1}{2}} \quad \ldots\ldots\ldots\ldots\ldots\ldots (3.7)$$

The ability of the fiber optic cable to accept light from more extreme angles increases as the numerical aperture increases.

3.3.2 Core Diameter

Light is transmitted along a fiber optic cable's core. The diameter of the core influences the amount of energy collected and transmitted by a fiber optic cable. As the core diameter of a fiber optic cable increases, so does the cone of acceptance. Hence, a greater amount of energy can be transported by large core diameter fiber optic cables.

3.3.3 Attenuation

Attenuation is the decrease in radiant power in a fiber optic cable due to absorption, scattering, micro-bending, and end loss reflection. An attenuation factor (α) in decibels per kilometer (dB/km) is calculated with Equation 3.8.

$$\alpha = 10\log_{10}(P_i/P_o)/x \quad \ldots\ldots\ldots\ldots\ldots\ldots \quad (3.8)$$

where; P_i = input power (W),
P_o = output power (W), and
x = length of fiber optic cable (km).

3.4 SUMMARY

The laws of geometrical optics must be considered when designing or analyzing an optical system. Fresnel lenses and fiber optic cables operate according to the laws of rectilinear propagation, reflection, and refraction. The aspects which influence a fresnel lens's ability to concentrate solar energy are the focal length and diameter of the lens. The aspects which influence a fiber optic cable's ability to collect and transmit solar energy are the numerical aperture, core diameter, and attenuation of the the fiber optic cable. When the fresnel lens and fiber optic cable are matched to form an optical system, the geometrical concentration ratio must be considered.

4. DESIGN OF PROTOTYPE DEVICE

The method proposed for irradiating horticultural crops in northern regions was to collect and transmit solar radiant energy to plants grown in an opaque, insulated structure. The opaque, insulated structure reduces the energy consumed for heating, while the use of solar energy reduces the energy consumed for generating light with electrical lamps. An evaluation of the options available for collecting and transmitting solar energy to a remote location, as presented in Chapter 2, indicated that fresnel lenses, flexible fiber optic cables, and an azimuth-elevation (az-el) solar tracker were best suited for design of the prototype device.

The design objective was to maximize the collection and transmission of photosynthetically active radiation from the sun, while still providing the necessary wavelengths for photomorphogenic responses. The selected design matches a single flexible fiber optic cable with a single fresnel lens to form a unit, referred to as a set. Multiple sets were then placed on a dual axis solar tracker to provide sufficient quantity of irradiation for plant growth. The flexible fiber optic cables simplify the solar tracking mechanism. The fresnel lenses produce chromatic aberrations which are useful for eliminating and/or reducing the ultraviolet and infra-red wavelengths.

The resulting design problem was to continually focus an image of the sun upon an object approximately the size of a pin head during winter

conditions at latitudes above the Arctic Circle. The following sections discuss details relating to the prototype device design.

4.1 GENERAL DESCRIPTION

A front view and a side view of the prototype light collection and transmission device are displayed in Figures 4.1 and 4.2, respectively. The prototype device consists of two identical collector panels, an azimuth-elevation (az-el) solar tracker, and a shadow band sensor, as well as two, detached electrical boxes and a remote control pendant. The electrical boxes and the remote control pendant are connected to the prototype device by electrical cables. The effective concentrator surface area on the prototype device is 0.30 m^2 and the length of the fiber optic cables attached to the prototype device are 5.00 m. The prototype device operates on 110 V AC electrical power at 60 Hz.

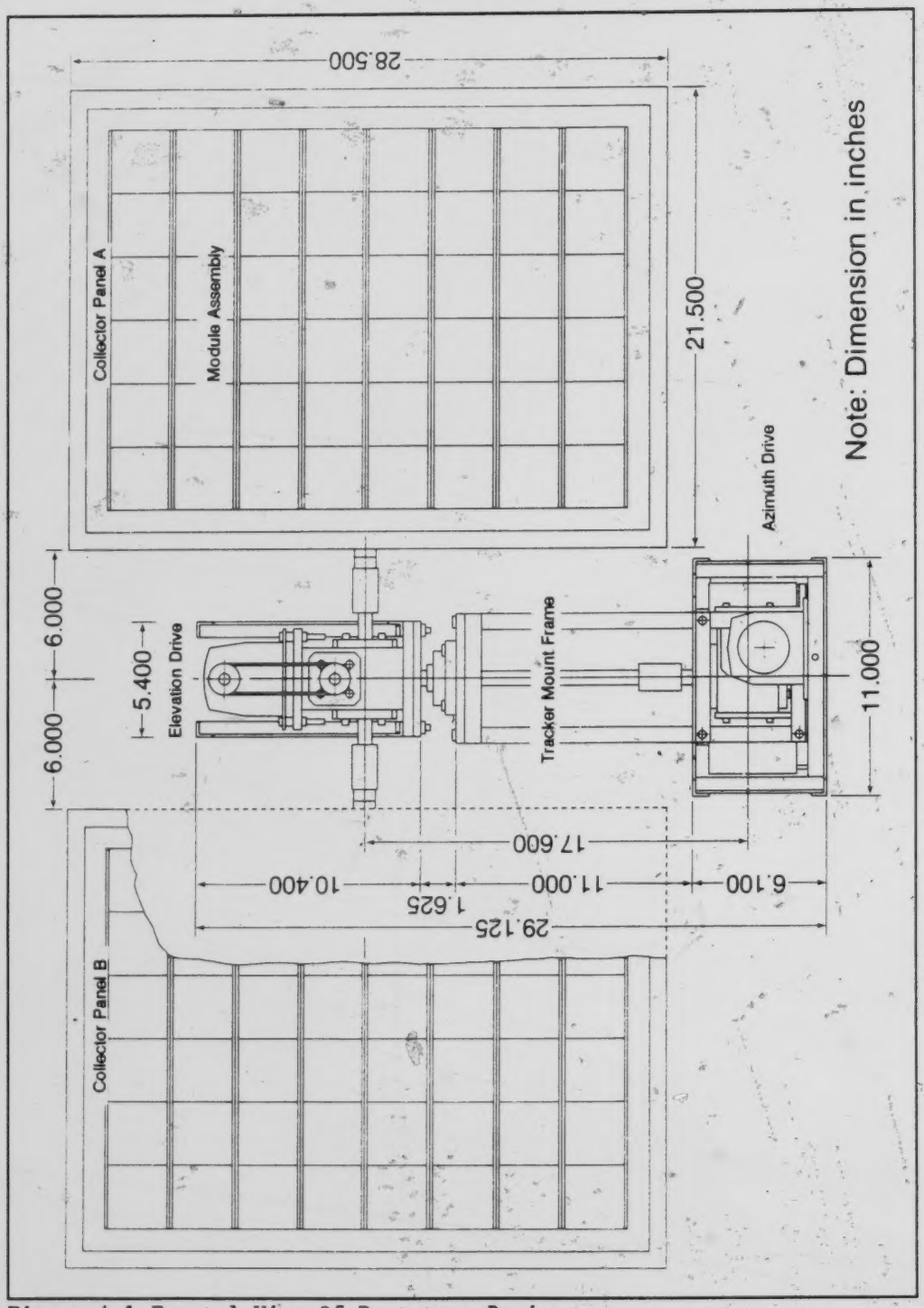

Figure 4.1 Frontal View Of Prototype Device

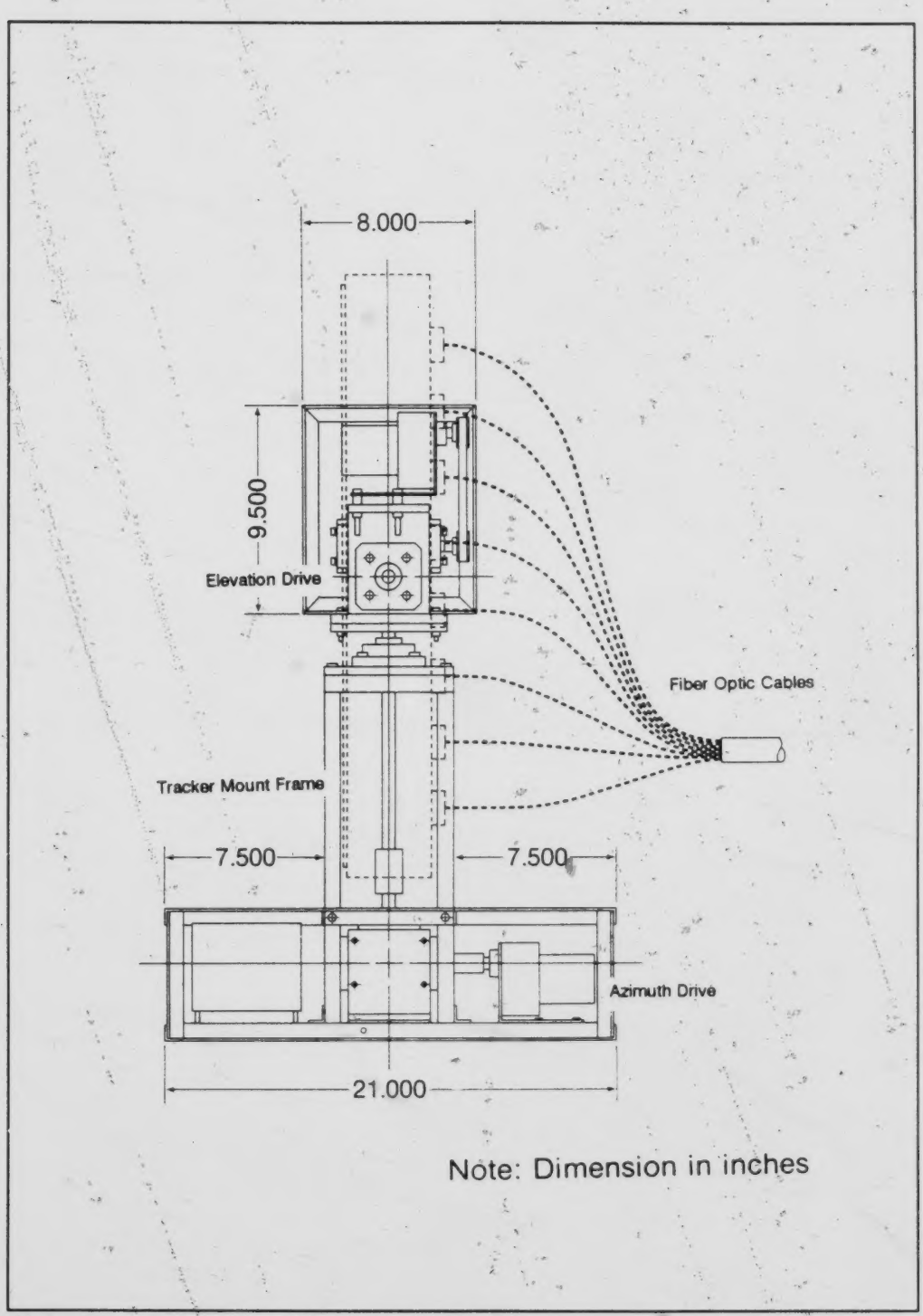

Figure 4.2 Side View Of Prototype Device

The collector panels are referred to as panel A and panel B. Panel A is located on the right side of the prototype device from a front view. The collector panels are positioned on either side of the az-el tracker's mount and attached to the output drive shaft of the az-el tracker's drive train. Each collector panel contains eight module assemblies arranged horizontally within the collector panel's frame. Each module assembly in turn contains six fresnel lens and fiber optic cable sets. An individual fiber optic cable is attached to a module assembly by a connector assembly. The collector panels are oriented such that the fresnel lenses' surfaces are aligned normal with the incoming solar rays.

The column and pedestal style mount contain the az-el tracker's drive train and actuators. The mount is divided into three sections, referred to as the base, tower, and head sections. The base contains the azimuth drive system, while the head contains the elevation drive system. The head rotates about the tower which connects the base to the head. The az-el drive train is capable of rotating the collector panels, one complete revolution about each axis.

The shadow band sensor is located between the collector panels above the solar tracker mount upon a rib plate. The rib plate is adjustable to align the shadow band sensor in a plane parallel with the fresnel lenses' surfaces. The shadow band sensor employs four photocells and two lobes to sense the position of the sun in the sky. A fifth photocell senses the quantity of sunlight available.

The az-el tracker's controller is contained in the detached electrical boxes. The controller interprets signals from the shadow band sensor and commands the actuators attached to the az-el tracker's drive train. Additional electric circuits contained in the electrical boxes ensure the prototype device does not overheat or rotate beyond the slack limit for the fiber optic cables. The remote control pendant allows the az-el tracker to be over ridden manually.

4.2 PRIMARY COMPONENTS

The four primary components on the prototype light collection and transmission device are the, fresnel lens, fiber optic cable, solar tracking kit, and gearmotors and gearboxes. The primary components are classified as such, since the prototype device is designed around these components.

4.2.1 Fresnel Lens

The primary function of the fresnel lens is to concentrate an image of the sun upon the end of a fiber optic cable's core. A secondary function of the fresnel lens is to produce chromatic aberrations of the sun's image.

The fresnel lens selected forms an image of the sun that is 0.61 mm in diameter and subtends a half angle (δ) of 25.7°. The image size and half

angle approximately match the fiber optic cable's core diameter of 0.600 ±0.024 mm and theoretical maximum acceptance angle of 23.6° (numerical aperture of 0.4). The fresnel lenses employed on the prototype device are a No. 5 positive focal length aspheric fresnel lens (Fresnel Technologies, Fort Worth, TX). The fresnel lens is corrected for spherical aberrations and measures 63.5 mm in diameter. The fresnel lens is cast in a square sheet of optical grade acrylic measuring 76.2 mm by 76.2 mm by 1.6 mm thick. The optic grade acrylic has an index of refraction of 1.49 and a transmissivity of 92% over the visible region of the spectrum. The fresnel lens has 49.2 grooves/cm and a 66.0 mm focal length. The fresnel lenses are oriented such that the grooved side of the lenses face the sun. A total of 96 fresnel lenses are used on the prototype device. Appendix A contains further information on the fresnel lenses.

A variation in the size of the fresnel lenses posed a problem during assembly. The majority of the optical grade acrylic sheets possessed a unilateral tolerance of +3 mm. Since the chosen allowance was ±0.5 mm, the edges of the fresnel lenses had to be shaved down with a hand plane to a tolerance of ±0.5 mm.

4.2.2 Fiber Optic Cable

The fiber optic cable's function on the prototype device is to transmit photosynthetic and photomorphogenic radiation from the focal point of the fresnel lens to a remote location. Once at the remote location, the radiation is dispersed to the plants from the end of the fiber optic cable.

The fiber optic cable selected has a large core diameter, large numerical aperture, low attenuation over the visible spectrum, and suitable temperature resistance. The cable employed on the prototype device is a PCS 600W plastic clad silica (Quartz & Silice, Cedex 27, 92096 Paris La Defense, France). The cable has a core diameter of 0.600 ±0.024 mm, cladding diameter of 0.750 ±0.060 mm, and overall outside diameter of 1.060 ±0.085 mm. The core-cladding eccentricity is specified as 0.030 mm. The fiber optic cable's coating material is a teflon type ETFE. The theoretical maximum numerical aperture is 0.40 (half acceptance angle of 23.6°). Appendix B displays the attenuation curve for the fiber optic cable. The recommended minimum and maximum operating temperatures for the fiber optic cable are -25°C and 130°C, respectively.

The light-receiving end of the fiber optic cable is referred to as the A end, while the light dispersing end of the cable is referred to as the B end. The length of the cables used on the prototype device is 5.00 m. The fiber optic cables were cut from a continuous length of cable wrapped on a spool. A 9 μm size diamond chip saw blade was used to cut

the cable in order to avoid chipping the silica core. Following the cutting operation, each end of the fiber optic cable was polished with the combination of a dry mylar backed aluminum oxide lapping film and wet aluminum oxide slurries. The polishing operation produced a 0.3 μm surface finish squared to a tolerance of less than 1°. The polishing operation proceeded as follows. The fiber optic cable was mounted in a polishing plate, such that the end of the fiber optic cable was flush with the face of the polishing plate. The face of the polishing plate was rotated counter-clockwise against four different polishing grit surfaces at one revolution per second for 30 to 45 revolutions. The polishing grit surfaces, in order of polishing, were a 32.0 μm dry film, a 15.0 μm wet slurry on a felt pad, a 3.0 μm wet slurry on a felt pad, and a 0.3 μm wet slurry on a felt pad. The cable and the polishing plate was rinsed with distilled water after each grit surface type. Lastly, the polishing plate was removed from the fiber optic cable and the end of the cable was visually inspected under a microscope for surface finish quality and cracks. Poor quality surfaces were re-polished and re-inspected, while surfaces displaying cracks were re-cut, re-polished, and re-inspected. The prepared ends of the fiber optic cables were covered with a plastic bag to prevent damage and contamination.

4.2.3 Solar Tracking Kit

The solar tracking system's function on the prototype device is to sense the position of the sun in the sky and position the collector panels perpendicular to the incoming rays from the sun. An az-el solar tracker is used on the prototype device. In comparison to a polar tracker, the az-el tracker is less complicated to build and requires minimal monitoring during operation. The solar tracking system consisted of an electronic dual axis solar tracking kit, two electrical gearmotors, two speed-reduction gearboxes, and miscellaneous drive train parts.

The solar tracking kit selected was rated to have a tracking accuracy of 0.1° when the drive train is tight and the drive speed is 0.025 rpm. The tracking kit employed on the prototype device is a Mark IV ST-2 Dual Axis Tracking System (Mann-Russell Electronics, Tacoma, WA). Appendix C contains further information on the solar tracking kit. The kit contains a microprocessor based relay-type controller, a shadow band sensor employing photocells, and a remote control pendant. The kit is capable of tracking the sun's azimuth and elevation positions for clear conditions (active tracking mode) and the sun's azimuth position for overcast conditions (synthetic tracking mode), as well as returning the collector panels to a sunrise position for the following day (night return mode). Attachment of the kit to an az-el tracker mount containing a drive train and actuators produces a feedback control system for tracking the sun's motion.

The controller includes a power supply, CMOS logic circuit, and a drive motor interface. The unit is housed in an oil tight enclosure that measures 20 cm by 15 cm by 9 cm. Deadband, balance sensitivity, low light level sensitivity, and synthetic track time intervals are adjusted with potentiometers on the controller. The az-el tracker can be operated manually with the remote control pendant.

The sensor head contains five photocells sealed in a 13 cm by 13 cm by 1.3 cm thick moulded assembly with 5 m of six-conductor shielded cable attached. Two vertically oriented, 7.5 cm-diameter, semi-circular shaped lobes positioned perpendicular to one another protrude from the face of the moulded assembly. The assembly is attached by three screws to the rib plate that spans between the collector panels above the head of the solar tracker's mount. The shielded cable extends from the sensor head to the controller. Two photocells associated with each lobe sense the position of the sensor head with respect to an axis. The photocells are positioned on either side of the lobe such that the center of the photocell is aligned with the outer edge of the lobe's rim. As a result, when the lobe is aligned with the sun, an equal shadow is cast upon each photocell. The controller interprets the sensor head to be in alignment with the sun when all four photocells are receiving the same amount of solar energy. The control objective is to maintain the lobe's alignment with the sun. The fifth photocell senses the quantity of sunlight available so the controller can determine whether to initiate synthetic tracking or night return functions.

4.2.4 Gearmotors And Gearboxes

Two identical electrical gearmotors are used as the actuators on the azimuth and elevation drive trains. The function of a gearmotor is to convert the controller's or the electrical safety circuits' commands to rotational motion in the drive train shafts. Two gearboxes are used as speed reducers for the azimuth and elevation drive trains. The function of the gearboxes is to reduce the speed of the rotation motion provided by the gearmotors to 0.025 rpm. The gearmotors and gearboxes selected match the controller and provide the required rotational speed, respectively.

The electrical gearmotors used on the prototype device are 110 V AC HY Sync model 23T1BEHY-D4 gearmotors (Bodine Electric Company, Chicago, Illinois, USA). The gearmotors feature low speed operation, high torque, reversibility, stall protection, and stopping and holding capability. The gearmotors require a capacitor and resistor in parallel with the line circuit to produce a phase shift network for operation. The output shaft speed for the gearmotor is 1 rpm. Appendix D contains further information on the gearmotors.

The speed reduction gearboxes are Flexaline 40:1 right angle worm gear style gearboxes (Grove Gear Division, Union Grove, WI). The azimuth gearbox is a style V, while the elevation gearbox is a style T. The azimuth gearbox is oriented such that the output shaft of the gearbox is in a vertical position, while the elevation gearbox is oriented such that the output shaft is in a horizontal position. The azimuth gearmotor and

gearbox are connected by a coupler and key. The key in the shafts' keyways prevent the shafts from slipping in the coupler. The elevation gearmotor and gearbox are connected by a timing belt and timing pulleys. The pulleys are attached to the shafts with a key in the shafts' keyways to prevent slippage of the pulleys on the shafts.

4.3 SECONDARY COMPONENTS

In addition to the three primary components, the prototype device has secondary components for supporting, postioning, retaining, and protecting the primary components. The secondary components are the collector panel, module assembly, connector assembly, rib plate, tracker mount frame, and auxiliary electrical box. The working drawings for the prototype device are shown in Appendix E.

4.3.1 Collector Panel

A collector panel consists of a casement-style window frame that contains eight module assemblies covered by a 4 mm-thick sheet of optical quality, tempered glass. The tempered glass, which protects the fresnel lenses within the module assemblies, has a transmissivity of 92% over the visible region of the spectrum. The collector panel's frame is 72.4 cm by 54.6 cm by 10.2 cm. The frame is constructed from an extruded aluminum tubing with a rectangular cross section of 10.2 cm by 4.5 cm and a nominal wall thickess of 3 mm. The frame has two functions on the prototype device. First, the frame provides a rigid structure to hold the module

assemblies and, secondly, the frame is a ventilation supply and exhaust ducting system. A fan was not sized for the system.

Each collector panel is mounted on the output shaft of the az-el drive system with a stub shaft, coupler, and key. The threaded end of a 15 mm-diameter, steel bar is screwed into the socket of a mounting bracket bolted midway up the side of the frame facing the tracker's mount to create a stub shaft. The key in the shafts' keyways prevent the stub shaft from rotating with respect to the az-el drive shaft. The stub shaft arrangement allows an incremental rotational adjustment of a panel about an axis through the az-el drive system. The adjustment is required to align the panels in the same plane as the fresnel lenses. The adjustment is accomplished by loosening the stub shaft lock nut, rotating the panel to obtain alignment, and re-tightening the stub shaft lock nut.

Access ports on the top and bottom of the frame provide a fan inlet and exhaust outlet for the ventilation system. Plugs inside the diagonally opposed corners of the frame separate the supply and exhaust duct sides of the frame. Ventilation air passes from the supply to the exhaust sides through 3.8 cm diameter holes on the inside vertical edge of the frame which match the module assemblies. The ventilation air removes moisture and/or excess heat from the module assemblies.

Studs on the frame are used to attach two aluminum brackets on the sides of the frame. The brackets form a ledge for supporting and fastening the module assemblies to the frame. Lastly, right-angle-shaped aluminum

brackets are attached to studs on the top, vertical sides of the frame facing the tracker's mount to form a ledge for supporting and fastening the rib plate.

4.3.2 Module Assembly

A module assembly is composed of a chassis, six fresnel lenses, and six connector assemblies with fiber optic cables attached. The module assembly is responsible for retaining and separating the fresnel lens and fiber optic cable sets by the focal distance of the fresnel lens. Incremental adjustments of the end of the fiber optic cables with respect to the focal distance and the optical axis of the fresnel lens are made with the connector assembly. The modular design facilitates setup, adjustment, and replacement of the fresnel lens and fiber optic cable sets.

Fresnel lenses and fiber optic cables are arranged in groups of six along the top and bottom, respectively, of a U shaped chassis. The chassis is referred to as a module. A cross sectional end view of a module with a fresnel lens and connector assembly with a fiber optic cable attached is displayed in Figure 4.3. The module measures 457.0 mm by 79.0 mm by 66.0 mm and is fabricated from 14 gauge aluminum sheet. Two 457.0 mm by 6.6 mm by 6.6 mm right angle shaped aluminum strips positoned back to back and separated by a distance of 1.6 +0.1 mm are glued with epoxy cement along both top inside edges of the module to produce two slots for the fresnel lenses. The fresnel lenses are butted against each other in the

slots and sealed in position with a silicon caulking compound. The outer ring of the connector assembly protrudes through a 38.1 +0.4 mm diameter access hole in the bottom underside of the module located under the center of each fresnel lens. Three 2.5 mm diameter holes around the circumference of the access hole at 120° intervals are used for attaching the connector assembly to the module. Two 4.9 mm diameter holes at each end of the module allow fasteners to connect the module to the collector panel's frame. A complete module assembly forms a tube which is open at each end, thereby, allowing ventilation air from the collector panel's frame to pass through.

4.3.3 Connector Assembly

A fiber optic cable is connected to the module by the connector assembly. The connector assembly is a micro-positioning device used to position the end of the fiber optic cable with respect to the focal point of the fresnel lens. The positioning is critical for maximizing the energy flux transported by the fiber optic cable, benefitting from the chromatic aberration phenomenon, and preventing heat damage to the fiber optic cable's end.

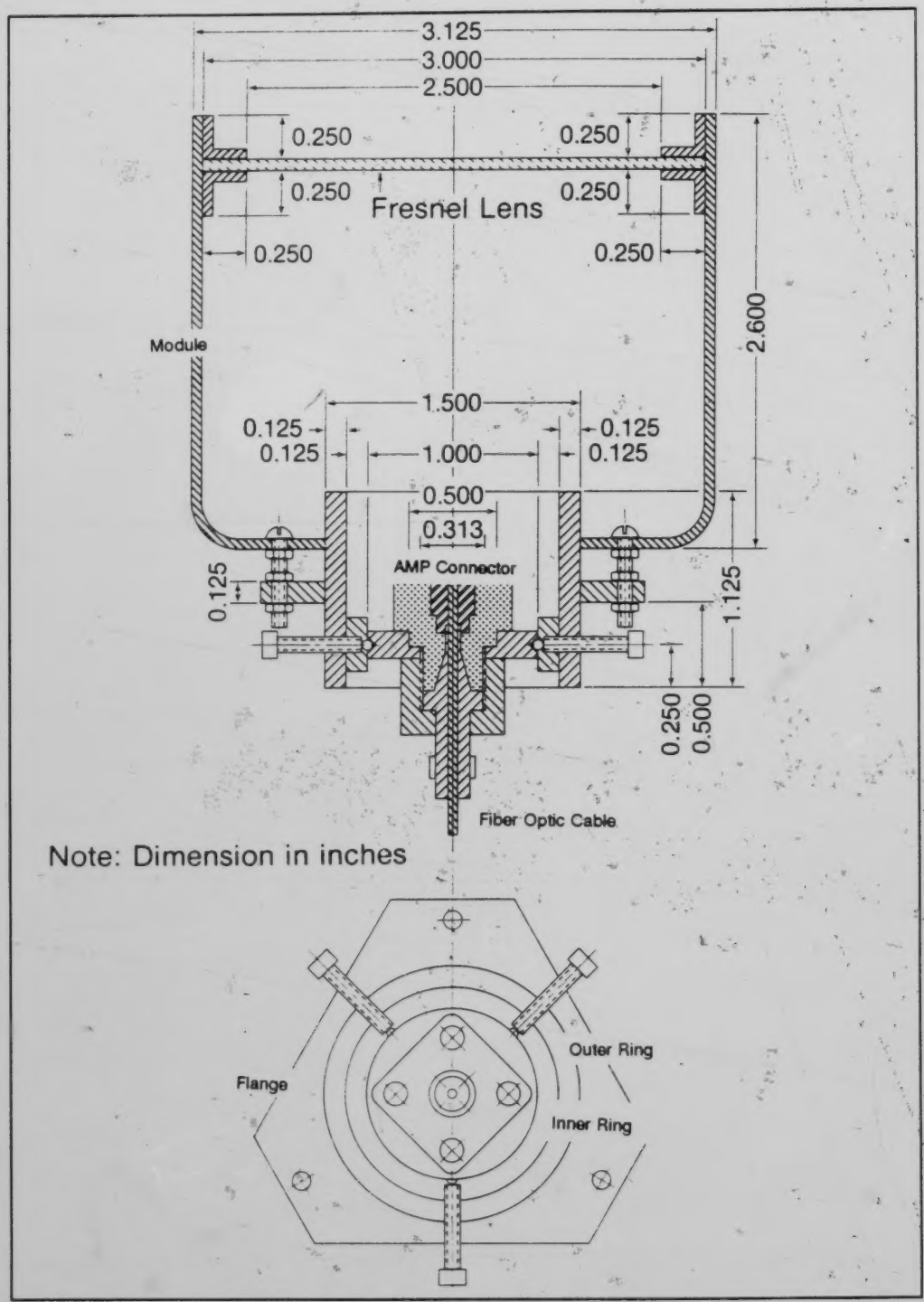

Figure 4.3 Cross Sectional Views Of Module Assembly

A cross sectional side view and a top view of the connector assembly are displayed in Figure 4.3. The connector assembly is composed of an aluminum connector plate, aluminum outer ring, aluminum inner ring, AMP fiber optic connector, six set screws with nuts, polyethylene foam dust cap, reflective aluminium foil tape, and a plastic-clad, silica fiber optic cable. The AMP connector in turn contains a plastic ferrule, plastic connector mount, plastic cap, and brass crimp ring. In addition, a 10 mm long layer of heat shrink tubing around the fiber optic cable provides a strain relief between the fiber optic cable and the AMP connector's ferrule.

The triangular shaped connector plate glued with epoxy cement to the middle of the outer ring produces a flange for attaching the connector assembly to the module. Three 2.5 mm diameter holes in the connector plate at 120° intervals match the three holes around the circumference of the module's access hole. Three No. 3 56UNF screws attach the connector assembly to the module. Adjustments to the focal distance are made by lateral movements of the connector assembly along the screws attaching the connector assembly to the module. The outer ring resembles a 28.6 mm-long tube measuring 38.1 mm in diameter with a 2.5 mm-thick wall. Three No. 3 56 UNF holes spaced at 120° intervals around the circumference midway up the side of the outer ring receive three No. 3 56UNF set screws. The set screws, which possess ends ground to a point, retain the inner ring to the outer ring. The inner ring resembles a 4 mm-thick, 25 mm-diameter washer with a 2.4 mm-deep by 12.7 mm-diameter counter bore in the 8.0 mm-diameter center hole. In addition, the inner ring has a V-shaped groove

around the circumference of the inner ring's edge. The counter bore is required for fitting the AMP connector to the inner ring and the groove is required to allow the set screws to rotate with respect to the inner ring and to retain the inner ring. The three set screws also allow adjustment of the fiber optic cable with respect to the optical axis of the fresnel lens. The AMP connector, which is fixed with respect to the inner ring, retains the fiber optic cable. The AMP connector is a single position fiber optic connector with a ferrule designed for large plastic fibers (AMP Optimate LRF, AMP Incorporated, Harrisburg, PA). The fiber optic cable is clamped to the AMP connector's ferrule by the brass ring which is crimped with a fiber optic crimp tool (AMP certi-crimp, AMP Incorporated, Harrisburg, PA).

The polyethylene foam dust cap over the end of the assembly prevents dust from entering the module. The reflective aluminum foil tape which possesses a 0.60 mm-diameter hole was placed over the end of the AMP connector under a microscope such that only the core of the fiber optic cable is visible. The tape reflects the solar energy not received upon the core of the fiber optic cable, thereby, preventing heat damage to the fiber optic cable's cladding and the AMP connector.

The fresnel lenses are held rigidly within the module, while the fiber optic cables are held rigidly within the connector assembly. The connector assembly's six set screws allow linear and rotational movements to the fiber optic cable end, thereby, provide a means to adjust the end of the fiber optic cable with respect to the focal point of the fresnel

lens. Adjustments to the focal distance are made by releasing the nut set on the connector assembly's flange and sliding the connector assembly laterally along the screws attaching the connector assembly to the module. The lateral movements are made by turning the nuts on the side opposing the desired direction of motion. Once positioning is complete, the nut set is re-tightened. Adjustments for aligning the fiber optic cable with the optical axis of the fresnel lens are made by releasing the nut set on the set screws retaining the inner ring and turning the set screws such that contact is maintained between the ends of the set screws and the inner ring. Once postioning is complete, the nut set is re-tightened.

4.3.4 Rib Plate

The rib plate connects the collector panels. The functions of the rib plate are to adjust the shadow band sensor with respect to the fresnel lens surfaces and prevent the collector panels from sagging on the az-el drive train shafts. The rib plate consists of two 127 mm by 305 mm by 10 mm plywood sheets. One sheet is attached to the top side of the rib plate mounting bracket, while the other sheet is attached to the bottom side of the rib plate mounting bracket. Adjusting the shadow band sensor is made by releasing the nuts retaining the rib plate's mounting brackets to the studs on the collector panels. The holes on the rib plate mounting brackets have sufficient clearance for incremental movement of the brackets and rib plate with respect to the collector panels. When the rib plate is properly positioned, the nuts are re-tightened.

4.3.5 Tracker Mount Frame

The tracker mount's frame supports the az-el drive train and the collector panels. The frame is fabricated from 19 mm by 19 mm, right-angle-shaped, 2.5 mm-thick steel members. The frame forms a column and pedestal style structure which is held together by a combination of welded connections and fasteners. The tracker mount's frame is covered by removable, sheet metal panels.

The tracker mount is divided into three sections, referred to as the base, tower, and head. As mentioned, the base and tower contain the azimuth drive train, while the head contains the elevation drive train. The head rotates about the tower which spans between the base and the head. The tower and the azimuth gearmotor and gearbox are mounted on a 19 mm-thick plywood base bolted to the mount's frame. The vertically-oriented, 16 mm-diameter azimuth drive shaft is connected to the azimuth gearbox's output shaft by a coupler and key. The azimuth drive shaft is supported below the head's base plate by a horizontally-mounted, flange-style bearing. The bearing is mounted on a 9.5 mm plywood plate bolted to the top of the tower section. The head section's 9.5 mm plywood base plate, which is sandwiched between two 3.2 mm-thick steel plates with a 14.3 mm diameter hole in the center of each, is attached to the azimuth drive shaft. The hole in the center of the base plate allows the base plate to be slipped over the threaded end of the azimuth drive shaft. The base plate rests upon a shoulder on the azimuth drive shaft and is fastened to the azimuth drive shaft by a nut and cotterpin. The

arrangement of the base plate on the azimuth drive shaft produces a rotating platform on which the elevation drive train is mounted. The frame is intended to be mounted on a level surface.

4.3.6 Additional Electric Circuits

The controller is interfaced with several emergency sensors to prevent damage to the prototype device. A limit switching circuit prevents the collector panels from rotating beyond one revolution and a thermal switching circuit detects overheating of the collector panels. The additional electrical circuits are contained in the auxilary electrical box. In addition, the phase shift network for the motors, hour meters, and a DC power supply for the gearmotors is contained in the auxiliary electrical box. The DC power supply is used for providing the gearmotors with an optional 1 A, 12 V, DC current to lock the gearmotors in position when AC current is not being provided.

Electrical current to the gearmotors is routed through limit switches located at the output shafts of the az-el drive train. The limit switches are mounted on the tracker's frame. When the limit switches are contacted, the electrical current is interrupted, thereby preventing the controller or manual operation from the remote control pendant from rotating the collector panels to a position where the fiber optic cables could be damaged. The prototype device is equipped with a default circuit in the right limit switch for operation above the Arctic Circle. Since the sun could be visible for 24 h/day above the Arctic Circle, the collector

panels must be prevented from rotating beyond the fiber optic cables slack limit, while still being able to re-position on the sun for the next 24 h period. Therefore, when the right limit switch is contacted, the controller is interrupted and the azimuth drive actuator is commanded to rotate the collector panels to the left until the left limit switch is contacted.

The controller is interfaced with an emergency thermal switch to prevent the collector panels from overheating. When the thermal switch is opened, the az-el tracker defocuses the collector panels until the thermal switch closes.

4.4 SUMMARY

The prototype light collection and transmission device is designed to optimize the collection and transmission of photosynthetically active radiation while not sacrificing wavelengths contributing to photomorphogenic responses. Fresnel lenses, flexible fiber optic cables, and an az-el solar tracker are used to accomplish the design objective. The prototype device is intended for evaluating the concept of irradiating horticultural crops grown in an opaque, insulated structure with sunlight in northern regions.

5. EVALUATION PROCEDURE

The second phase of the research project was the evaluation of the prototype light collection and transmission device. The procedures required for evaluating the prototype device include the setup of the prototype device, selection of the instrumentation, and setup of the experiment. First, the prototype device was set up to maximize the radiant energy output, while preventing heat damage to the fiber optic cables. Secondly, the instruments were selected to measure the physical properties which influenced the performance of the prototype device. Thirdly, the experiment was set up to monitor the performance of the prototype device for various sky conditions.

5.1 PROTOTYPE DEVICE SETUP

The setup of the prototype device attempts to maximize the collection and transmission of photosynthetically active radiation, while still providing sufficient radiation for photomorphogenic responses. In addition, the setup prevents damage to the fiber optic cables from heat damage and movement. Three adjustments are required to properly align the prototype device with the sun and a fourth adjustment is required to limit the movement of the prototype device's collector panels. First, the fiber optic cables are aligned with the focal points of the fresnel lenses. Secondly, the shadow band sensor is aligned with the surfaces' of the fresnel lenses. Thirdly, the shadow band sensor is aligned with the sun

in the sky. The fourth adjustment involves setup of the limit switches located at the output shafts of the az-el drive train.

5.1.1 Alignment Of The Sets

An optical alignment is required between the fresnel lens and fiber optic cable sets to maximize the collection and transmission of radiant energy, benefit from the chromatic aberration phenomenon, and prevent heat damage to the A ends of the fiber optic cable. The optical alignment is accomplished by reversing the direction of light flow through each set and creating an image with an optical geometry resembling that existing between the fresnel lens and the sun in the sky. The optical alignment procedure was performed in a laboratory at the Alberta Telecommunications Research Center in Edmonton, Alberta.

The alignment procedure is described as follows: A module assembly is attached to a stand on an optical bench. The stand held a module assembly such that the surfaces' of the fresnel lenses in the module assembly are parallel with a wall 3.650 m away and the centers' of the fresnel lenses align with bulls-eyes on a horizontal target line marked on the wall. The bulls-eyes are centered on the target line and separated by 76.2 mm. As well, a 33.6 mm-diameter target circle is centered on each bulls-eye. The optical bench provided a level surface for precise alignment of the setup stand and module assembly with respect to the target line. The setup stand is levelled by adjusting four set screws at the base of the setup stand.

Next, the B end of a fiber optic cable is mounted in a three axis micro-positioning device attached to the optical bench. The micro-positioning device is used to hold and position the B end of the fiber optic cable near the focal point of a 4.5 mm focal length lens. A HeNe laser is mounted on the opposite side of the lens from the B end. The laser and lens combination are used for creating a divergent light beam to fill the numerical aperture of the fiber optic cable. The A end of the fiber optic cable is aimed at a photo-dector (Newport Corporation model 818-SL) which is connected to a power meter (Newport Corporation model 835). A 0.9 mm-diameter laser light beam with a wavelength of 632.8 nm is passed through the 4.5 mm focal length lens to produce a divergent light beam. The B end of the fiber optic cable is adjusted with respect to the focal point of the lens until the photodetector senses the maximum energy flux at the 632.8 nm wavelength.

Then, the A end of the fiber optic cable is attached to a connector assembly on the module. The divergent light beam emitted from the A end of the fiber optic cable passes through the fresnel lens and is collimated into a direct light beam. The direct light beam produces a spot on the wall marked with the target line. The set screws on the connector assembly are adjusted until the spot produced by the light beam is centered on the bulls-eye opposing the fresnel lens and the spot is the same diameter as the target circle. The geometry between the optical axis of the fresnel lens and the position and diameter of the direct light beam's spot on the target line replicates an angle of 0.53° (angle subtended by the sun). This

optical geometry replicates the angle subtended by the sun in the sky with respect to the optical axis of the fresnel lens. The fiber optic cable is assumed to be positioned at the focal point of the fresnel lens. The set screws on the connector assembly are locked in position and the B end of the fiber optic cable is removed from the micro-positioning device. This procedure is repeated for the remainder of the fresnel lens and fiber optic cable sets on a module assembly.

5.1.2 Alignment Of Fresnel Lenses To The Shadow Band Sensor

An alignment of the shadow band sensor to the surfaces' of the fresnel lenses is required to maximize the collection and transmission of radiant energy, benefit from the chromatic aberration phenomenon, and prevent heat damage to the A ends of the fiber optic cable. The alignment of the shadow band sensor in a parallel plane with the surfaces' of the fresnel lenses is accomplished in two steps. First, collector panel A is aligned with collector panel B and, secondly, the rib plate is aligned with the fresnel lenses such that the output from the fiber optic cables is maximized.

The collector panels are aligned with one another by adjusting the stub shaft connection of panel A to the az-el drive train until the light from the B ends of the fiber optic cable is uniform. This adjustment is delayed until after the prototype device is positioned on site. The shadow band sensor is then aligned with the surfaces' of the fresnel lenses by adjusting the position of the rib plate's mounting brackets. A quantum

sensor, connected to a radiometer, is positioned at the B ends of the fiber optic cable. Once the energy flux from the fiber optic cables is maximized, the shadow band sensor and fresnel lenses are assumed to be aligned. The adjustments are made on a clear, sunny day with the prototype device under manual operation.

5.1.3 Alignment Of Shadow Band Sensor To The Sun

The shadow band sensor and sun must be aligned to maximize the collection and transmission of solar energy, benefit from the chromatic aberration phenomenon, and prevent heat damage to the A ends of the fiber optic cable. The alignment is accomplished by adjusting potentiometers on the controller's circuit board and monitoring the radiant energy from the B end of the fiber optic cables with a quantum sensor connected to a radiometer. Once the radiant energy is maximized and the solar tracking is accurate and stable under a variety of sky conditions, the alignment is assumed to be complete. The alignment is performed according to the manufacturer's instructions when the prototype device is operating under both sunny, clear conditions and overcast conditions.

Seven potentiometers on the controller are used for adjusting the alignment of the shadow band sensor and the sun. The potentiometers are divided between the active and synthetic solar tracking modes. The commencement of synthetic tracking and night return modes is adjusted by the synthetic track adjustment. The time interval for synthetic tracking is adjusted by the base time adjustment. The length of time the azimuth

gearmotor is powered during synthetic tracking is adjusted with the movement time adjustment. The active solar tracking mode is divided between the azimuth and elevation axes which both contain window and balance adjustments. The window adjustment determines the amount of deadband between tracking commands, while the balance adjustment balances the ratio of solar energy to shadow received on the photocells on either side of a lobe. The potentiometers can be rotated up to five turns from the end of travel. The manufacturer recommends setting all the potentiometers two turns clockwise from the end of travel with the exception of the window potentiometers which are set one turn clockwise from the end of travel. The sensitivity is increased or the time interval is decreased on the controller by turning a potentiometer counter-clockwise.

The instructions provided by the manufacturer describing the location of the azimuth and elevation potentiometers are incorrect. This presented a problem during the initial adjustments for aligning the shadow band sensor and the sun. The instructions were corrected by interchanging the position identified for the azimuth and elevation potentiometers.

5.1.4 Limit Switch Setup

The prototype device possesses limit and thermal type emergency switches for preventing damage to the fiber optic cables during operation. However, only the limit switching circuit is used on the prototype device during testing. The azimuth limit switches are set up to allow the

collector panels to be rotated 180° from due East to due West, while facing the sun. The elevation limit switches are set up to allow a normal from the collector panels' surfaces to be rotated 90° from a horizontal to a vertical position. The motion of the collector panels is restricted to reduce the amount of slack in the fiber optic cables for movement of the collector panels and, thereby, allow the fiber optic cables to reach from the prototype device to the opaque, insulated structure.

5.2 INSTRUMENTATION

Instruments are required to measure direct solar radiation, photon flux, spectral photon flux, and temperature. In addition, a data aquisition system is used to record the measurements provided by the instruments. The instruments are selected to comply with ASAE (1989) Engineering Practices.

5.2.1 Photon Flux

The photon flux was measured inside the opaque, insulated structure. Photon flux measurements are made with a model LI 185 radiometer and model LI 190 quantum sensor (LI-COR Inc., Lincoln, NE, USA). A quantum sensor is used since the irradiation is intended for plant growth. The manufacturer states that the accuracy of the radiometer is ±1% over the full scale. The radiometer produces an analog output voltage signal between 0 to 100 mV corresponding to the photon flux in $\mu mol/s/m^2$ on the quantum sensor and the range setting on the radiometer. The analog output

signal was connected to a data aquisition system. Equation 5.1 is used to convert the output voltage signal (P) and the range setting (RS) to photon flux (PF). The range settings used on the radiometer during the testing are 30, 100, and 300 mV/mV.

$$PF = P\,(10^{RS}) \quad \ldots\ldots\ldots\ldots\ldots\ldots\ldots\ldots \quad (5.1)$$

5.2.2 Spectral Photon Flux

Spectral photon flux was measured outside beside the prototype device and inside the opaque, insulated structure. Spectral photon flux measurements were made with a portable spectroradiometer (LI COR model LI 1800). The spectroradiometer is calibrated for a wavelength range from 380 to 750 nm in 5 nm bandwidths. Five scans are automatically averaged for each spectral photon flux measurement. The spectral photon flux data was recorded in $\mu W/cm^2/nm$ according to the LI 1800 calibration file and a quantum conversion to $\mu mol/s/m^2/nm$ was made by the LI 1800 prior to downloading the data to an IBM Personal Computer. The spectroradiometer's readings from a clear, sunny day matched with spectral scans presented by Hart (1988).

5.2.3 Direct Solar Radiation

Direct solar radiation was measured outside near the prototype device. Direct solar radiation measurements are made with a pyrheliometer mounted on an equatorial solar tracker (Eppley models NIP and EQM). The pyrheliometer possesses a one second response time, 7.38×10^{-6} $V/W/m^2$

sensitivity, and ±0.5 percent accuracy. The measurement range of the pyrheliometer is 0 to 1400 W/m^2. The instrument is set up according to the manufacturer's instructions. The voltage output signal (S) in V from the pyrheliometer was increased with an amplifier to voltage (S') in V, according to Equation 5.2, in order to improve the readability of the signal by the data acquisition system. The direct solar radiation (D) in W/m^2 is calculated from Equation 5.3.

$$S' = 20.67 S + 72 \quad \ldots\ldots\ldots\ldots\ldots\ldots \quad (5.2)$$

$$D = S(7.38\times10^{-6})^{-1} \quad \ldots\ldots\ldots\ldots\ldots\ldots \quad (5.3)$$

5.2.4 Temperature

Air temperatures were measured inside and outside the opaque, insulated structure, as well as, inside a control type opaque, insulated structure. The thermistors (Fenwal Electronics Model UUB31J1, Milford, MA) were interfaced with the data aquisition system. A constant 1 mA current source on the data aquisition system was used to excite the thermistors. The resistance of the thermistor is calculated by dividing the voltage measurement by the 1 mA current source. Equations 5.4 and 5.5 were provided by the manufacturer to calculate the temperature T' in Kelvin and T in Celcius from a thermistor's resistance (R) in ohms.

$$T' = (2.0909905\times10^{-7}[\log(R)]^3 + 2.75851225\times10^{-4}[\log(R)] + 1.37958851\times10^{-3})^{-1} \quad (5.4)$$

$$T = T' - 273.16 \quad \ldots\ldots\ldots\ldots\ldots\ldots \quad (5.5)$$

5.2.5 Data Acquisition System

The data acquisition system consisted of a screw terminal connection board interfaced with a Dascon-1 analog/digital I/O expansion board (MetraByte Corporation, Taunton, MA, USA) which is installed in an IBM Personal Computer. An Advanced Basic computer program running on the microcomputer reads the four analog-to-digital channels on the screw terminal connection board, converts the voltages to meaningful units, and stores the data on a computer diskette. The radiometer's output signal is read from channel 1, the pyrheliometer's amplified output signal is read from channel 2, the thermistors are read from channels 3 and 4.

5.3 EXPERIMENTAL SETUP

The experiment was set up in order to evaluate the prototype device under sunny and clear, partly overcast, and overcast conditions. The direct solar radiation was measured to identify the amount of radiant energy available to the prototype device. The photon flux was measured in order to identify the quantity of photosynthetically active radiation provided by the prototype device. Correlation of the direct solar radiation and the photon flux provided an estimate of the performance of the prototype device. The air temperatures were measured to indicate whether the radiant energy from the prototype device contained a significant proportion of infra-red radiation. The spectral photon flux was measured to identify the quality of the irradiation provided by the prototype device and the efficiency of the prototype device.

5.3.1 Location Of Testing

The prototype device was located on the roof of the Agriculture Forestry Center at the University of Alberta Campus, Edmonton, Alberta. The prototype device, as displayed in Plates 5.1 and 5.2, was mounted outside on a 2 m-high platform with an exposure from due East to due West. The fiber optic cables from the prototype device were run through an access hole into an opaque, insulated structure located in the greenhouse complex on the roof.

5.3.2 Opaque, Insulated Structure

The opaque, insulated structure consisted of an Environator growth cabinet. The inside dimensions of the growth cabinet were 68 cm by 58 cm by 61 cm. The inside surfaces of the growth cabinet were a white enamel with the exception of the rear vertical surface which was stainless steel. The outside of the growth cabinet was painted white. The growth cabinet was modified with an access hole to allow the fiber optic cables to be run through the top of the cabinet. Access ports on the side of the cabinet were used for routing cables from the quantum sensor, thermistor, and spectroradiometer. The growth cabinet was located inside a greenhouse on a bench in the southwest corner of the greenhouse. A ventilation inlet was located underneath the bench. A second, similar growth cabinet was located next to the growth cabinet containing the fiber optic cables. The second growth cabinet was used as a control for temperature measurements.

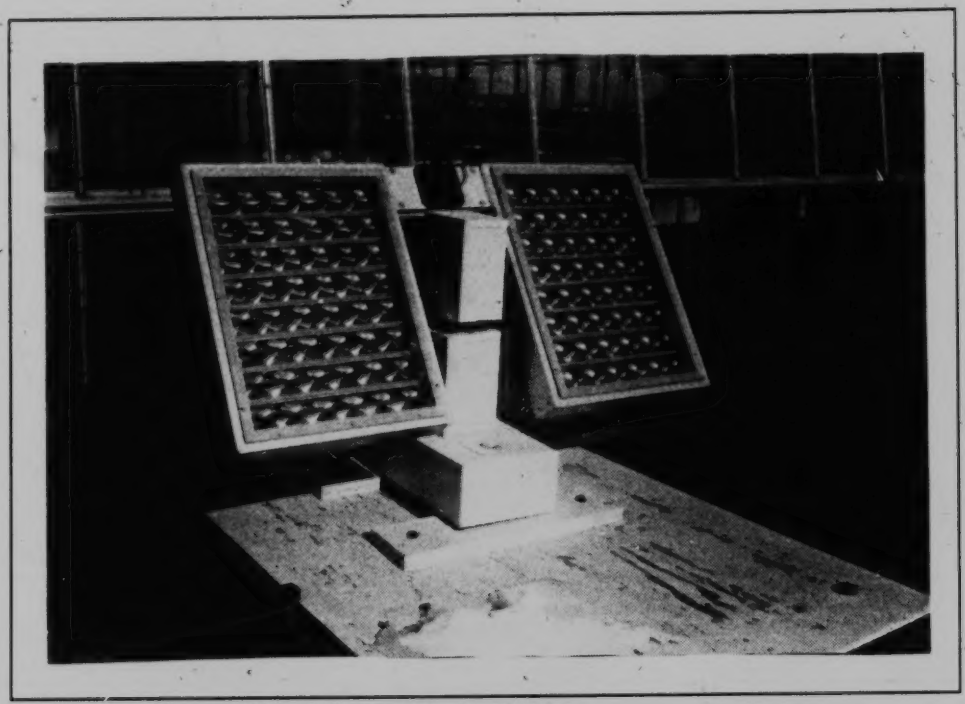

Plate 5.1 Front View Of Prototype Device

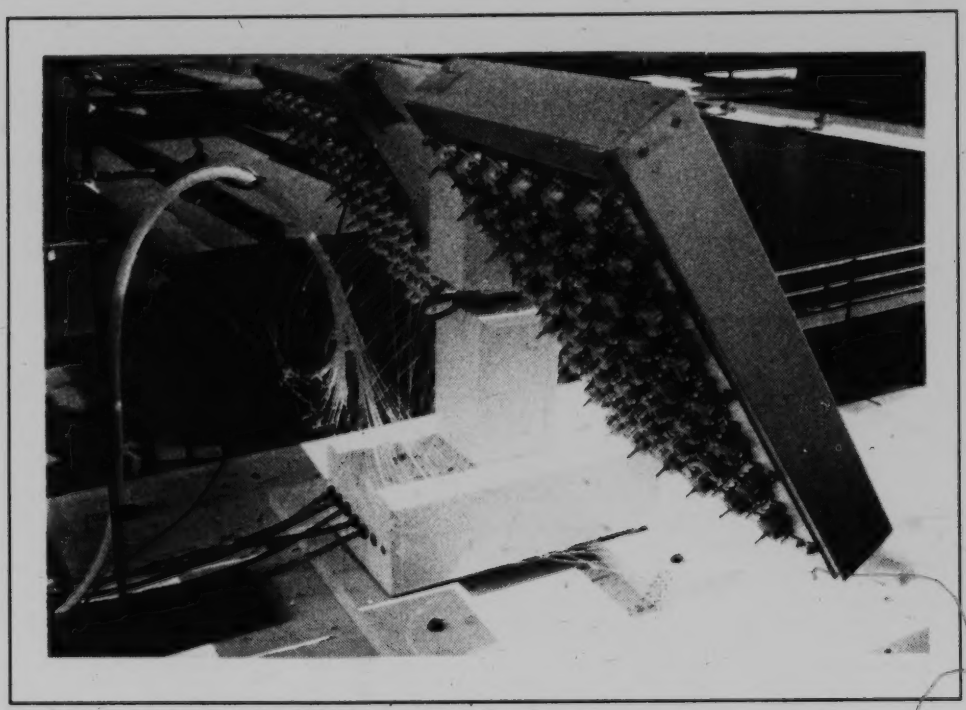

Plate 5.2 Back View Of Prototype Device

5.3.3 Orientation Of The Fiber Optic Cables

The B ends of the fiber optic cable are attached to a panel in the Environator growth cabinet, as displayed in Plate 5.3. The panel resembles a pegboard with 1.2 mm-diameter holes spaced 35 mm apart. The fiber optic cables are positioned in the panel's holes such that the B ends of the fiber optic cable extend below the panel and face the bottom of the growth cabinet. The fiber optic cables are oriented in a rectangular pattern of 8 fibers by 12 fibers.

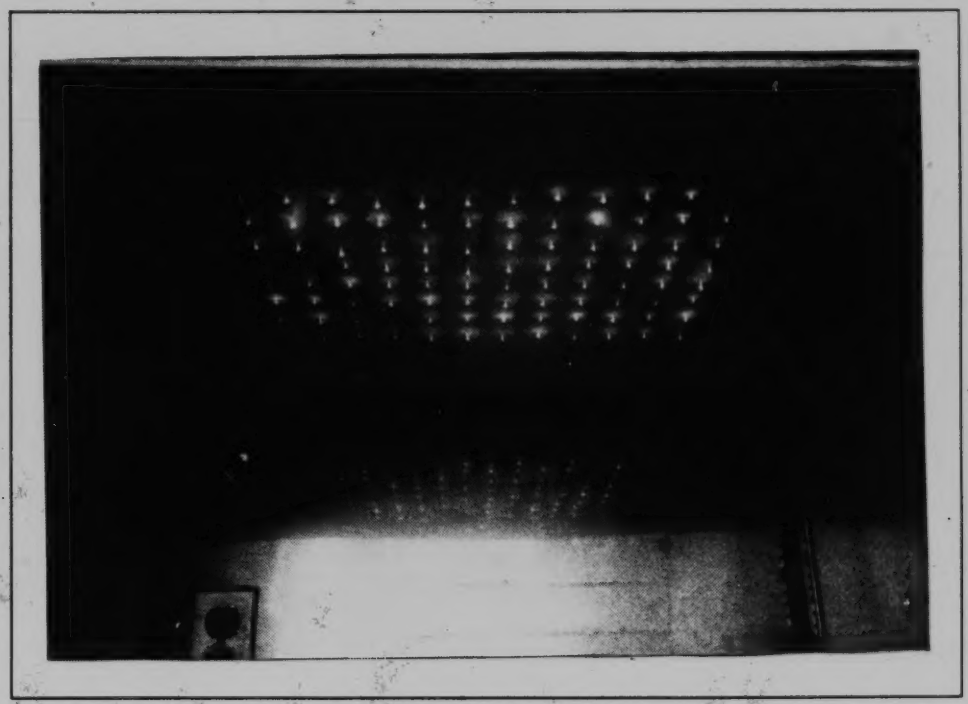

Plate 5.3 Orientation Of Fiber Optic Cables

5.3.4 Orientation Of Instruments

Plate 5.4 shows the quantum sensor, spectroradiometer, and a thermistor inside the growth cabinet. During testing, the quantum sensor was located at the center, bottom of the growth cabinet. The quantum sensor was 40 cm from the B ends of the fiber optic cable when placed at the bottom of the cabinet. The spectroradiometer's photodetector was located at the bottom, center of the growth cabinet 30 cm from the B ends of the fiber optic cable. The thermistor inside the growth cabinet was hung in the upper, left corner of the growth cabinet. Communication cables from the instruments inside the growth cabinet were run through the access port to the data aquisition system. A second thermistor was located outside the growth cabinet on top of the bench in order to measure the ambient temperature within the greenhouse near the growth cabinet. The pyrheliometer displayed in Plate 5.5 is located outdoors near the platform on which the prototype device was situated. The pyrheliometer was adjusted daily to account for the changes in the sun's declination angle. The second Environator growth cabinet, used as a control for temperature measurements, was located next to the growth cabinet with the fiber optic cables.

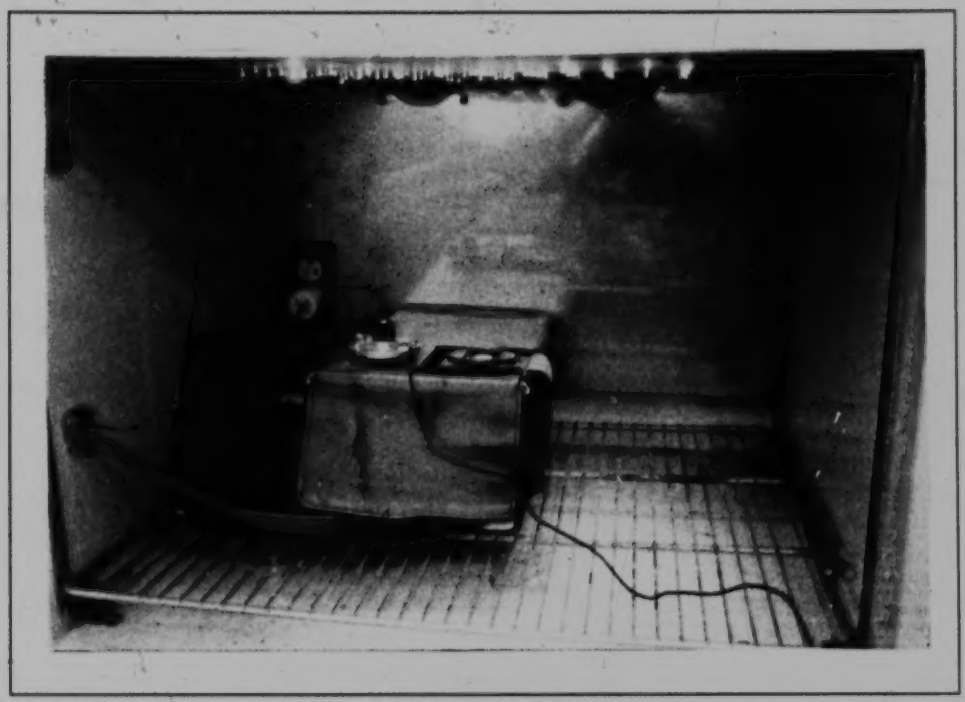

Plate 5.4 Instruments Inside Growth Cabinet

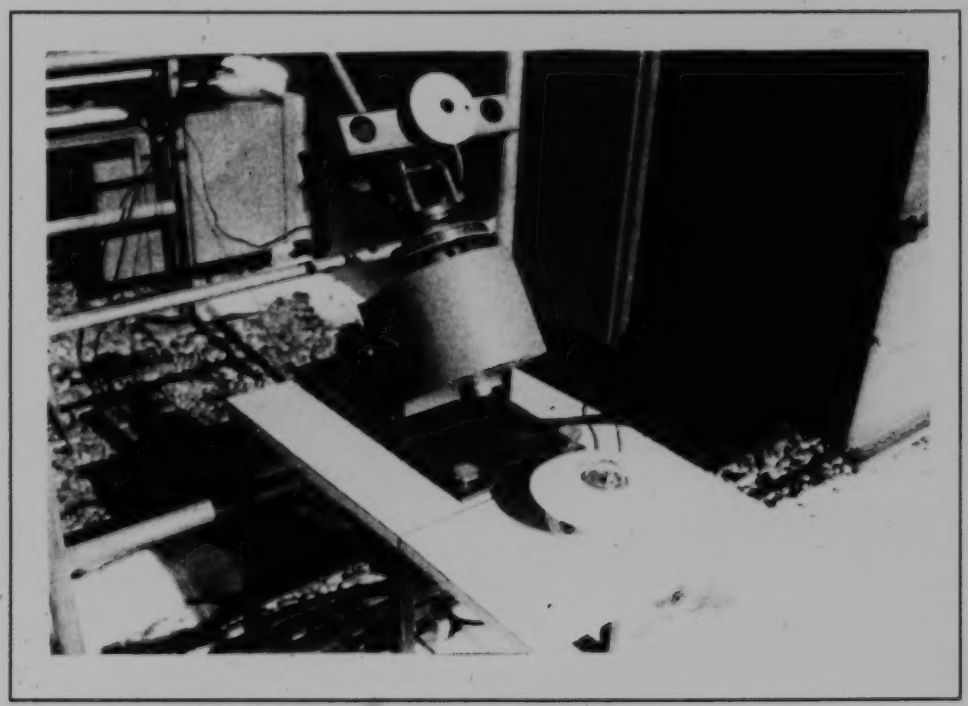

Plate 5.5 Pyrheliometer

5.3.5 Measurement Technique

The direct solar radiation, photon flux, and temperatures were sampled at three second intervals and averaged after five samples. The averaged readings were recorded along with the time. The three second sampling rate was selected to adequately monitor changes in the physical variables, while still providing a manageable amount of data for analysis.

6. TESTING AND RESULTS

The prototype light collection and transmission device was set up for testing on two occasions. The first occasion was in the Fall of 1989, while the second occasion was in the Winter of 1990. The prototype device was operated for three days during the Fall testing and eight days during the Winter testing. The Fall testing involved operation of the prototype device under predominantly clear sky conditions, while the Winter testing involved operation of the prototype device under clear and sunny, partly overcast, and overcast sky conditions. On both occasions, the prototype device was located on the roof of the Agriculture Forestry Centre at the University of Alberta. The direct solar radiation to the prototype device, the photon flux inside the growth cabinet, and the temperature inside the growth cabinet were measured during operation of the prototype device. In addition, the ambient temperature outside the growth cabinet was measured on five dates in order to determine whether the ambient temperature in the greenhouse was influencing the temperature inside the growth cabinet. Similarly, the temperature inside the control cabinet was measured on two dates in order to determine whether the radiant energy emitted from the fiber optic cables was influencing the temperature inside the growth cabinet. As well, the operating time for the elevation and azimuth gearmotors was recorded on two dates. Lastly, spectral photon flux was measured near the prototype device and inside the growth cabinet on three dates. The quantum sensor was located at the center of the growth cabinet near the bottom, unless otherwise stated. Similarly, the spectroradiometer was placed on the bottom of the growth cabinet, such that the sensor was

located under the center of the panel holding the fiber optic cables. Table 6.1 summarizes the dates, times, sky conditions, and measurements taken during the prototype device's testing.

Table 6.1 Summary Of Testing On The Prototype Device

Date	Start Time	End Time	Sky Condition	* Measurement (Yes/No) 1	2	3	4	5	6	7
89/11/29	1011h	1420h	Clear	Y	Y	Y	N	N	N	Y
89/12/03	1142h	1645h	Clear	Y	Y	Y	Y	N	N	N
89/12/04	1051h	1657h	Clear	Y	Y	Y	Y	N	N	N
90/02/28	1120h	1642h	Overcast	Y	Y	Y	Y	N	N	N
90/03/01	0937h	1649h	Varied	Y	Y	Y	Y	N	N	N
90/03/02	0939h	1611h	Varied	Y	Y	Y	Y	N	Y	N
90/03/13	0945h	1600h	Clear	Y	Y	Y	N	N	N	Y
90/03/14	1036h	1635h	Clear	Y	Y	Y	N	Y	N	N
90/03/15	0912h	1630h	Clear	Y	Y	Y	N	Y	Y	N
90/03/16	0950h	1500h	Overcast	Y	Y	Y	N	N	N	N
90/03/21	1010h	1330h	Varied	Y	Y	Y	N	N	N	Y

* 1 Direct Solar Radiation Outside
2 Photon Flux Inside Growth Cabinet
3 Air Temperature Inside Growth Cabinet
4 Air Temperature Outside Growth Cabinet
5 Air Temperature Inside Control Cabinet
6 Operating Time On Gearmotors
7 Spectral Photon Flux Measurements

6.1 FALL 1989 TESTING

The prototype light collection and transmission device was operated on three days between November 28, 1989 and December 4, 1989. The sky conditions were predominantly clear with cloud on the horizon. The prototype device operated as designed and the fiber optic cables did not suffer any observable damage. Overall, the Fall testing did not provide

adequate information on the performance of the prototype device, since most of the operating time was devoted to improving the solar tracking accuracy.

6.1.1 November 29, 1989

The first day of operation for the prototype light collection and transmission device was November 29, 1989. Generally, the sky conditions throughout the day were clear and sunny with cloud present on the horizon. The alignment of the fresnel lenses to the shadow band sensor was completed the previous day. The first three hours of the test were devoted to adjusting the alignment of the shadow band sensor to the sun. The direct solar radiation, photon flux, temperature inside the growth cabinet, and spectral photon flux were measured. The test began at 1011h and was interrupted on three occasions prior to ending at 1420h. Measurements were recorded for a total of 3.56 h. The first and second interruptions were to determine why the direct solar radiation being recorded would jump from 0 to 700 W/m^2, even though, the sky conditions were not changing. Figure 6.1a displays the direct solar radiation measurements. The test was interrupted at 1123h in order to check the data aquisition hookup and program. However, no faults were found and the test was resumed at 1131h. The direct solar radiation measurements did not stabilize and the test was interrupted again at 1149h to continue troubleshooting. The amplifier used to condition the pyrheliometer's output signal was identified to be the cause of the erratic direct solar radiation measurements. Unfortunately, the amplifier could not be replaced

immediately, so the test was resumed at 1159h. The test was interrupted for a third time at 1330h in order to perform spectral photon flux measurements inside the growth cabinet. The test was resumed again at 1351h. The photon flux displayed in Figure 6.1b varied from 0 to 80 $\mu mol/s/m^2$. The controller was adjusted between 1010h and 1300h to align the shadow band sensor with the sun. The photon flux dropped to nearly zero inside the growth cabinet between 1155h and 1225h when the sun's rays were obstructed by the Student's Union Building. The photon flux ranged from 0 to 40 $\mu mol/s/m^2$ between 1351h and 1420h. Figure 6.1c displays the temperature measurements inside the growth cabinet. The inital rise in the temperature at 1011h was the result of replacing the thermistor inside the growth cabinet with another thermistor. The temperature measurements between 1351h and 1420h were likely influenced by opening the growth cabinet. The air temperature increased 3°C inside the growth cabinet during the test. Overall, the day was devoted to setting up and becoming familiar with the prototype device. Figure 6.2a displays the spectral photon flux measurement made near the prototype at 1356h with the spectral photon flux measurements made inside the growth cabinet at 1342h, 1345h, and 1348h. Figure 6.2b displays the spectral photon flux measurements from inside the growth cabinet at 1342h, 1345h, and 1348h, as well as, at 1608h when the sun was setting. The scans inside the growth cabinet differ, since the solar tracker was not maintaining an accurate alignment of the collector panels with the sun. The spectral photon flux distribution was continuous and possessed a higher proportion of red wavelengths (700 nm) than blue wavelengths (400 nm).

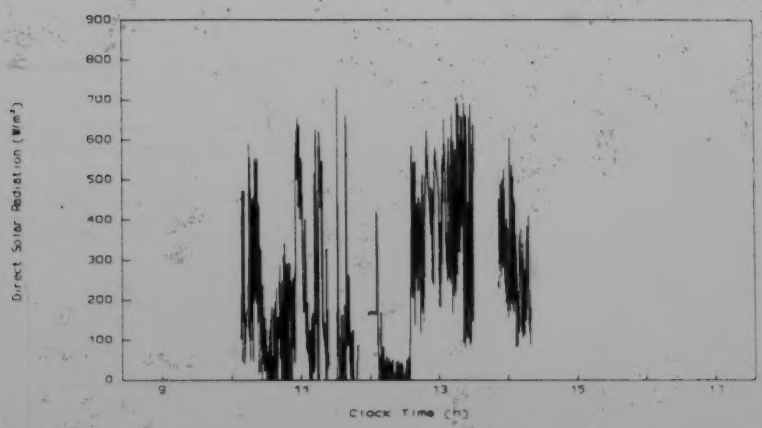

Figure 6.1a Direct Solar Radiation (1989-11-29)

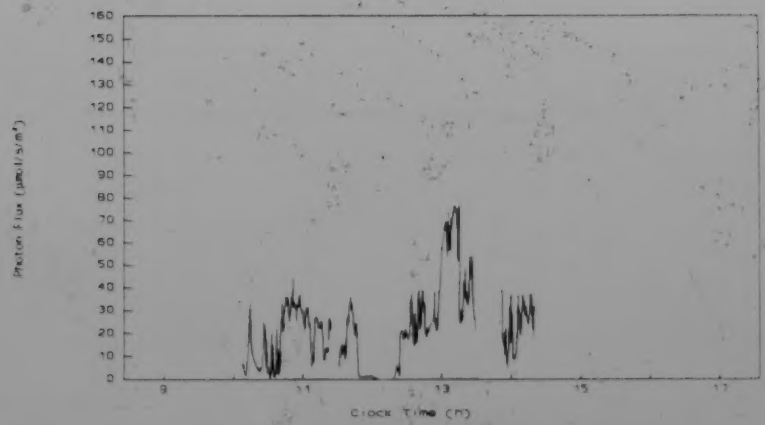

Figure 6.1b Photon Flux Inside Cabinet (1989-11-29)

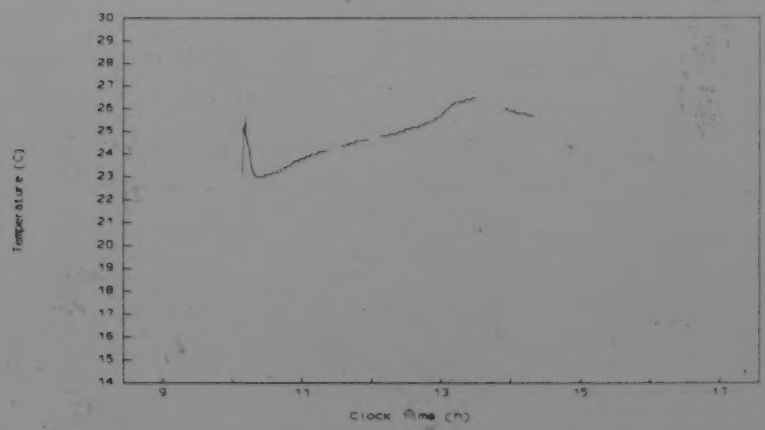

Figure 6.1c Temperature Inside Cabinet (1989-11-29)

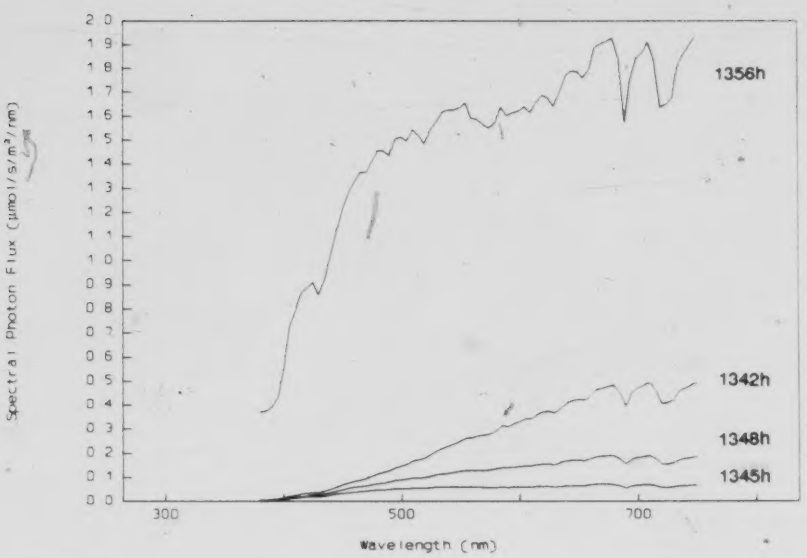

Figure 6.2a Spectral Photon Flux (1989-11-29)

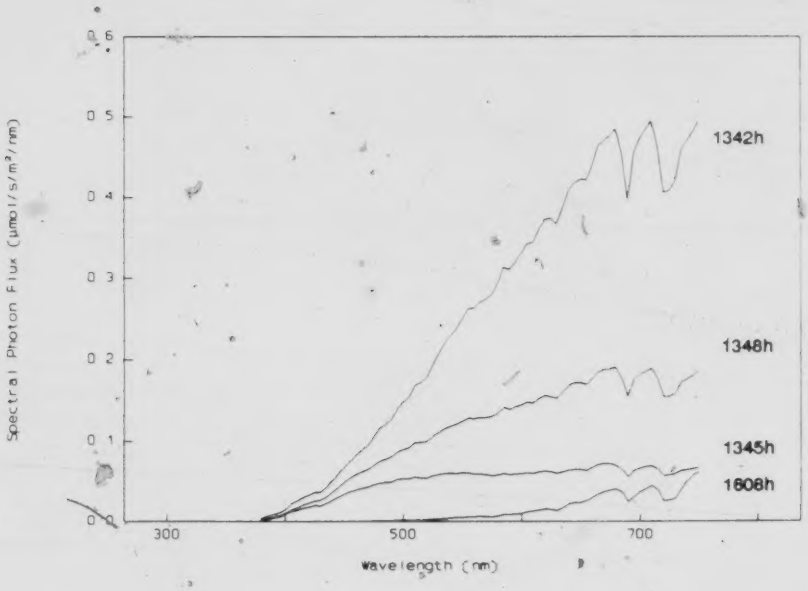

Figure 6.2b Spectral Photon Flux With Greater Resolution (1989-11-29)

6.1.2 December 3, 1989

On December 3, 1989, the sky conditions changed from overcast to clear and sunny with cloud on the horizon. The direct solar radiation, photon flux, temperature inside the growth cabinet, and temperature outside the growth cabinet were measured. The test run began at 1142h and ended at 1645h. The amplifier used to condition the pyroheliometer's output signal on November 29, 1989 was replaced with another amplifier available in the Department of Agricultural Engineering. The direct solar radiation measurements displayed in Figure 6.3a responded as expected to changes in the sky conditions. The controller was adjusted from 1300h to 1520h in order to align the shadow band sensor to the sun. As a result, the photon flux displayed in Figure 6.3b varied from 0 to 80 $\mu mol/s/m^2$. Figure 6.3c indicates that the temperature inside the growth cabinet ranged between 22°C and 23°C during the test, while the temperature outside the growth cabinet ranged between 14°C and 25°C during the test. The temperature variation outside the growth cabinet was due to ventilation air entering the greenhouse through a ventilation inlet under the bench on which the growth cabinet was located. When the ventilation system was not operating, the ambient temperature around the growth cabinet increased due to solar heat gain in the greenhouse. Overall, the day was devoted to improving the prototype device's solar tracking accuracy.

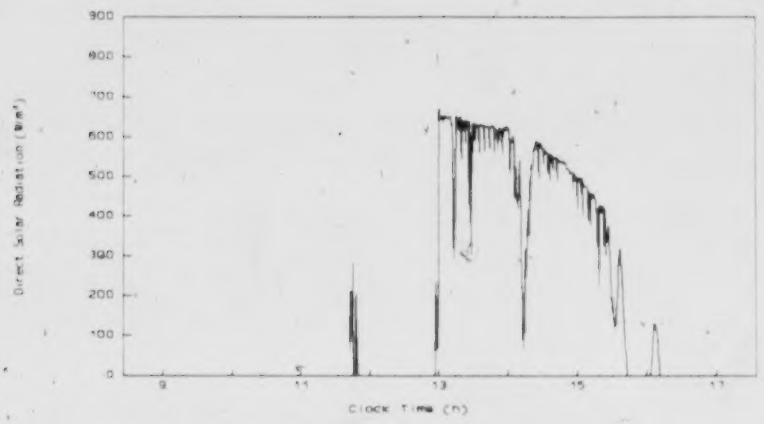

Figure 6.3a Direct Solar Radiation (1989-12-03)

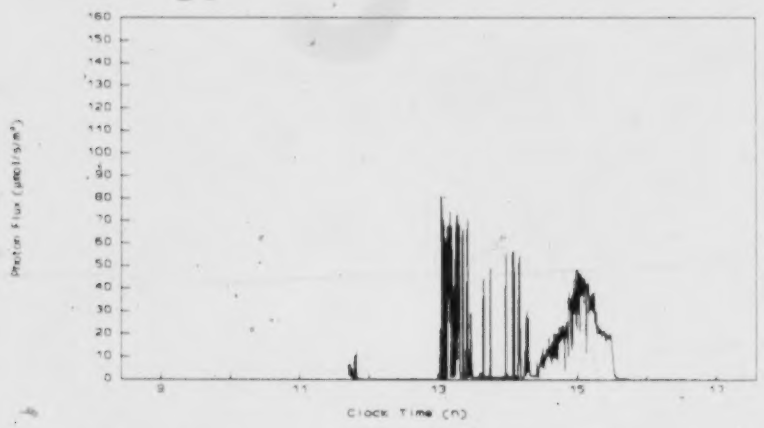

Figure 6.3b Photon Flux Inside Cabinet (1989-12-03)

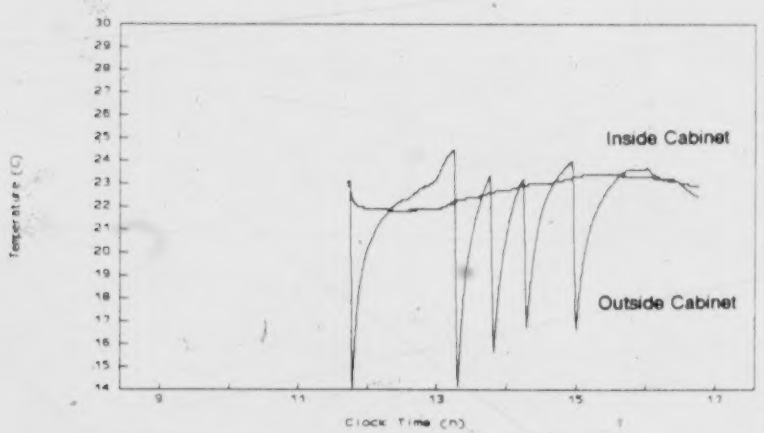

Figure 6.3c Temperature Inside And Outside Cabinet (1989-12-03)

6.1.3 December 4, 1989

On December 4, 1989, the sky conditions were generally clear and sunny with cloud present on the horizon. The direct solar radiation, photon flux, temperature inside the growth cabinet, and temperature outside the growth cabinet were measured. The test run began at 1051h and ended at 1657h. Figure 6.4a shows the direct solar radiation measured near the prototype device. The photon flux measurements shown in Figure 6.4b were essentially zero until 1430h. The prototype device's controller was adjusted from 1330h to 1445h in order to align the shadow band sensor to the sun. The temperature measurements displayed in Figure 6.4c indicate that the temperature inside the growth cabinet ranged between 22°C and 25°C, while the ambient temperature outside the the growth cabinet ranged between 14°C and 24°C. Ventilation air entering the greenhouse caused the ambient temperature around the growth cabinet to drop, while solar heat gain in the greenhouse caused the ambient temperature around the growth cabinet to rise. Overall, the day was devoted to improving the prototype device's solar tracking accuracy with little success.

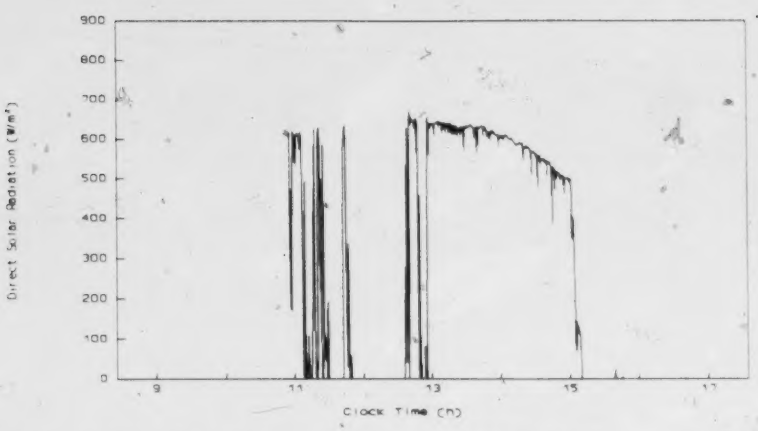

Figure 6.4a Direct Solar Radiation (1989-12-04)

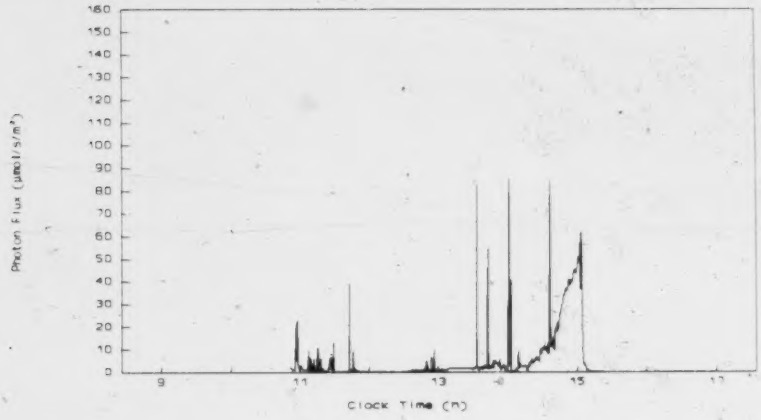

Figure 6.4b Photon Flux Inside Cabinet (1989-12-04)

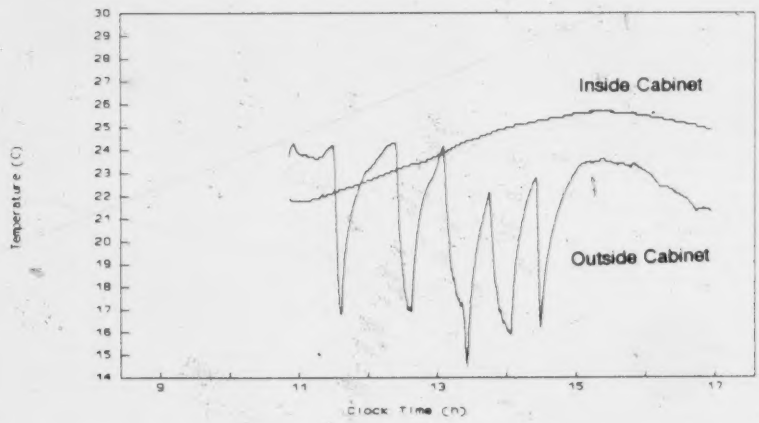

Figure 6.4c Temperature Inside And Outside Cabinet (1989-12-04)

6.2 WINTER 1990 TESTING

The second testing session for the prototype light collection and transmission device occurred between February 28, 1990 and March 21, 1990. The sky conditions during the testing period included clear and sunny, partly overcast, and overcast. The prototype device was operated for eight days during the second testing period. The primary objective was to improve the solar tracking accuracy of the prototype device. The prototype device withstood strong winds and cold temperatures with no apparent damage to the fiber optic cables.

6.2.1 February 28, 1990

February 28, 1990 was the first day that the prototype device was operated during the Winter testing session. The day was devoted to adjusting the alignment of the shadow band sensor to the sun. Direct solar radiation, photon flux, temperature inside the growth cabinet, and temperature outside the growth cabinet were measured. The alignment of the shadow band sensor and the fresnel lenses was completed prior to the start of testing at 1120h. Figure 6.5a shows the direct solar radiation measured throughout the test. The prototype device's controller was adjusted from 1135h to 1140h in order to align the shadow band sensor with the sun. The solar tracking improved as indicated by the photon flux measurements displayed in Figure 6.5b. However, at 1230h overcast sky conditions prevented any further assessment of the prototype device's solar tracking capabilities. Figure 6.5c indicates that the temperature inside the growth

cabinet rose from 21°C to 23°C, while the ambient temperature outside the growth cabinet ranged between 19°C and 23°C. Again, the incoming ventilation air influenced the temperature measurements outside the growth cabinet. The test was stopped at 1642h, since overcast conditions persisted.

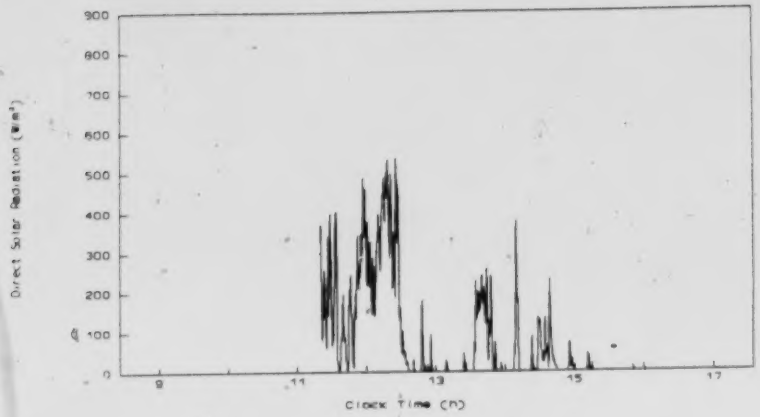

Figure 6.5a Direct Solar Radiation (1990-02-28)

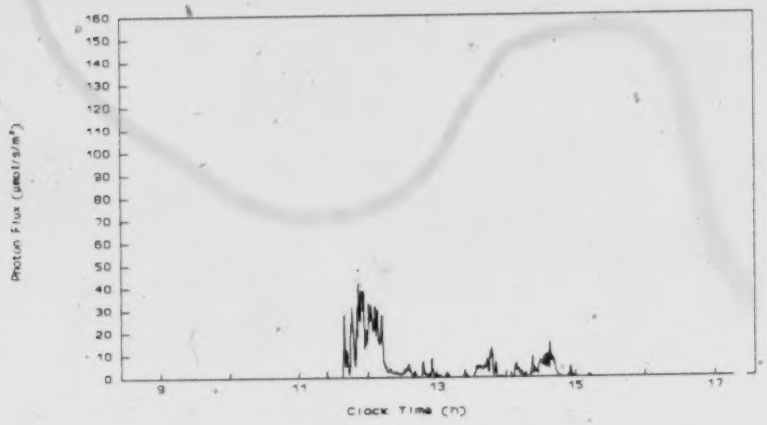

Figure 6.5b Photon Flux Inside Cabinet (1990-02-28)

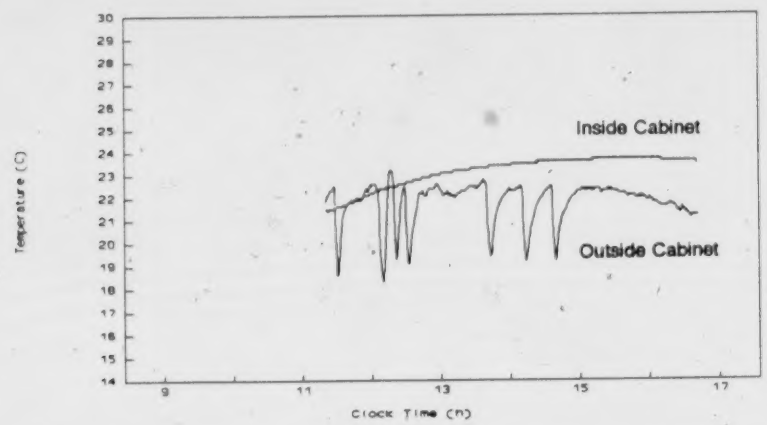

Figure 6.5c Temperature Inside And Outside Cabinet (1990-02-28)

6.2.2 March 1, 1990

On March 1, 1990, the sky conditions varied between sunny and clear to partly cloudy. The direct solar radiation, photon flux, temperature inside the growth cabinet, and temperature outside the growth cabinet were measured. The test run began at 0937h and was interrupted on two occasions prior to ending at 1649h. Measurements were recorded for a total of 4.16 h. Figures 6.6a and 6.6b display the direct solar radiation and the photon flux measurements, respectively. The first interruption occurred at 1215h when the microcomputer hung up and stopped recording data. The test run was resumed at 1245h, but, was interrupted a second time at 1307h. The test was interrupted in order to examine the controller's circuit board and potentiometers. The shadow band sensor was continually leading the sun and a fault with the controller was suspected. No faults were found with either the circuit board or the potentiometers and the test run was resumed at 1538h. The solar tracking was eventually improved by adjusting the controller's azimuth potentiometers. Figure 6.6c displays the temperature measurements throughout the test. As with prior temperature measurements, the ventilation air entering the greenhouse influenced the ambient temperature around the growth cabinet. The test was completed at 1649h. Overall, the day was devoted to improving the prototype device's solar tracking accuracy.

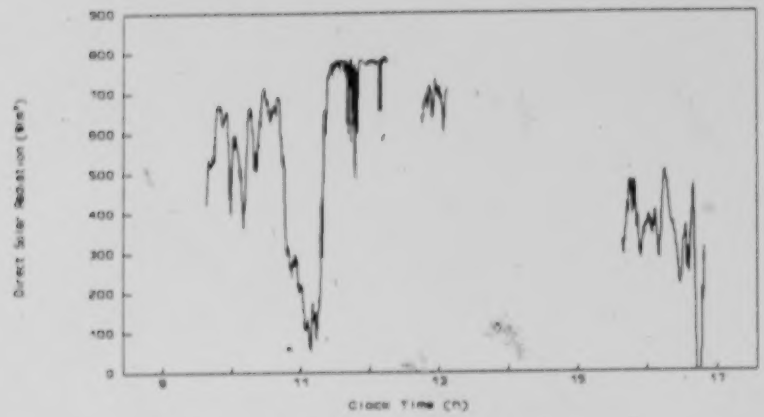

Figure 6.6a Direct Solar Radiation (1990-03-01)

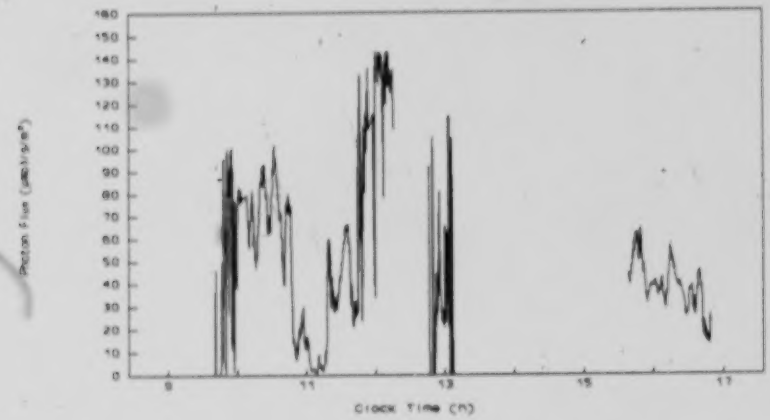

Figure 6.6b Photon Flux Inside Cabinet (1990-03-01)

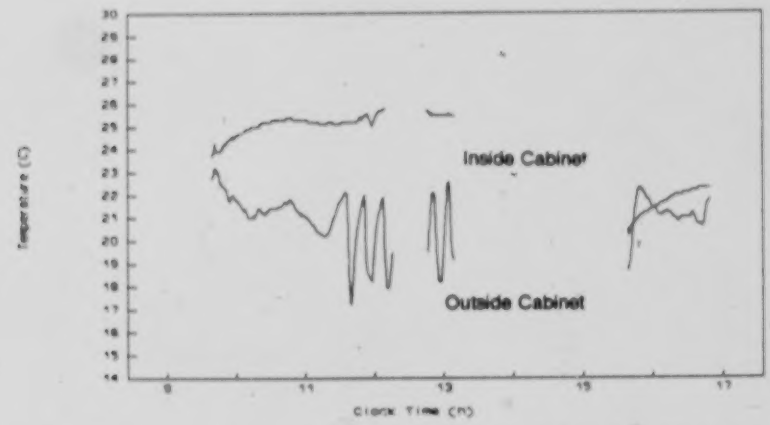

Figure 6.6c Temperature Inside And Outside Cabinet (1990-03-01)

6.2.3 March 2, 1990

On March 2, 1990, the prototype device was operated without any interruptions or adjustments for the entire day. The sky conditions varied from sunny and clear to partly overcast to overcast. Direct solar radiation, photon flux, temperature inside the growth cabinet, temperature outside the growth cabinet, and operating time on the gearmotors were measured. The test run began at 0939h and finished at 1611h. Figure 6.7a displays the direct solar radiation measured, while Figure 6.7b displays the photon flux measured. In general, the photon flux corresponded to changes in the direct solar radiation. Figure 6.7c indicates that the temperature inside the cabinet rose from 21°C to 24°C, while the ambient temperature outside the growth cabinet rose from 18°C to 21°C. In addition, the ambient temperature outside the growth cabinet fluctuated between 16°C and 21°C due to the incoming cooler ventilation air and solar heat gain in the greenhouse. The hour meters indicated that the elevation gearmotor operated for 58 s, while the azimuth gearmotor operated for 8 min, 38 s during the 6.51 h test run. Overall, March 2, 1990 was a day for evaluating the prototype device under a variety of sky conditions.

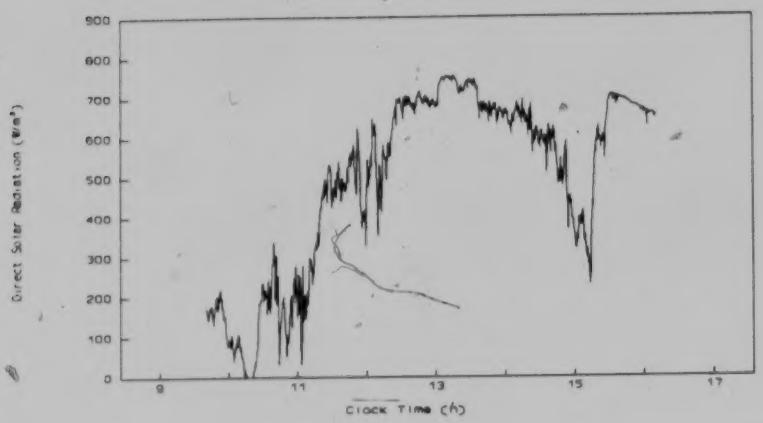

Figure 6.7a Direct Solar Radiation (1990-03-02)

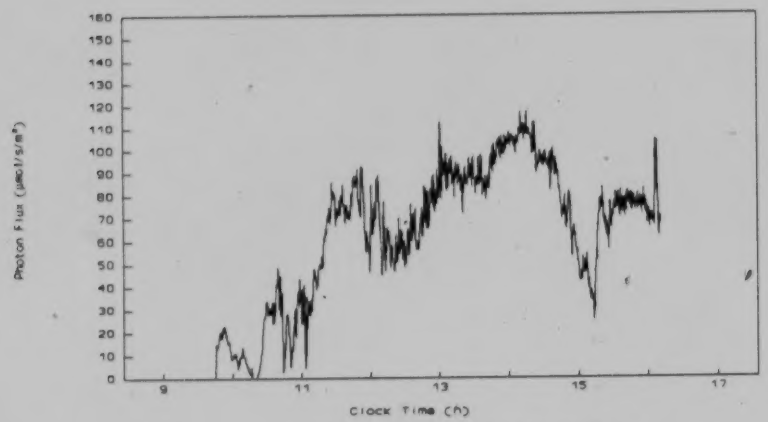

Figure 6.7b Photon Flux Inside Cabinet (1990-03-02)

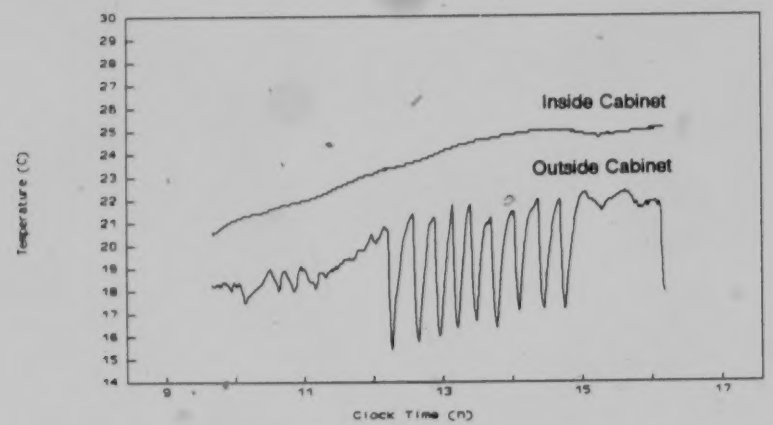

Figure 6.7c Temperature Inside And Outside Cabinet (1990-03-02)

6.2.4 March 13, 1990

March 13, 1990 was a clear, sunny day as indicated by the direct solar radiation measurements in Figure 6.8a. In addition, photon flux, temperature inside the growth cabinet, and spectral photon flux were measured. Following the test run, the photon flux at nine different locations near the bottom of the growth cabinet were measured. The test run began at 0945h and finished at 1600h. The prototype device was not checked after startup until 1050h, at which time, the photon flux, as displayed in Figure 6.8b, was under 10 $\mu mol/s/m^2$. The door to the growth cabinet was opened in order to ensure the quantum sensor was correctly positioned. Further examination indicated that the low photon flux was caused by the shadow band sensor leading the sun. Opening the door on the growth cabinet allowed a flood of light and warm air to create spikes in both the photon flux and temperature at 1050h. Figure 6.8c displays the temperature measurements. The controller was adjusted from 1052h to 1100h in order to improve the solar tracking accuracy. Two additional adjustments to the controller were made at 1300h and 1545h. Overall, March 13, 1990 was a day for evaluating the prototype device under clear and sunny sky conditions. Figure 6.9a displays the spectral photon flux measurements made near the prototype device at 1551h and inside the growth cabinet at 1604h. Figure 6.9b displays the spectral photon flux measurement at 1604h with greater resolution. The spectral distribution of the photon flux was continuous and possessed a higher proportion of red wavelengths (700 nm) than blue wavelengths (400 nm).

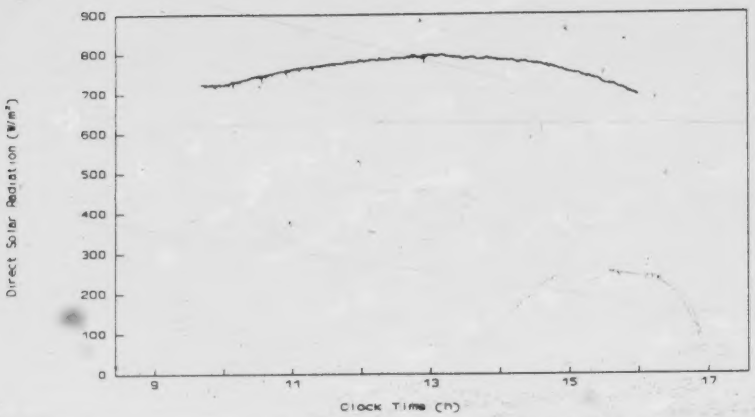

Figure 6.8a Direct Solar Radiation (1990-03-13)

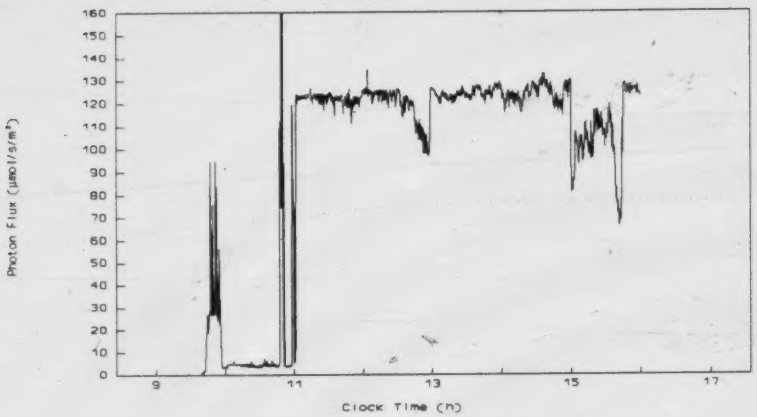

Figure 6.8b Photon Flux Inside Cabinet (1990-03-13)

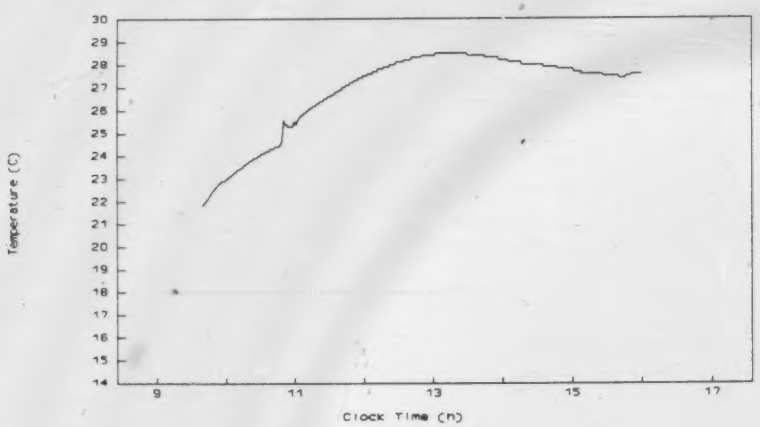

Figure 6.8c Temperature Inside Cabinet (1990-03-13)

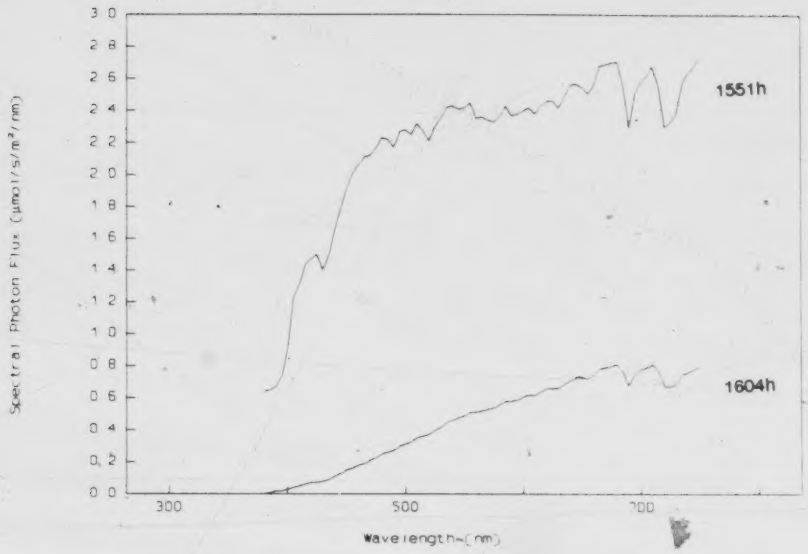

Figure 6.9a Spectral Photon Flux (1990-03-13)

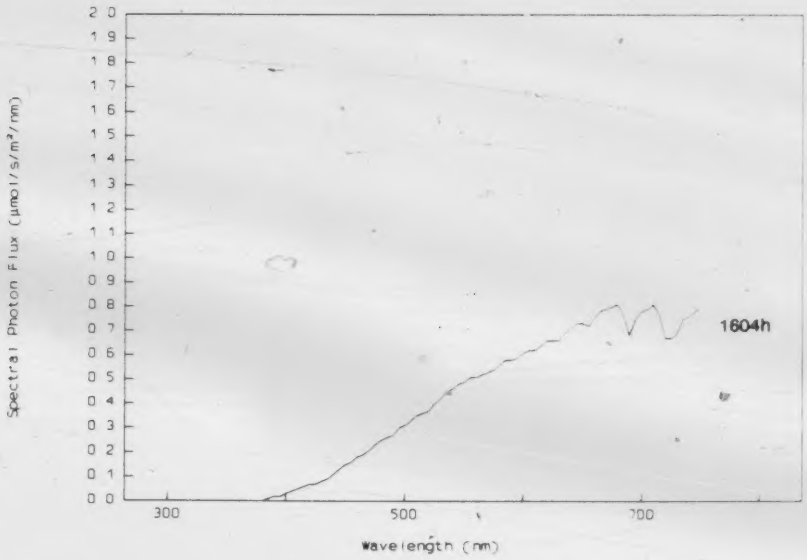

Figure 6.9b Spectral Photon Flux With Greater Resolution (1990-03-13)

Table 6.2 outlines the average photon flux measured at nine locations near the bottom of the growth cabinet (Figure 6.10) along with the average direct solar radiation measured outside. The photon flux was recorded for a two minute interval at each location and averaged. The photon flux was lowest in the corners and greatest at the center of the cabinet. The photon flux ranged from 21.8 to 87.2 $\mu mol/s/m^2$.

Table 6.2 Photon Flux Near Bottom Of Growth Cabinet

Location Of Quantum Sensor	Clock Time	Photon Flux Ave. *(a)	Photon Flux S.D. *(a)	Direct Radation Ave. **(b)	Direct Radation S.D. **(b)
1 15 cm Left Of Center	1618h	70.8	3.6	666	1
2 15 cm Right Of Center	1621h	84.0	1.1	661	1
3 15 cm Front Of Center	1624h	57.0	1.0	655	1
4 15 cm Back Of Center	1627h	46.6	1.1	649	1
5 Back Left Corner	1630h	21.8	1.7	644	2
6 Back Right Corner	1633h	39.1	6.0	639	1
7 Front Right Corner	1636h	32.1	1.9	633	1
8 Front Left Corner	1639h	30.4	3.1	625	2
9 Center	1641h	87.2	2.4	619	2

* a $\mu mol/s/m^2$ ** b W/m^2

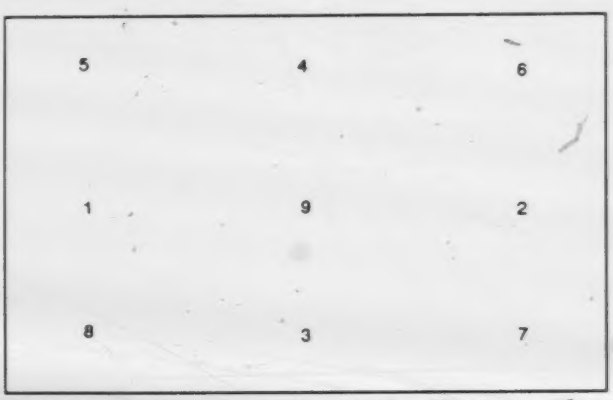

Figure 6.10 Location Of Photon Flux Measurements

6.2.5 March 14, 1990

March 14, 1990 was a clear, sunny day as indicated by the direct solar radiation measurements in Figure 6.11a. In addition, photon flux, temperature inside the growth cabinet, and temperature inside the control cabinet were measured. The test run began at 1036h and ended at 1635h. The dips in the photon flux measurements displayed in Figure 6.11b were caused by a misadjustment of the controller or a wind load disturbing the collector panels. The dips in the photon flux at 1140h, 1200h to 1240h, and 1320h to 1340h were representative of wind load disturbances, since the solar tracking accuracy improved without any adjustments to the controller. The controller was adjusted at 1100h and 1630h in order to improve the solar tracking accuracy. The decrease in the photon flux at 1420h was likely related to a misadjustment of the controller, since the photon flux remained below 30 $\mu mol/s/m^2$ until 1630h. Figure 6.11c indicates that the temperatures inside the growth cabinet and control cabinet differed by 2°C at the start of the test and by 0.5°C at the end of the test. The temperatures in the two cabinets also rose at different rates when the test began, but converged by 1300h. The radiant energy emitted from the fiber optic cables does not appear to influence the temperature within the growth cabinet. Overall, March 14, 1990 was a day for evaluating the prototype device under clear, sunny sky condition.

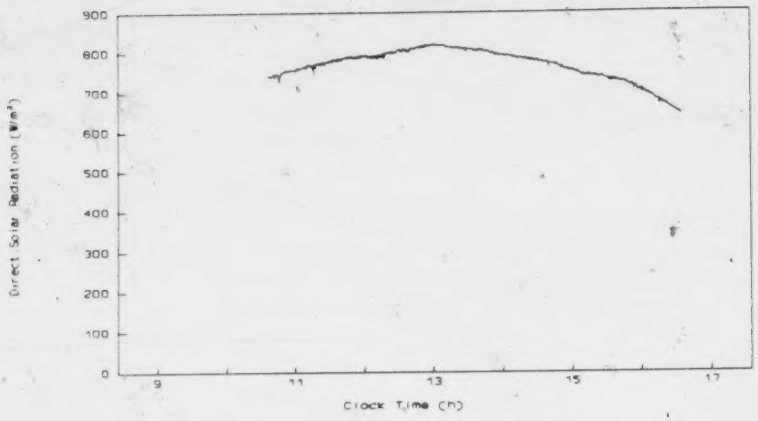

Figure 6.11a Direct Solar Radiation (1990-03-14)

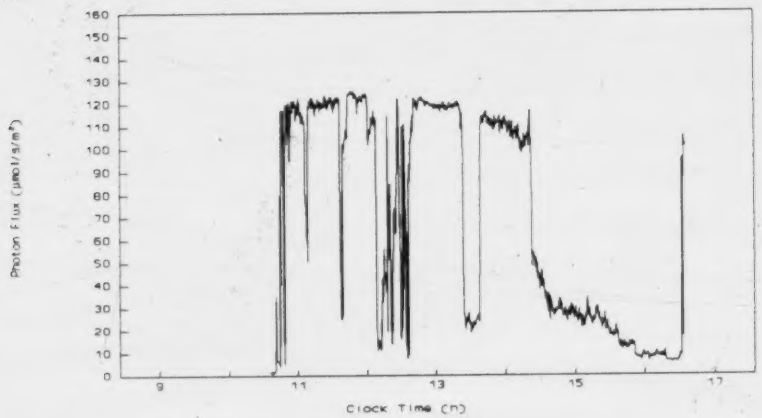

Figure 6.11b Photon Flux Inside Cabinet (1990-03-14)

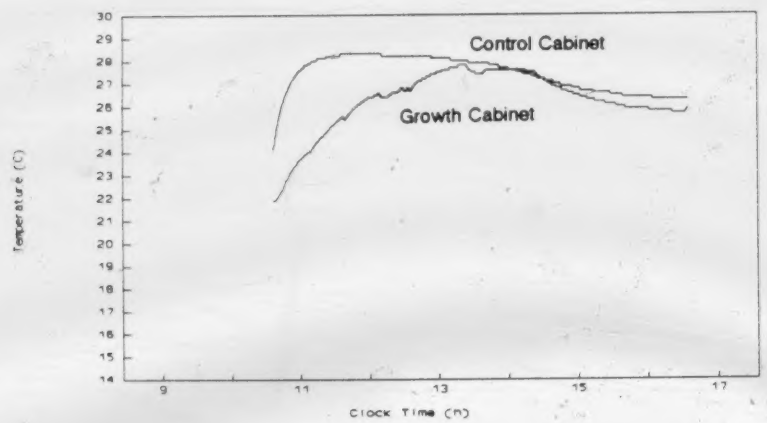

Figure 6.11c Temperature Inside Both Cabinets (1990-03-14)

6.2.6 March 15, 1990

March 15, 1990 was a clear, sunny day as indicated by the direct solar radiation measurements displayed in Figure 6.12a. In addition, the photon flux, temperature inside the growth cabinet, temperature inside the control cabinet, and operating time on the gearmotors were measured. The test run began at 0912h and ended at 1630h. The prototype device was not checked after startup until 1025h when the photon flux was observed to be erratic, as displayed in Figure 6.12b. The controller was adjusted at 1025h in order to improve the solar tracking. A second adjustment was made to the controller at 1245h. The cause of the drop in the photon flux between 1100h and 1130h was not discerned. The duration of the low photon flux rules out the likelihood of wind disturbances. A more plausible explanation for the drop in photon flux was due to a mis-adjustment of the controller. Figure 6.12c indicates that the temperatures inside the growth cabinet and control cabinet both started the test at 22°C and ended the test at 28°C and 26°C, respectively. The hour meters indicated that the elevation gearmotor operated for 34 s, while the azimuth gearmotor operated for 27 min, 36 s during the 7.3 h test. Overall, March 15, 1990 was an evaluation day for the prototype device under clear, sunny sky conditions.

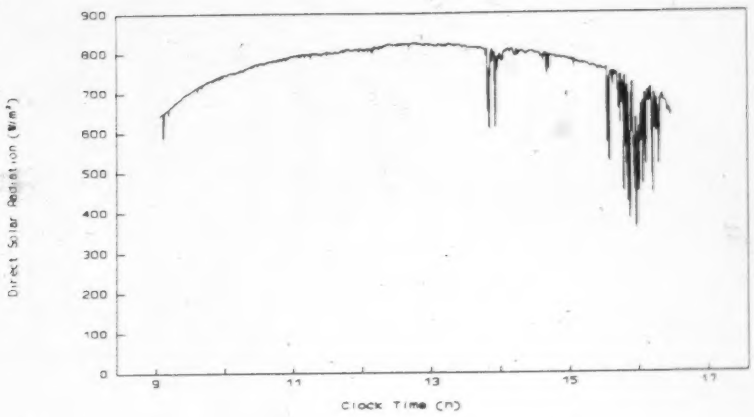

Figure 6.12a Direct Solar Radiation (1990-03-15)

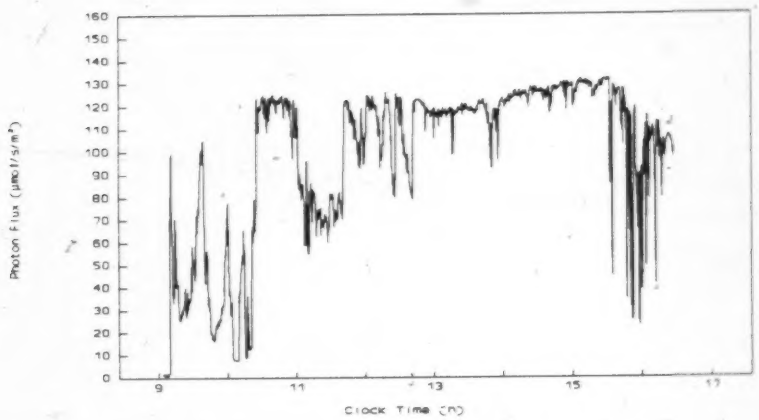

Figure 6.12b Photon Flux Inside Cabinet (1990-03-15)

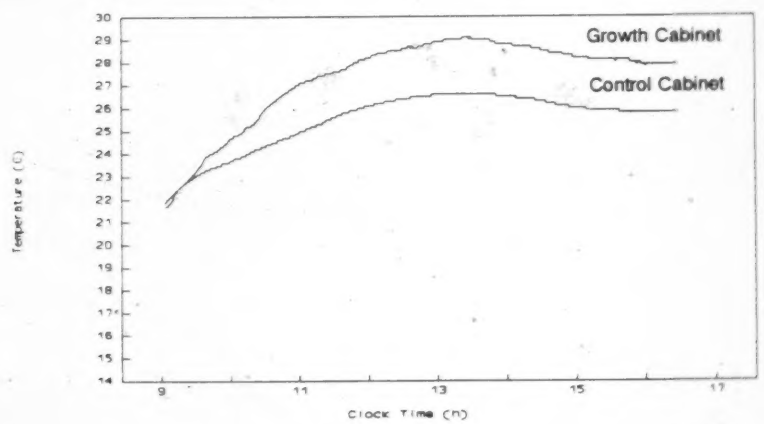

Figure 6.12c Temperature Inside Both Cabinets (1990-03-15)

6.2.7 March 16, 1990

March 16, 1990 had overcast sky conditions for most of the day. Direct solar radiation, photon flux, and temperature inside the growth cabinet were measured. Shadows were visible at 0950h when the test started. However, the shadows had disappeared by 1130h. An adjustment was made to the controller at 1000h to determine whether the solar tracking could be improved. The test was stopped at 1500h, since the sky conditions remained overcast. The direct solar radiation meaurements displayed in Figure 6.13a indicate that no radiant energy was available to the prototype device after 1130h. The photon flux measurements responded in turn and were essentially zero after 1130h, as displayed in Figure 6.13b. The fiber optic cables do not transmit a significant amount of radiant energy on an overcast day. The temperature measured inside the growth cabinet rose by 2°C during the test, as displayed in Figure 6.13c. Overall, March 16, 1990 was a day for evaluating the prototype device under overcast sky conditions.

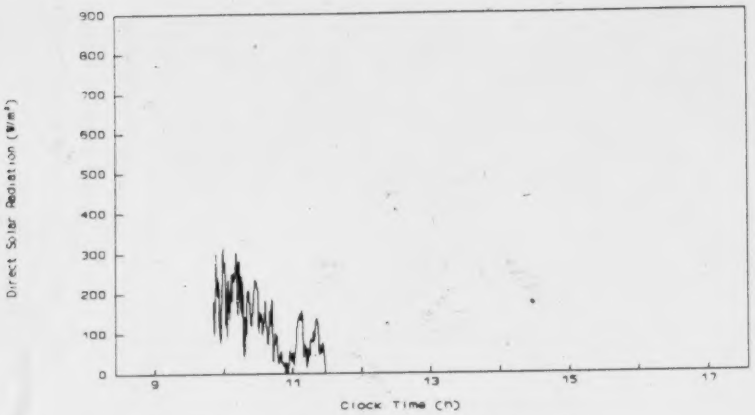

Figure 6.13a Direct Solar Radiation (1990-03-16)

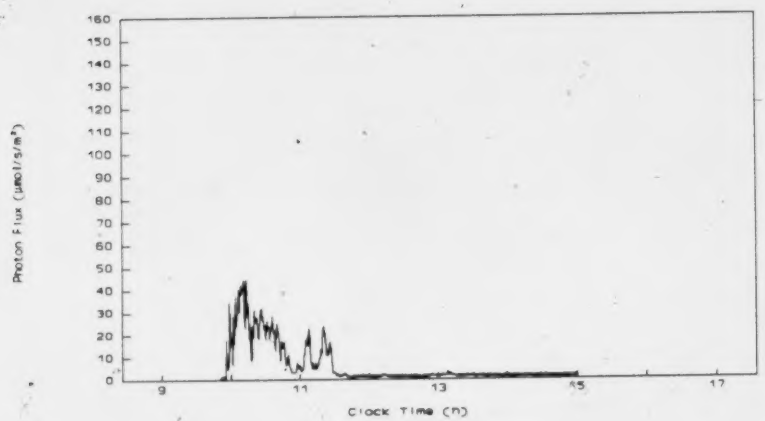

Figure 6.13b Photon Flux Inside Cabinet (1990-03-16)

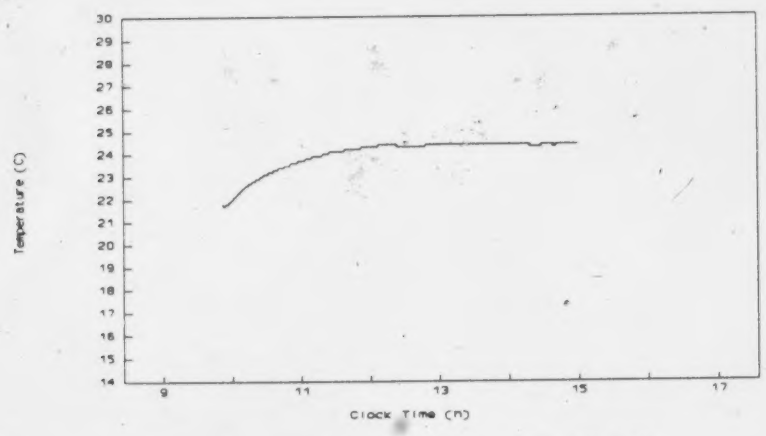

Figure 6.13c Temperature Inside Cabinet (1990-03-16)

6.2.8 March 21, 1990

On March 21, 1990, partly cloudy sky conditions prevailed as shown by the direct solar radiation measurements in Figure 6.14a. In addition, photon flux, temperature inside the growth cabinet, and spectral photon flux were measured. The test run began at 1010h and ended at 1330h. The controller was adjusted between 1152h and 1204h in order to initiate synthetic tracking under cloudy sky conditions. The collector orientation tended to wander during the testing period. Figure 6.14b shows the photon flux measured during the test. The photon flux varied erratically from 0 to 75 $\mu mol/s/m^2$ between 1010h and 1100h and from 0 to 25 $\mu mol/s/m^2$ between 1220h and 1330h. Between 1100h and 1220h, the photon flux was essentially zero, since the prototype device was in synthetic tracking mode. The temperature measurements displayed in Figure 6.14c indicate that the temperature rose from 22°C to 23°C during the testing period. Overall, March 21, 1990 was a day for evaluating the prototype device under varying sky conditions. The spectral photon flux measurements displayed in Figure 6.15a were made near the prototype device at 1323h and inside the growth cabinet at 1336h. Figure 6.15b displays the spectral photon flux measurement at 1336h with greater resolution.

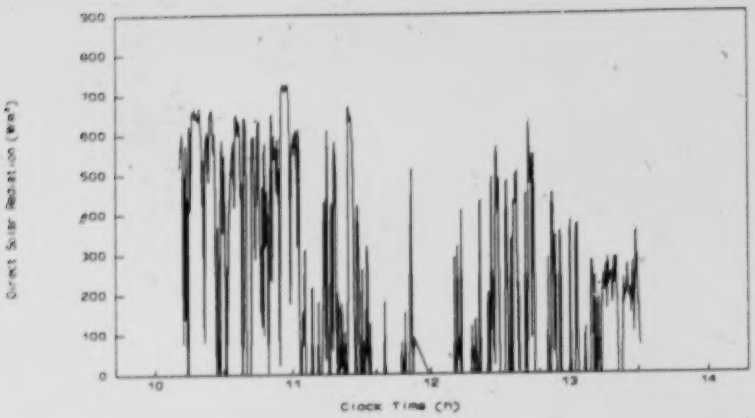

Figure 6.14a Direct Solar Radiation (1990-03-21)

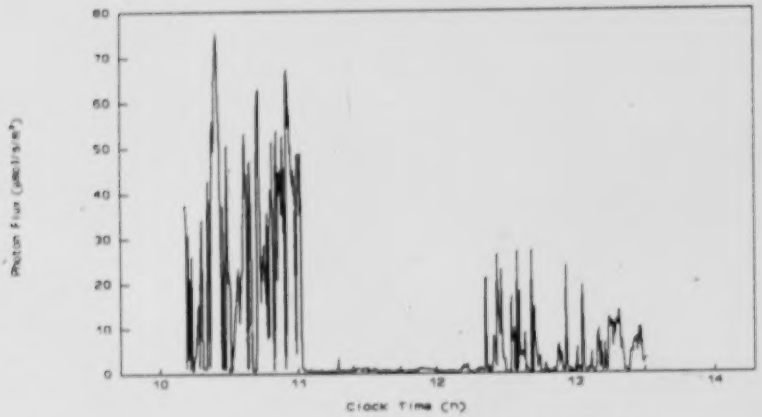

Figure 6.14b Photon Flux Inside Cabinet (1990-03-21)

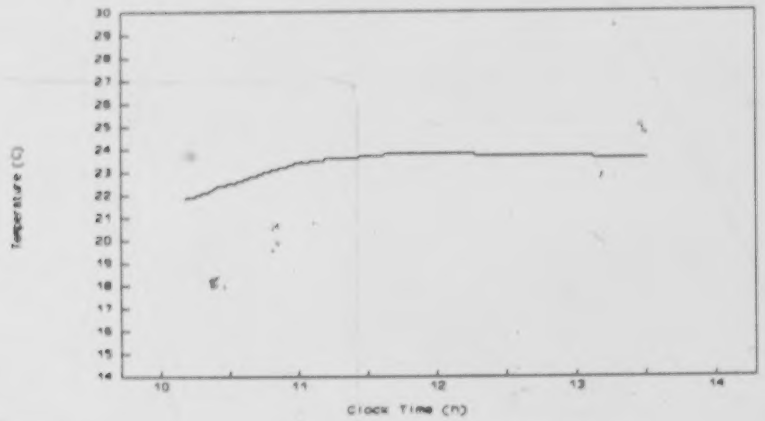

Figure 6.14c Temperature Inside Cabinet (1990-03-21)

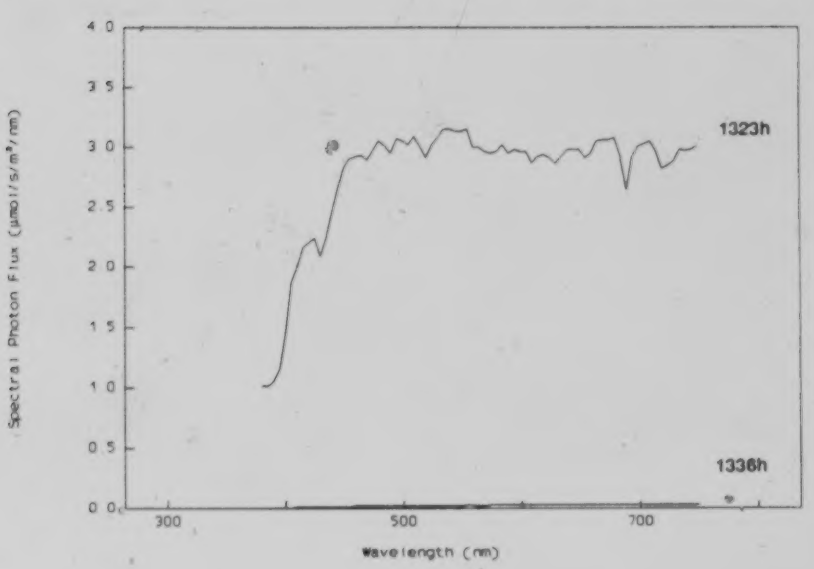

Figure 6.15a Spectral Photon Flux (1990-03-21)

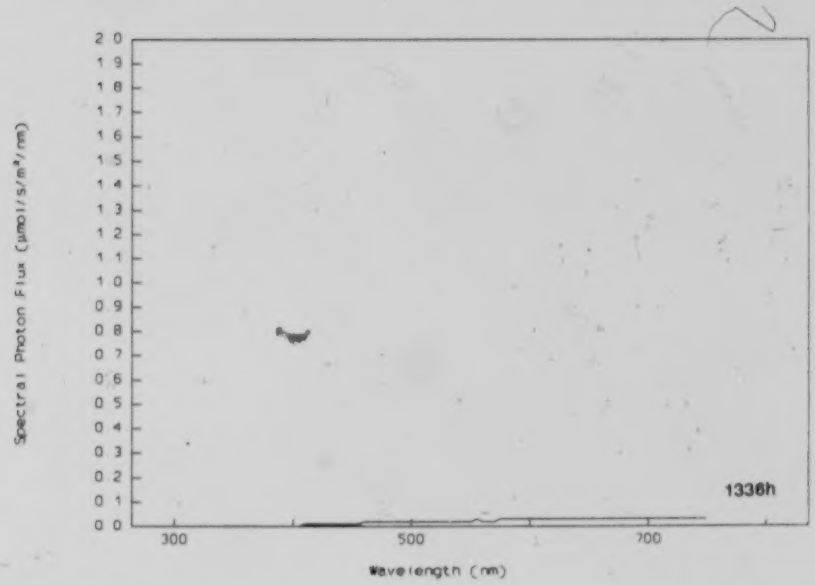

Figure 6.15b Spectral Photon Flux With Greater Resolution (1990-03-21)

6.3 SUMMARY

The prototype light collection and transmission device was operated for a total of eleven days on two different occasions. Table 6.3 summarizes the total, average, and standard deviation for the direct solar radiation and photon flux measured during the tests.

Table 6.3 Results Calculated From Measurements

Date	Test Time	* Direct Radiation			** Photon Flux		
yy/mm/dd	(h)	Tot. (a)	Ave. (b)	S.D. (b)	Tot. (c)	Ave. (d)	S.D. (d)
89/11/29	3.56	28050	226	193	2797	22.5	17.5
89/12/03	5.05	47266	257	287	1632	8.9	16.3
89/12/04	6.11	54941	247	306	973	4.4	11.1
90/02/28	5.37	9981	52	135	614	3.2	7.3
90/03/01	4.16	72854	504	212	7161	49.6	35.6
90/03/02	6.51	113389	490	224	14625	63.2	30.2
90/03/13	6.34	176188	763	26	22467	97.3	46.2
90/03/14	5.99	167108	766	42	14863	68.1	47.2
90/03/15	7.41	206009	764	67	26375	97.8	35.0
90/03/16	5.15	1346	7	90	1163	6.2	9.3
90/03/21	3.33	20477	179	264	1049	9.2	15.7

* a J/m^2 near prototype device
b W/m^2 near prototype device
** c $\mu mol/m^2$ inside cabinet
d $\mu mol/s/m^2$ inside cabinet

7. DISCUSSION

A prototype device capable of collecting and transmitting sunlight via fiber optic cables for the irradiation of horticultural crops grown within an opaque, insulated structure was designed and tested. The results indicate that the concept of transmitting photosynthetic and photomorphogenic radiation from the sun via fiber optic cables was viable. However, the quantity and duration of irradiation were dependent upon the prevailing atmospheric conditions. The irradiation in the visible region was characterized by a continuous spectrum with a higher proportion of radiant energy in the red region than the blue region. Lastly, the contribution of radiant energy in the infra-red region emitted from the fiber optic cables was minimal.

7.1 DESIGN

Overall, the prototype device operated as designed. The three primary functions of light collection, light transmission, and solar tracking were achieved. The az-el tracker positioned the fresnel lenses perpendicular to the sun's incoming rays, such that concentrated images of the sun were focused upon the ends of the fiber optic cables. The modular design facilitated construction, setup, and adjustment of the prototype device.

The rigidity of the prototype device was a concern. A combination of backlash in the output shafts of the gearboxes and flexibility in the

10 mm-thick plywood headplate allowed the collector panels to rock with respect to the solar tracker mount's frame. Edwards (1980) indicates that a solar collector system with a lack of rigidity is susceptible to solar tracking errors caused by wind disturbances and sagging. The lack of rigidity was suspected as the cause of inaccurate solar tracking on March 14, 1990. The sheltered location where the prototype device was tested probably reduced wind loading. The weight of the collector panels tended to hold the collector panels to one side of the backlash and damp motions in the headplate.

7.2 EVALUATION

As previously outlined, the quantity, quality, duration, and direction of irradiance influence the growth of a plant. Testing on two separate occasions gave an indication of the quantity, quality, and duration of irradiation that was supplied by the prototype device. The results obtained during the Fall, 1989, testing indicated the importance of accurate solar tracking for maintaining photon flux inside the growth cabinet. The solar tracking accuracy could not be assessed on November 29, 1989, since the direct solar radiation was not measured correctly. Both, December 3 and 4, 1989 were devoted to adjusting the controller in order to align the shadow band sensor or the collector panels with the sun. The Fall 1989 testing was completed without the accuracy of the solar tracker improving. The results obtained in the Winter 1990 testing were more informative, since the solar tracking accuracy was improved and the prototype device was operated under a variety of sky conditions. February

28, 1990 and March 1, 1990 were devoted to adjusting the controller in order to align the shadow band sensor with the sun. By the end of the day on March 1, 1990, accurate solar tracking had been obtained. The following evaluation of the prototype device has been made.

7.2.1 Solar Tracking Accuracy

As mentioned, the solar tracking accuracy of the prototype device was critical for maintaining photon flux within the growth cabinet. If the alignment of the fresnel lenses to the shadow band sensor or the shadow band sensor to the sun was not accurate, the setup of the fiber optic cable and fresnel lens sets was of no consequence. By operating the prototype device manually, the photon flux inside the growth cabinet was reduced from 120 to 0 $\mu mol/s/m^2$ in approximately 5 s. Since the collector panels rotate 0.75° in 5 s, the solar tracking accuracy required for best performance is estimated to be ±0.20°. The solar tracking accuracy was assessed by (1) a visual comparison of photon flux to direct solar radiation, (2) a linear regression analysis of photon flux vs direct solar radiation, and (3) the calculation of a performance ratio. Table 7.1 summarizes the assessment of the prototype device's solar tracking accuracy.

The visual comparison identified the following peculiarities with the solar tracking accuracy. On March 14, 1990, the direct solar radiation was constant at 750 W/m^2, yet the photon flux inside the growth cabinet would dip to 10 $\mu mol/s/m^2$ from 120 $\mu mol/s/m^2$. The short duration dips are

attributed to wind loads disturbing the collector panels. The long duration dips are attributed to unexplained erratic behaviour of the controller and/or shadow band sensor. Fortunately, the solar tracking accuracy tended to recover from the drops without adjustment of the controller. The results indicate that the rigidity of the prototype device influences the solar tracking accuracy and the sensitivity of the control system tends to vary. The visual assessment of the solar tracking accuracy for each test run is presented in Table 7.1.

A linear regression analysis of photon flux vs direct solar radiation assisted in qualifying the solar tracking accuracy of the prototype device. The hypothesis is that a high correlation coefficient indicates accurate solar tracking. Intuitively, the photon flux inside the growth cabinet should only respond to the direct solar radiation outside if the solar tracking is accurate. If the photon flux responds to other variables, such as wind load disturbances or controller mis-adjustments, then the corresponding correlation coefficient is low and the implication is that solar tracking is not accurate. The correlation coefficients are presented in Table 7.1. On February 28 and March 1, 1990, the prototype device did not track the sun accurately, since the controller was being adjusted. As expected, the corresponding correlation coefficient was 0.57 for both days. The linear regression analyses for February 28 and March 1, 1990 are displayed in Figures 7.1 and 7.2, respectively. On March 2, 1990, when the controller's adjustment was complete, the correlation coefficient was 0.91. The linear regression analysis for March 2, 1990 is displayed in Figure 7.3. Similarly, on March 16, 1990, when the sky

conditions were overcast, the correlation coefficient was 0.88. The correlation coefficient calculated from the regression analysis on March 21, 1990 was 0.70. The direct solar radiation on March 21, 1990 varied from 0 to 700 W/m^2 within minutes. This variation influenced the prototype device's solar tracking accuracy. The linear regression analyses are presented in Appendix F for each test run.

Table 7.1 Assessment Of Solar Tracking Accuracy

Date	Visual Assessment	Correlation Coefficient	Performance Ratio
89/11/28	Poor	0.42	0.100
89/12/03	Poor	0.50	0.034
89/12/04	Poor	0.33	0.018
90/02/28	Fair	0.57	0.062
90/03/01	Fair	0.57	0.098
90/03/02	Excellent	0.91	0.129
90/03/13	Excellent	0.53	0.128
90/03/14	Good	0.61	0.089
90/03/15	Excellent	0.44	0.128
90/03/16	Excellent	0.88	0.864
90/03/21	Poor	0.70	0.051

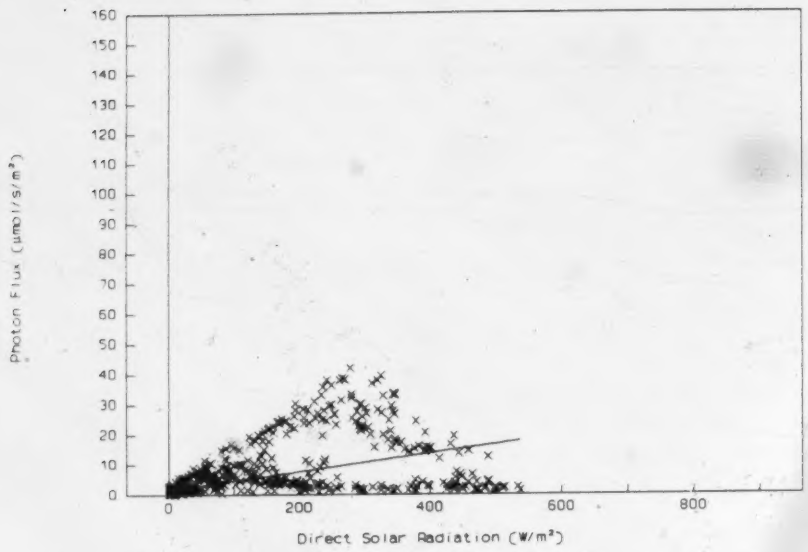

Figure 7.1 Linear Regression Analysis (1990-02-28)

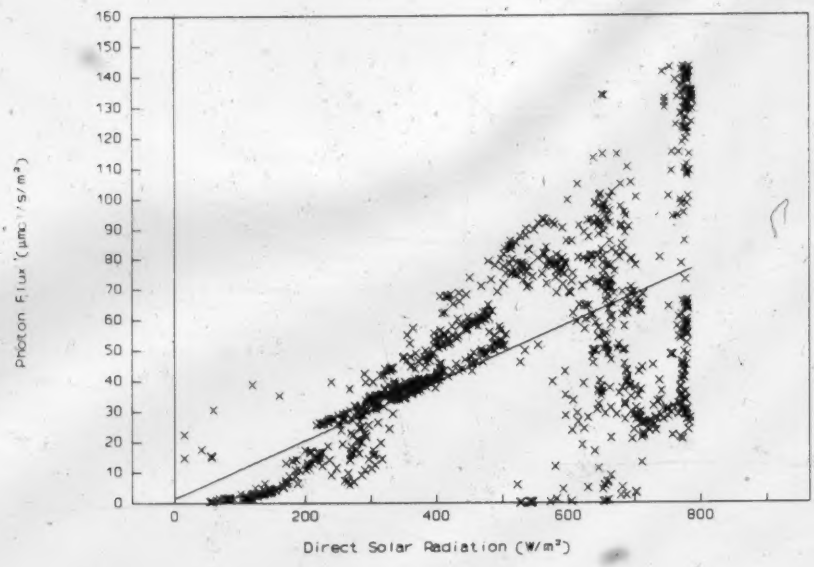

Figure 7.2 Linear Regression Analysis (1990-03-01)

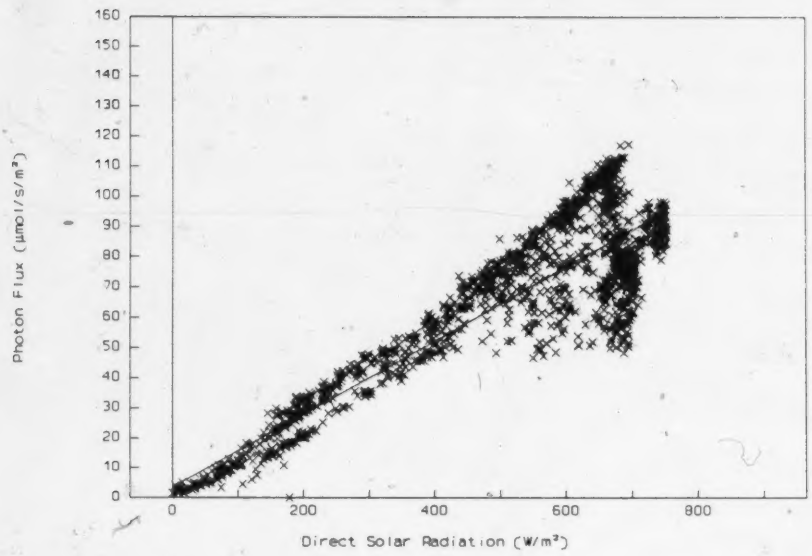

Figure 7.3 Linear Regression Analysis (1990-03-02)

Unfortunately, a linear regression and/or a scatter diagram are not useful for analyzing solar tracking accuracy under clear, sunny sky conditions, since the direct solar radiation is constant. In order to assess the solar tracking accuracy under clear, sunny sky conditions and to compare different test runs, a performance ratio was calculated. The performance ratio is the integral of the photon flux measurements inside the growth cabinet to the integral of the direct solar radiation measurements outside. The performance ratio should not be confused with efficiency, since the wavelength ranges for the photon flux and direct solar radiation differ. The resulting performance ratios for the test runs are presented in Table 7.1. The performance ratios indicate that the most accurate solar tracking occurred on March 2, 13, and 15, 1990. The

performance ratio for these dates is 0.13. The performance factor indicates that the prototype device can maintain accurate solar tracking under sunny, clear sky conditions, as well as, varying sky conditions. The 0.09 performance ratio for March 14, 1990 indicates that wind load disturbances and controller/shadow band sensor behaviour influenced the solar tracking accuracy. The 0.86 performance ratio for March 16, 1990 is misleading, since the total direct solar radiation during the test run was minimal. The 0.05 performance ratio for March 21, 1990 indicates that the solar tracking was influenced by rapidly varying sky conditions.

7.2.2 Efficiency

The efficiency of the prototype device for collecting and transmitting solar radiant energy was calculated by dividing the spectral photon flux inside the growth cabinet by the spectral photon flux outside. This calculation of efficiency relates the quantity of radiant energy supplied for photosynthesis to the quantity of radiant energy available for photosynthesis. Figure 7.4 displays the efficiency of the prototype device for collecting and transmitting wavelengths between 380 and 750 nm. The indication is that the prototype device collects and transmits wavelengths for the blue and red regions of the spectrum at 5% and 30% efficiency, respectively. Intuitively, the result is reasonable, since the attenuation of the fiber optic cable is greater for the blue wavelengths than the red wavelengths (Appendix B). The overall efficiency of the prototype device for collecting and transmitting photosynthetically active irradiation is 19.2%.

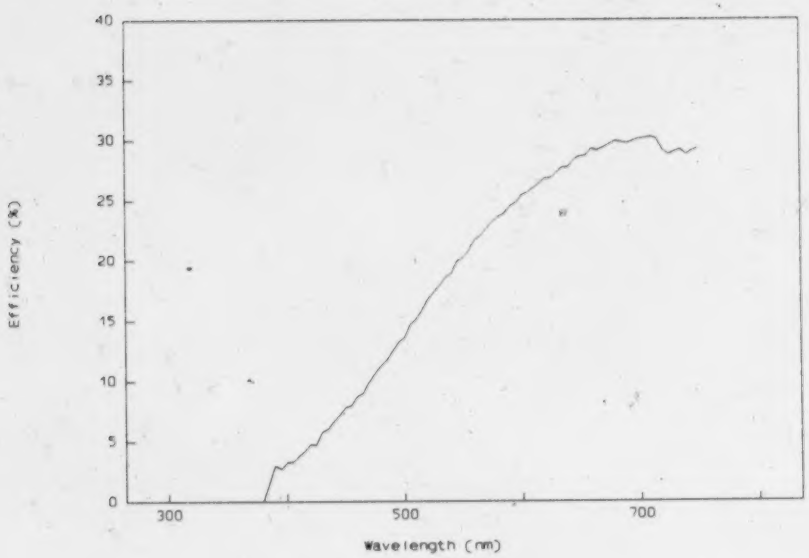

Figure 7.4 Efficiency Of Prototype Device (1990-03-13)

7.2.3 Quantity

The quantity of radiant energy is important for plant growth. The guidelines available for predicting a plant's growth with a specific irradiation level are vague. Cathey and Campbell (1980) recommend 18 W/m^2 (approximately 80 $\mu mol/s/m^2$) of irradiation between 400 and 850 nm for rapid propagation of plants. Research conducted by Craker and Seibert (1982) on lettuce plants indicates that the selection of a low light level with a long photoperiod produces the most lettuce leaf area per unit light energy. For instance, a light intensity of 14.1 W/m^2 (approximately 65 $\mu mol/s/m^2$) and a photoperiod of 24 h, converted 11% of the available

photosynthetically active radiation to lettuce tissue. Craker and Seibert (1982) also determined that low light intensities and long photoperiods represented the most efficient use of light energy for radish plants. The linear regression analysis from March 2, 1990 indicates that the prototype device can produce a photon flux near the bottom, center of the growth cabinet described by Equation 7.1.

$$PF = 0.12D + 3.55 \quad \ldots\ldots\ldots\ldots\ldots\ldots \quad (7.1)$$

where; PF = Photon Flux ($\mu mol/s/m^2$) and
D = Direct Solar Radiation (W/m^2).

Examples of the photon fluxes produced are, 28 $\mu mol/s/m^2$ at 200 W/m^2, 52 $\mu mol/s/m^2$ at 400 W/m^2, 77 $\mu mol/s/m^2$ at 600 W/m^2, and 101 $\mu mol/s/m^2$ at 800 W/m^2 near the bottom of the growth cabinet. The maximum photon flux achieved inside the growth cabinet was 130 $\mu mol/s/m^2$ when the direct solar radiation was 800 W/m^2. The results indicate that the prototype device can supply sufficient radiant energy for plant growth when sky conditions permit. The distribution of the radiant energy near the bottom of the growth cabinet, as measured on March 13, 1990, was not uniform. A non-uniform distribution could influence plant growth under the irradiation emitted from the prototype device.

7.2.4 Quality

The quality of radiant energy is important for plant growth. The radiant energy provided by the prototype device was characterized by a

continuous spectrum between 380 and 750 nm with a higher proportion of radiant energy in the red region (700 nm) than the blue region (400 nm). The spectral photon flux from March 13, 1990 indicates that an average of 0.1 $\mu mol/s/m^2/nm$ was provided between 400 and 500 nm and an average of 0.7 $\mu mol/s/m^2/nm$ was provided between 600 and 700 nm. Although not directly measured, the thermal component of the radiant energy was low. The temperature rise inside the growth cabinet was minimal and tended to correspond with the temperature rise within the greenhouse. As well, the temperature inside the growth cabinet and the control cabinet were similar. This indicates that the infra-red component of the radiant energy emitted from the fiber optic cables was minimal. The radiant energy was considered to be sufficient quality for photomorphogenic responses.

7.2.5 Duration

The duration of irradiation is important for plant growth. The duration of irradiation provided by the prototype device was dependent upon the sun being visible in the sky. On a clear, sunny day the duration of irradiation would be the time between sunrise and sunset, while on an overcast day, no irradiation would be available. The duration of irradiation cannot be controlled unless a backup electrical lighting system is interfaced with the prototype device.

7.3 SUMMARY

The research performed contributes to energy efficient control of plant environments. With a backup lighting system, the concept of irradiating horticultural crops grown in an opaque, insulated structure with sunlight supplied via fiber optic cables appears viable. However, economic conditions will determine when and if the technology will become commercially marketable. The design employing an az-el solar tracker and one fiber optic cable with one fresnel lens appears to work well.

8. CONCLUSIONS

A prototype light collection and transmission device has been designed and tested. The test results indicate that the prototype device is capable of collecting and transmitting sunlight via fiber optic cables. The following conclusions are drawn from the evaluation of the test results:

1. The orientation of a single flexible fiber optic cable with a single fresnel lens and an azimuth-elevation solar tracker is effective for collecting and transmitting radiant solar energy.

2. A solar tracking accuracy of ±0.20° is critical for maintaining the photon flux inside the growth cabinet at levels for plant growth.

3. A correlation coefficient of 0.9 and/or a performance ratio of 0.13 indicates that the prototype device is accurately tracking the sun.

4. The prototype device is capable of supplying a photon flux of 130 $\mu mol/s/m^2$ (400-700 nm) near the bottom of the growth cabinet when the direct solar radiation outside is 800 W/m^2 (300-2500 nm).

5. The prototype device is capable of supplying blue (400 nm) and red (700 nm) wavelengths of irradiation with an efficiency of 5% and 30%, respectively.

6. The irradiation supplied by the prototype device contains a minimal amount of infra-red radiant energy.

7. The duration and quantity of irradiation supplied by the prototype device are dependent upon the availability of direct solar radiation.

8. The prototype device's overall collection and transmisssion efficiency for photosynthetically active radiation is 19.2%.

9. RECOMMENDATIONS

The prototype device requires two design modifications. First, the plywood head plate should be replaced with a rigid steel plate to improve the rigidity of the solar tracker. Second, the worm gears in the gearboxes should be fitted tighter to reduce backlash in the output shaft.

The prototype light collection and transmission device requires further testing. First, the solar tracking accuracy must be evaluated in order to identify the cause of the erratic behaviour of the controller/shadow band sensor under clear, sunny sky conditions. Second, the set up of the fresnel lens and fiber optic cable sets should be examined to determine if the alignment is correct. Lastly, an actual horticultural crop should be grown under the irradiation emitted from the fiber optic cables in order to assess the actual performance of the prototype device.

REFERENCES

ASAE. 1989. ASAE Engineering Practice: ASAE EP411. Guidelines for measuring and reporting environmental parameters for plant experiments in growth chambers. 456-459. 1989 Agric. Eng. Yearbook., Am. Soc. Agric. Eng., St. Joseph, MI.

ASHRAE. 1981. Environmental control for animals and plants. 9.10-9.15. In ASHRAE Handbook 1981 Fundamentals. Am. Soc. Heat. Refri. Air Cond. Eng. Inc., Atlanta, GA.

BICKFORD, E.D. and DUNN, S. 1972. Lighting for Plant Growth. The Kent State University Press, Kent, OH.

BULLEY, N.R. and PHILLIPS, D. 1984. Horticultural lighting using HID/light pipe systems. Paper No. 84-4532. Am. Soc. Agric. Eng., St. Joseph, MI.

BURDETT-MOULTON, HAY, D., ROMER, M., MACKAY & PARTNERS. 1988. Iqaluit greenhouse feasibility study. Unpublished report by Burdett-Moulton Architects & Engineers Ltd., Frobisher Bay, N.W.T..

CARIOU, J.M., MARTIN, L., and DUGAS, J. 1982. Transport of solar energy with optical fibers. Solar Energy 29(5): 397-406.

CATHEY, H.M. and CAMPBELL, L.E. 1980. Light and lighting systems for horticultural plants. Horticultural Reviews 2: 491-537.

CRAKER, L.E. and SEIBERT, M. 1982. Light energy requirement for controlled environment growth of lettuce and radish. Trans. Am. Soc. Agric. Eng. 12(1): 214-216.

D'AZZO, J.J. and HOUPIS, C.H. 1981. Linear Control System Analysis and Design. McGraw-Hill Book Company, Toronto, ON.

DUGUAY, M.A. and EDGAR, R.M. 1977. Lighting with sunlight using sun tracking concentrators. Applied Optics 16(5): 1444-1446.

EDWARDS, B. 1980. Collector deflections due to wind gusts and control scheme design. Solar Energy 25: 231-234.

FRAAS, L.M., PYLE, W.R. and RYASON, P.R. 1983. Concentrated and piped sunlight for indoor illumination. Applied Optics 22(4): 578-582.

HARMON, S. 1977. Solar-optical analysis of a mass-produced plastic circular fresnel lens. Solar Energy 19: 105-108.

HART, J.W. 1988. Light and Plant Growth. Unwin Hyman Ltd., Boston, MA.

HOLMS, M.G., KLIEN, W.H., and SAGER, J.C. 1985. Photons, flux and some light on philology. Hortscience 20(1): 29-31.

HUGHES, R.O. 1979. Optimal control of sun tracking solar concentrators. Trans. Am. Soc. Mech. Eng., Journal of Dynamics Systems, Measurement, and Control. 101: 157-161.

HUGHES, R.O. 1980. Effects of tracking errors on the performance of point focusing solar collectors. Solar Energy 24: 83-92.

IZAWA, T. and SUDO, S. 1987. Optical Fibers: Materials and Fabrication. D. Reidel Publishing Company, Boston, MA.

KATO, D. and NAKAMURA, T. 1976. Application of optical fibers to the transmission of solar radiation. J. Appl. Phys. 47(10): 4528-4531.

KLEIN, M.V. and FURTAK, T.E. 1986. Optics 2nd Ed. John Wiley & Sons, Inc., Toronto, ON.

KRITCHMAN, E.M.,FRIESEM, A.A., YEKUTIELI, G. 1979. Efficient fresnel lens for solar concentration. Solar Energy 22: 119-123.

LANGHANS, R.W. and DREESEN, D.R. 1988. Challenges of growing plants in space. Hortscience 23(2): 286-293.

LEWIS, C.E., THOMAS, W.C., and NORTON, R.A. 1978. Controlled environment agriculture. Bulletin 55, Agricultural Experiment Station, University of Alaska, Fairbanks, AK.

LOOMIS, J. 1987. Produce production centre. Unpublished report by Produce North Ltd., Norman Wells, N.W.T..

MORI, K., TANATSUGU, N., and YAMASHITA, M. 1984. Visible solar ray supply system for space station. Paper No. IAF-84-39. Am. Inst. Aero. Astro., New York, NY.

MORI, K. 1985. Photoautotrophic bioreactor using visible solar ray condensed by fresnel lenses and transmitted through optical fibers. Biotechnology and Bioengineering Symp. No. 15 331-345.

MORI, K. 1987. Solar ray collection apparatus. Canadian Patent 1229273. Ottawa, ON.

OLSEN, R.L., OLESON, M.W., and SLAVIN, T.J. 1988. CELSS for advanced manned mission. Hortscience 23(4): 275-286.

OSHIDA, I. 1961. Step lenses and step prisms for utilization of solar energy. UN Conference On New Sources Of Energy 15(22): 598-603.

POOLE, P. 1985. Polar solar, report on the design, construction, and installation of a greenhouse at Pond Inlet, Northwest Territories. Unpublished report by Peter Poole, Alcove, PQ.

PRINCE, R.P., BARTOK, J.W., and ALDRICH, R.A. 1982. Controlled environment vegetable production technology projection. Paper 82-4050. Am. Soc. Agric. Eng., St. Joseph, MI.

SAGER, J.C., EDWARDS, J.L., and KLEIN, W.H. 1982. Light energy utilization efficiency for photosynthesis. Trans. Am. Soc. Agric. Eng. 25(6): 1737-1746.

ST. GEORGE, D.R. and FEDDES, J.J.R. 1988. Production of greenhouse crops in Northern Canada. Paper 88-124. Can. Soc. Agric. Eng., Ottawa, ON.

SEIPPEL, R.G. 1981. Optoelectronics. Reston Publishing Company, Virginia, IL.

SESCI. 1986. Solar light pipe replaces lightbulbs. SOL 55, Ottawa, ON.

STINE, W.B. and HARRIGAN, R.W. 1985. Solar Energy Fundamentals and Design with Computer Applications. John Wiley & Sons, Inc., Toronto, ON.

WELFORD, W.T. and WINSTON, R. 1978. The Optics of Nonimaging Concentrators; Light and Solar Energy. Academic Press, New York, NY.

WHITEHEAD, L.A., NODWELL, R.A., and CURZON, F.L. 1982. New efficient light guide for interior illumination. Applied Optics 21(15): 2755-2757.

APPENDIX A

Appendix A, pp 124, contained spectral transmission curve of the 0.125 inch optical grade acrylic for the fresnel lenses. It has been removed due to the in-availability of copyright permission.

APPENDIX B

Appendix B, pp 125-126, contained attenuation curve and specifications for PCS 600W fiber optic cable. It has been removed due to the in-availability of copyright permission.

APPENDIX C

Appendix C, pp 127-131, contained specifications and operating instructions for the Mark IV ST-2 Dual Axis solar tracking kit. It has been removed due to the in-availability of copyright permission.

APPENDIX D

Appendix D, pp 132-133, contained specifications for the 23T-D electric gearmotors. It has been removed due to the in-availability of copyright permission.

APPENDIX E

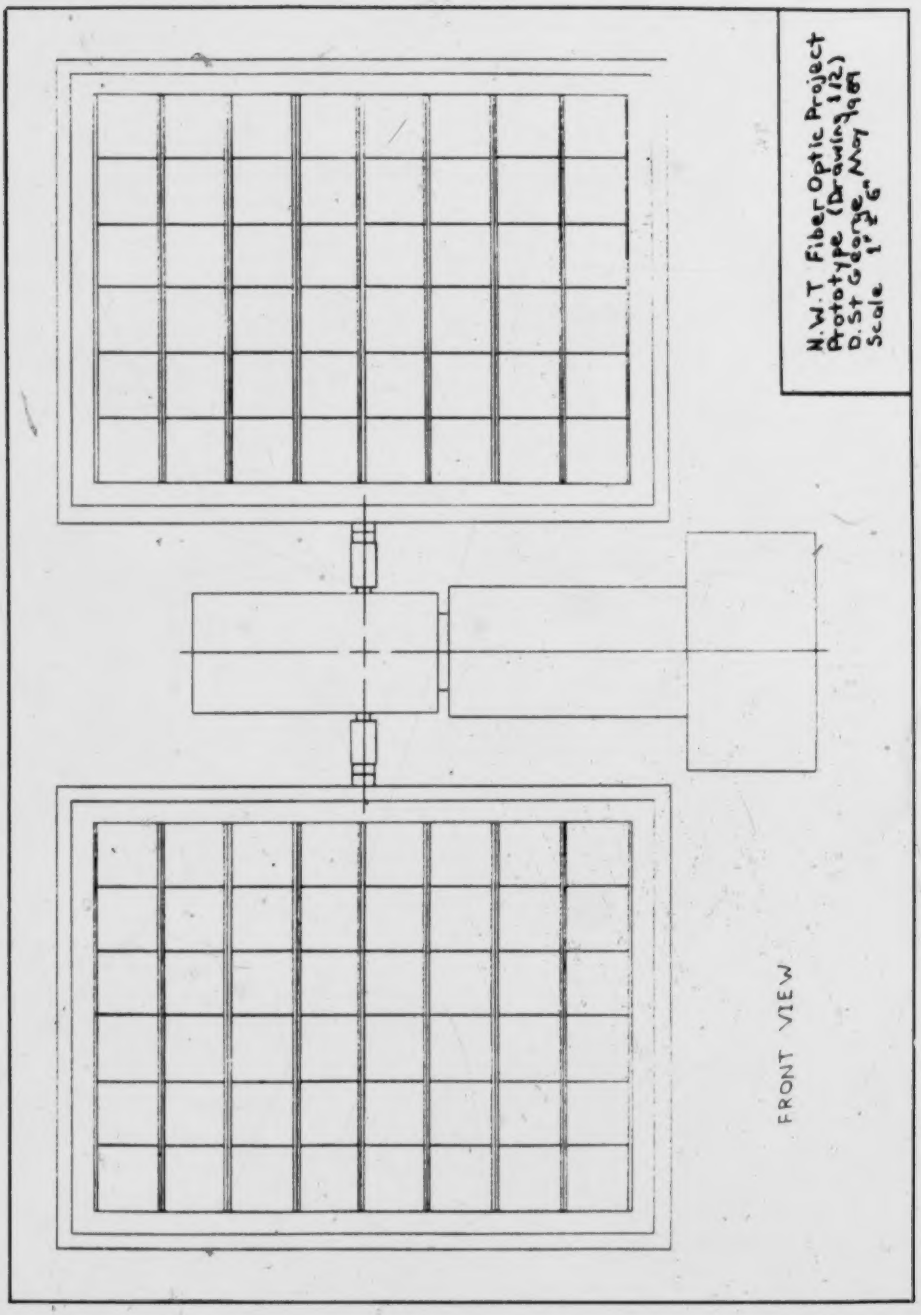
N.W.T Fiber Optic Project
Prototype (Drawing 1/2)
D.St Georges May 1989
Scale 1"=6"
FRONT VIEW

APPENDIX E

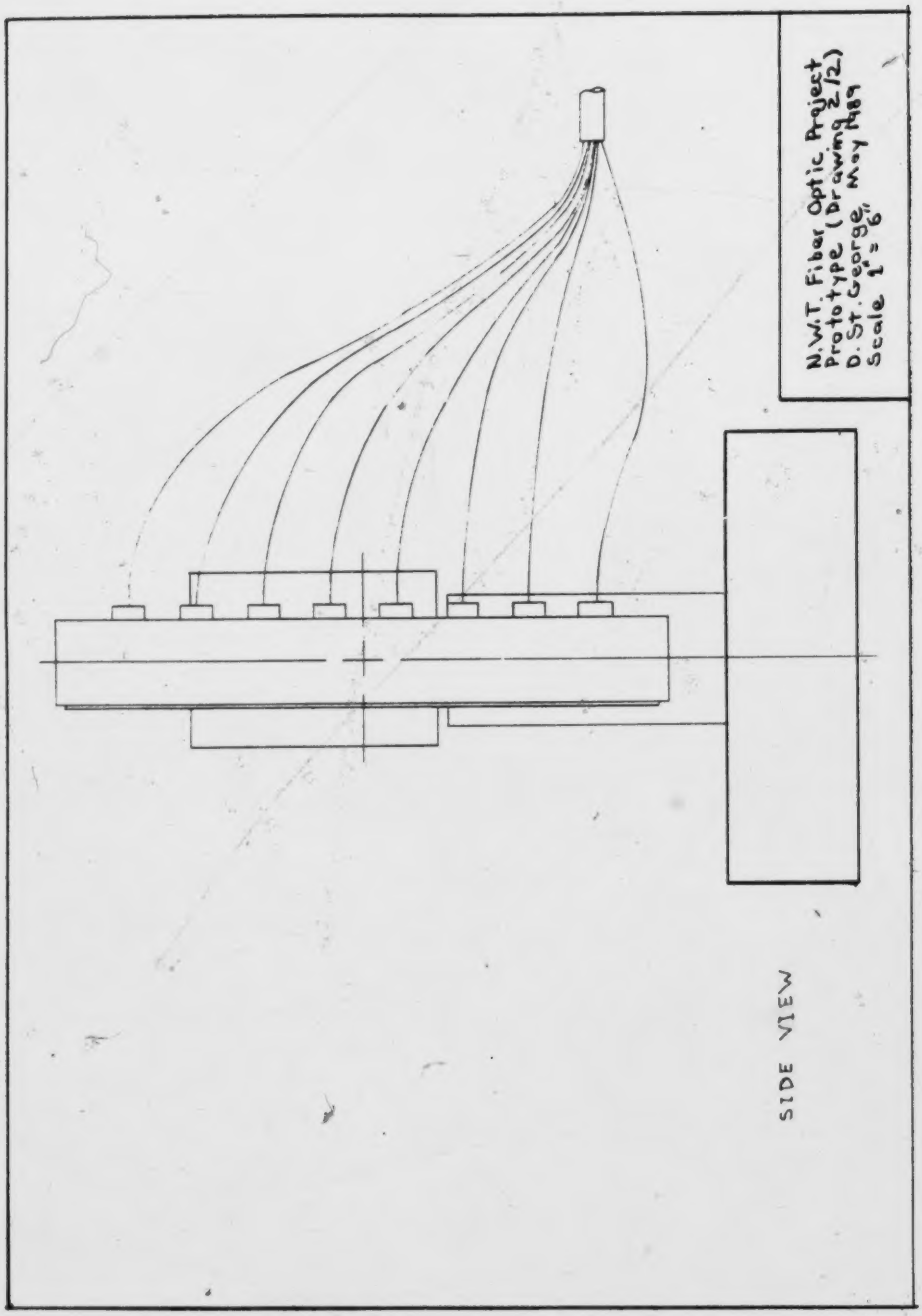
N.W.T. Fiber Optic Project
Prototype (Drawing 2/2)
D. St. George, May 1989
Scale 1" = 6"
SIDE VIEW

APPENDIX E

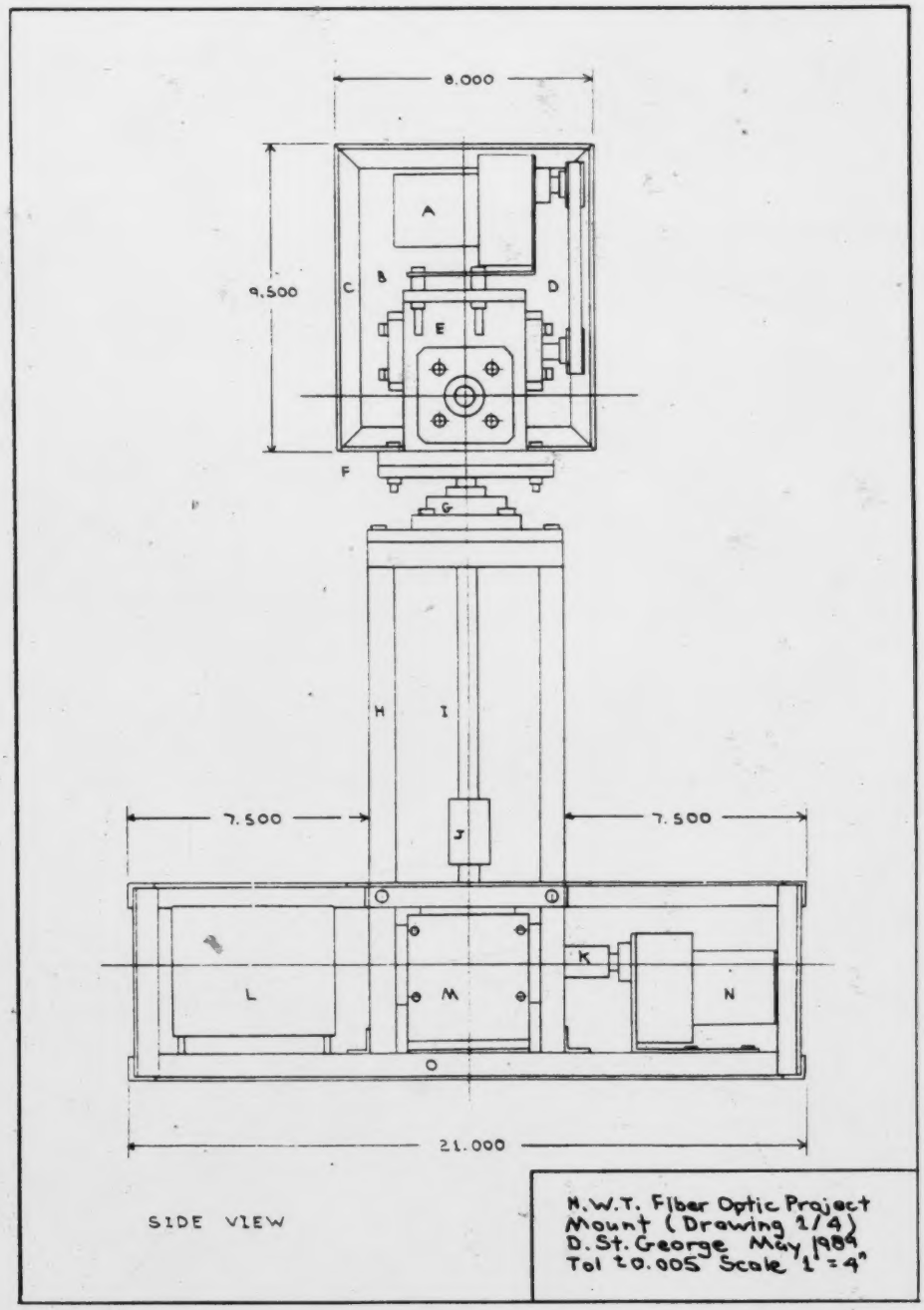
8.000
9.500
A
B
C
D
E
F
G
H
I
J
7.500
7.500
K
L
M
N
21.000
SIDE VIEW
N.W.T. Fiber Optic Project
Mount (Drawing 1/4)
D. St. George May 1989
Tol ±0.005 Scale 1" = 4"

APPENDIX E

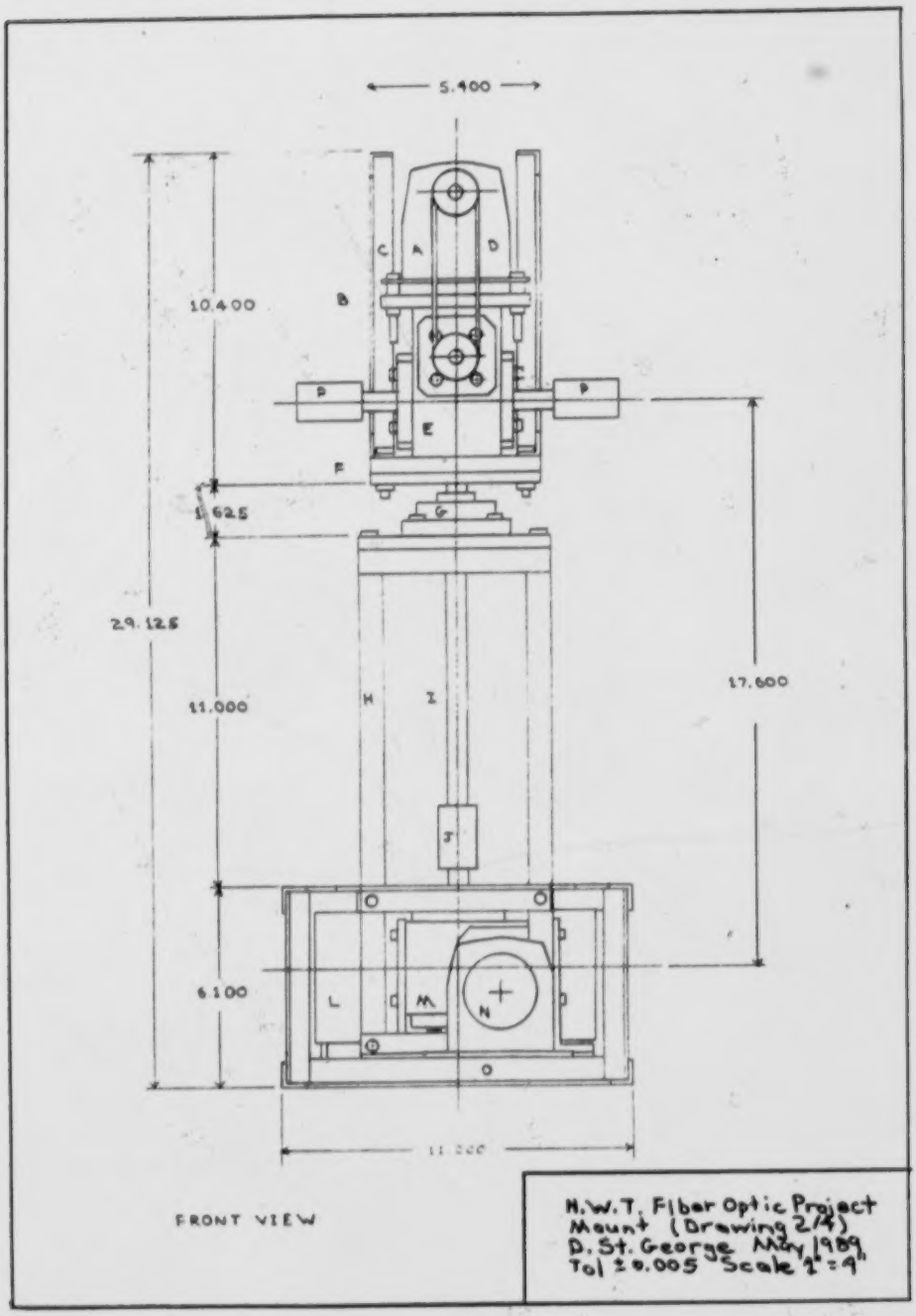
5.400
10.400
1.625
29.125
11.000
17.600
6.100
11.000
A
B
C
D
E
F
G
H
I
J
L
M
N
O
P
FRONT VIEW
M.W.T. Fiber Optic Project
Mount (Drawing 2/4)
D. St. George May 1989
Tol ± 0.005 Scale 1" = 4"

APPENDIX E

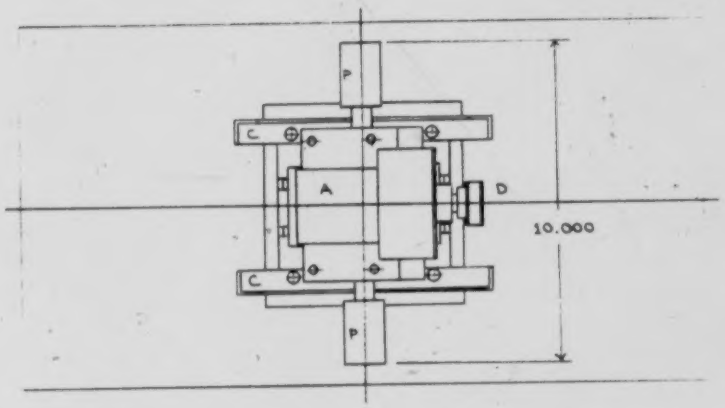

TOP VIEW ELEVATION

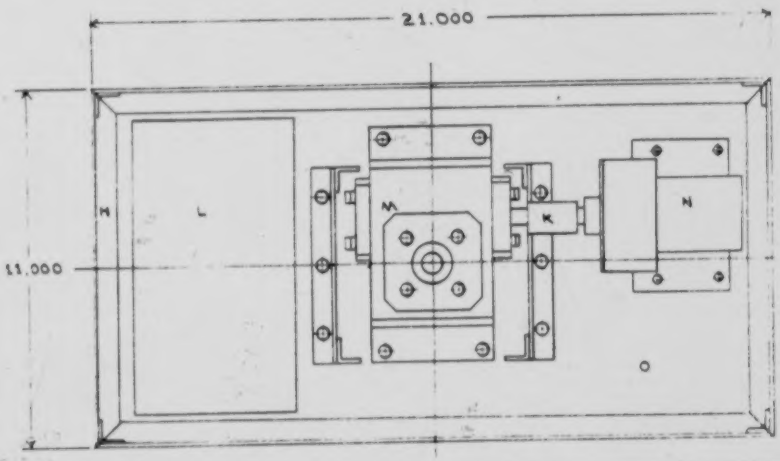

TOP VIEW AZIMUTH

N.W.T. Fiber Optic Project
Mount (Drawing 3/4)
D. St. George May 1984
Tol ±0.005" Scale 1"=4"

APPENDIX E

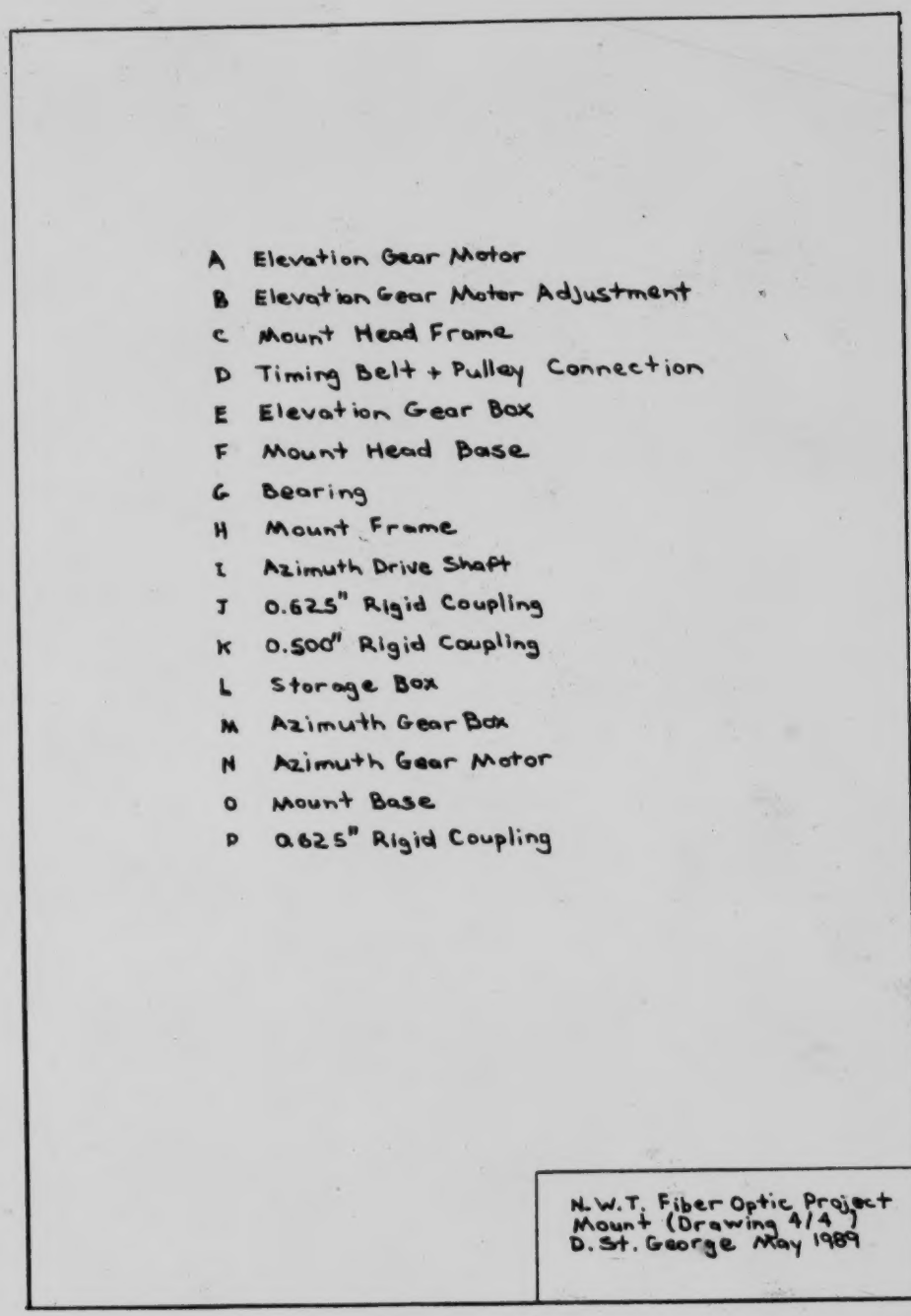
A Elevation Gear Motor
B Elevation Gear Motor Adjustment
C Mount Head Frame
D Timing Belt + Pulley Connection
E Elevation Gear Box
F Mount Head Base
G Bearing
H Mount Frame
I Azimuth Drive Shaft
J 0.625" Rigid Coupling
K 0.500" Rigid Coupling
L Storage Box
M Azimuth Gear Box
N Azimuth Gear Motor
O Mount Base
P 0.625" Rigid Coupling
N.W.T. Fiber Optic Project
Mount (Drawing 4/4)
D. St. George May 1989

APPENDIX E

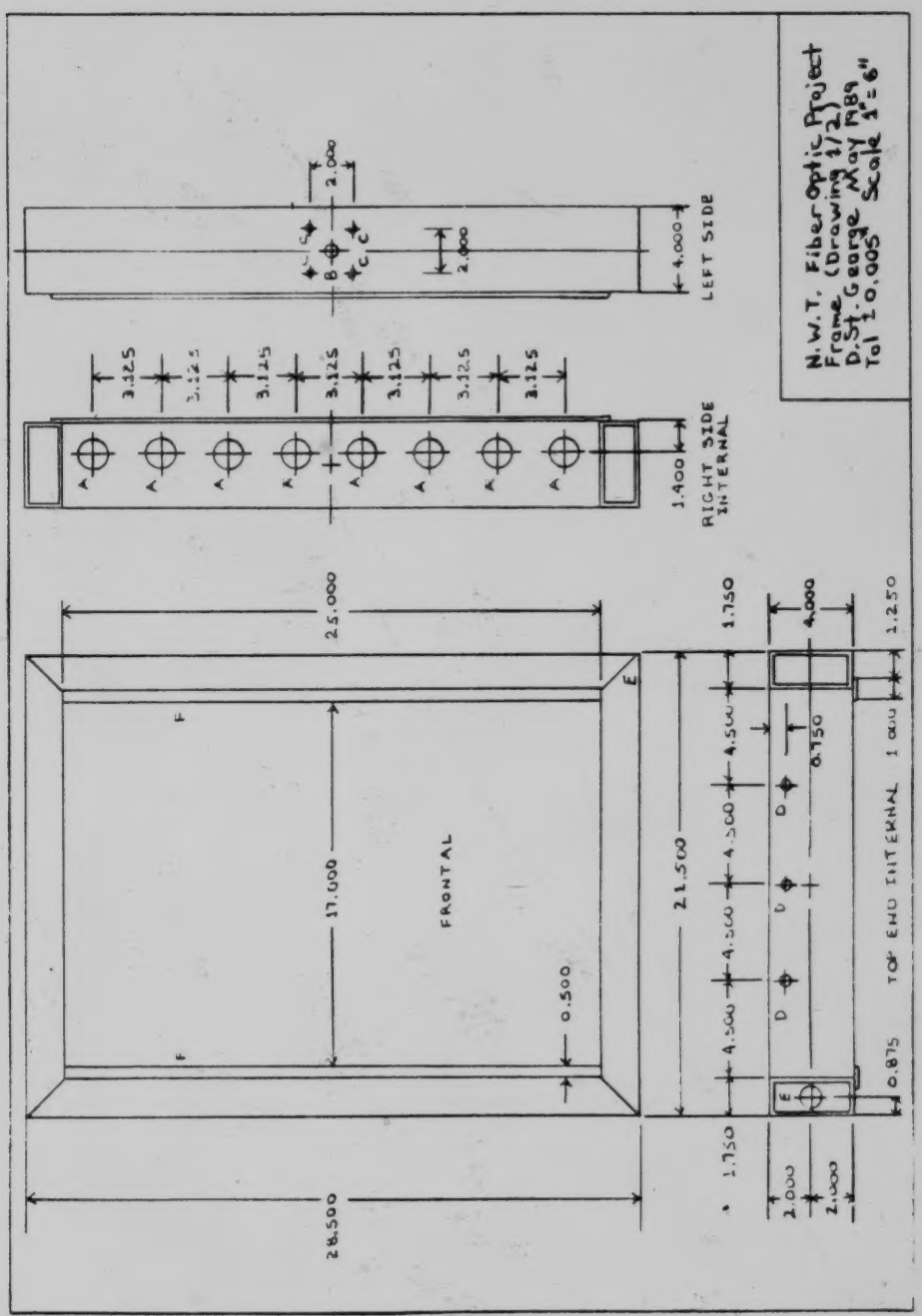
N.W.T. Fiber Optic Project
Frame (Drawing 1/2)
D.St.George May 1989
Tol ± 0.005" Scale 1"=6"
LEFT SIDE
RIGHT SIDE INTERNAL
TOP END INTERNAL
FRONTAL
25.000
17.000
0.500
28.500
21.500
1.750
4.000
1.250
0.750
0.875
2.000
3.125
4.000
1.900

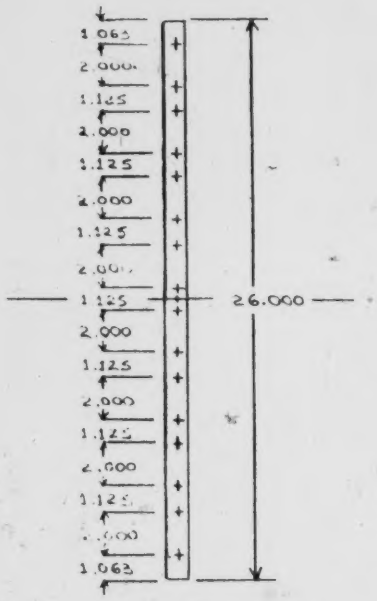

PART F
0.194 Dia. Hole No. 10 Drill Size
Fuse Part F To Frame

A	1.500	Dia Hole Thru Inside Edge
B	0.688	Dia Hole Thru Outside Edge
C	0.344	Dia Hole Thru Outside Edge
D	0.500	Dia Hole Thru Inside Edge
E	1.000	Dia. Hole Thru Outside Edge

N.W.T. Fiber Optic Project
Frame (Drawing 2/2)
D. St. George May 1989
Tol. ±0.005 Scale 1" = 6"

APPENDIX E

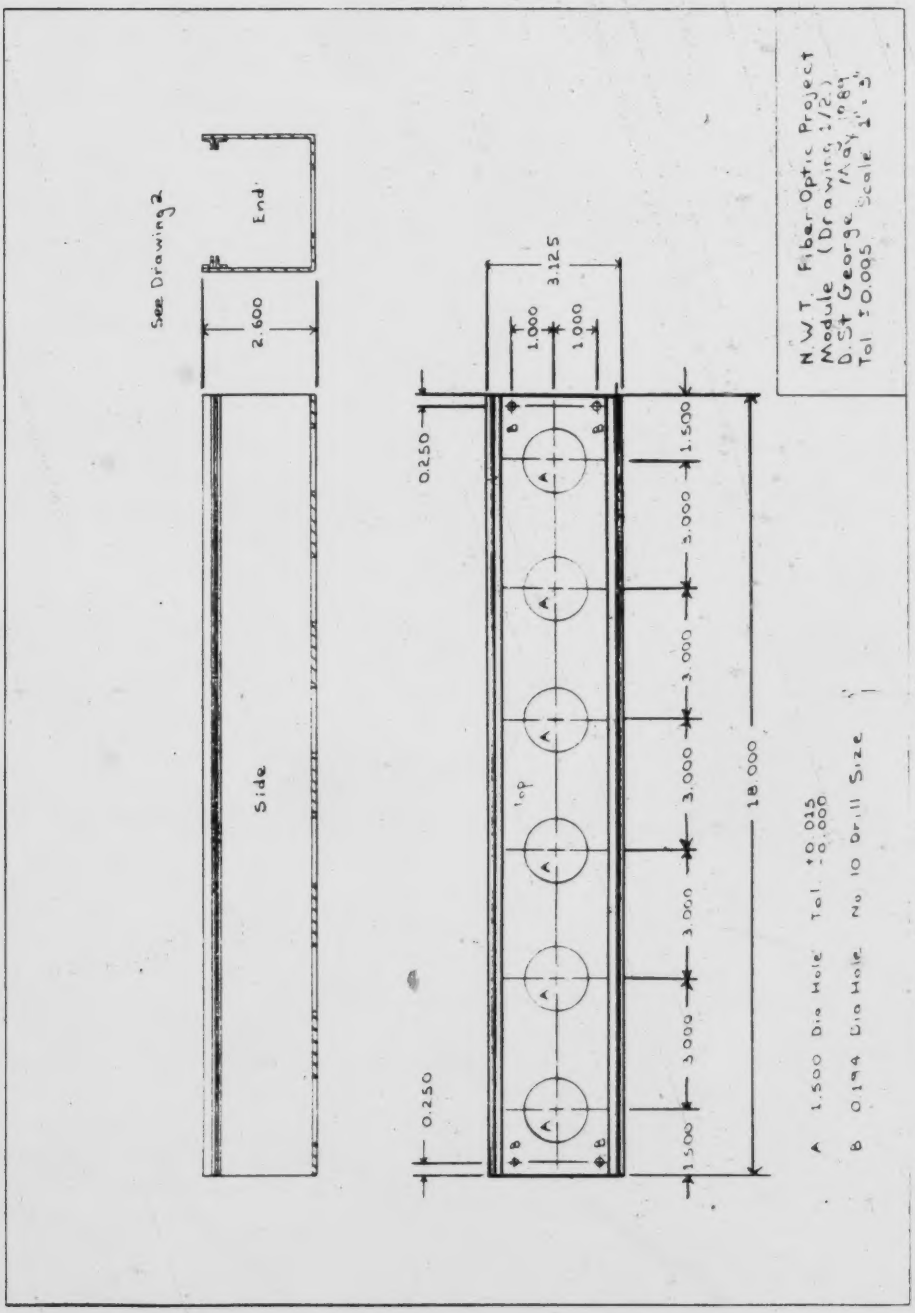
See Drawing 2
End
2.600
Side
3.125
1.000
1.000
0.250
0.250
1.500
3.000
3.000
3.000
3.000
3.000
1.500
18.000
Top
A
B
A 1.500 Dia Hole Tol +0.015 -0.000
B 0.194 Dia Hole No 10 Drill Size
N.W.T. Fiber Optic Project
Module (Drawing 1/2)
D.St George
Tol ±0.005

APPENDIX E

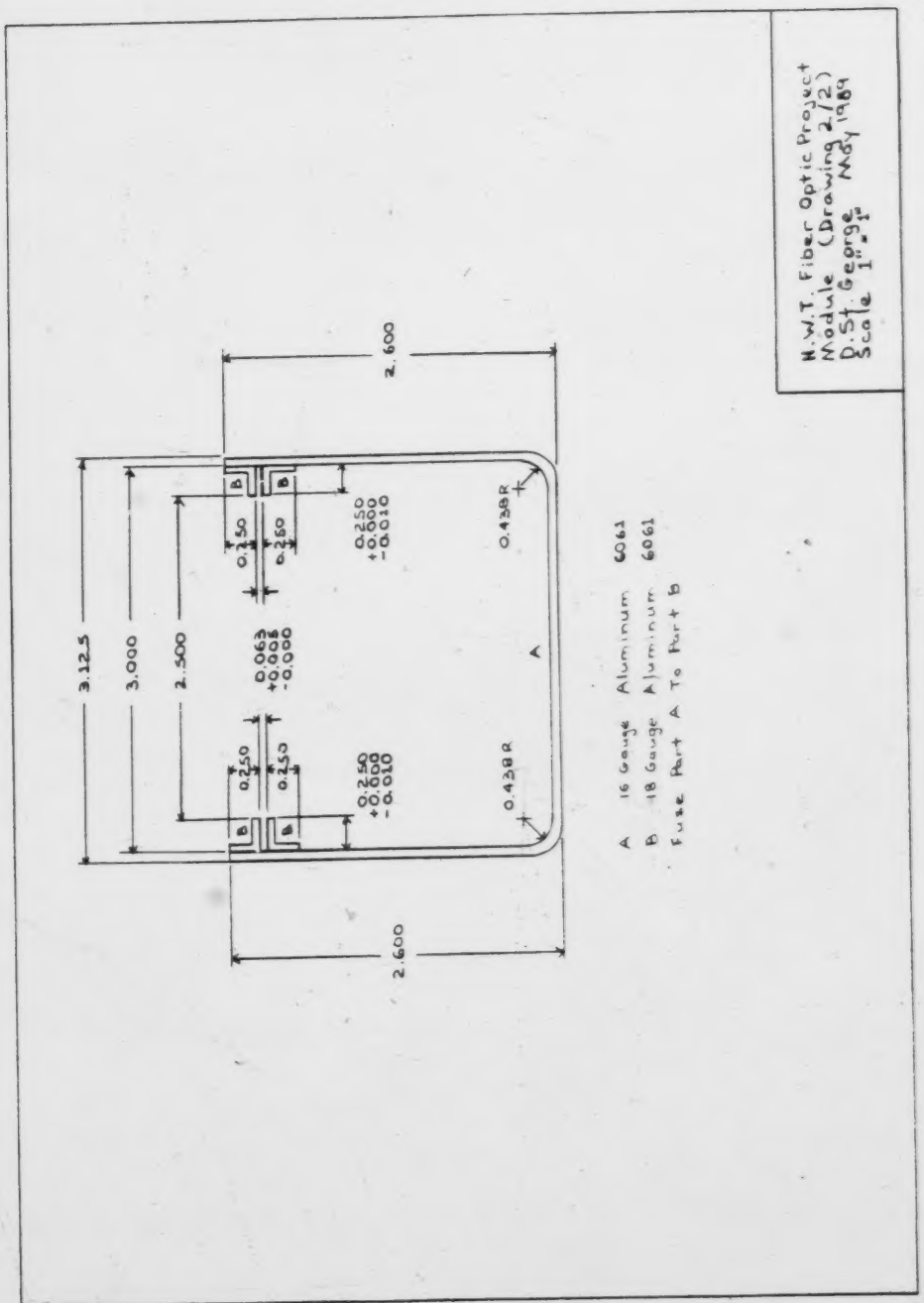
N.W.T. Fiber Optic Project
Module (Drawing 2/2)
D.St.George May 1969
Scale 1"=1"
2.600
3.125
3.000
2.500
0.250 +0.000 -0.010
0.063 +0.005 -0.000
0.438R
0.250
A 16 Gauge Aluminum 6061
B 18 Gauge Aluminum 6061
Fuse Part A To Part B

APPENDIX E

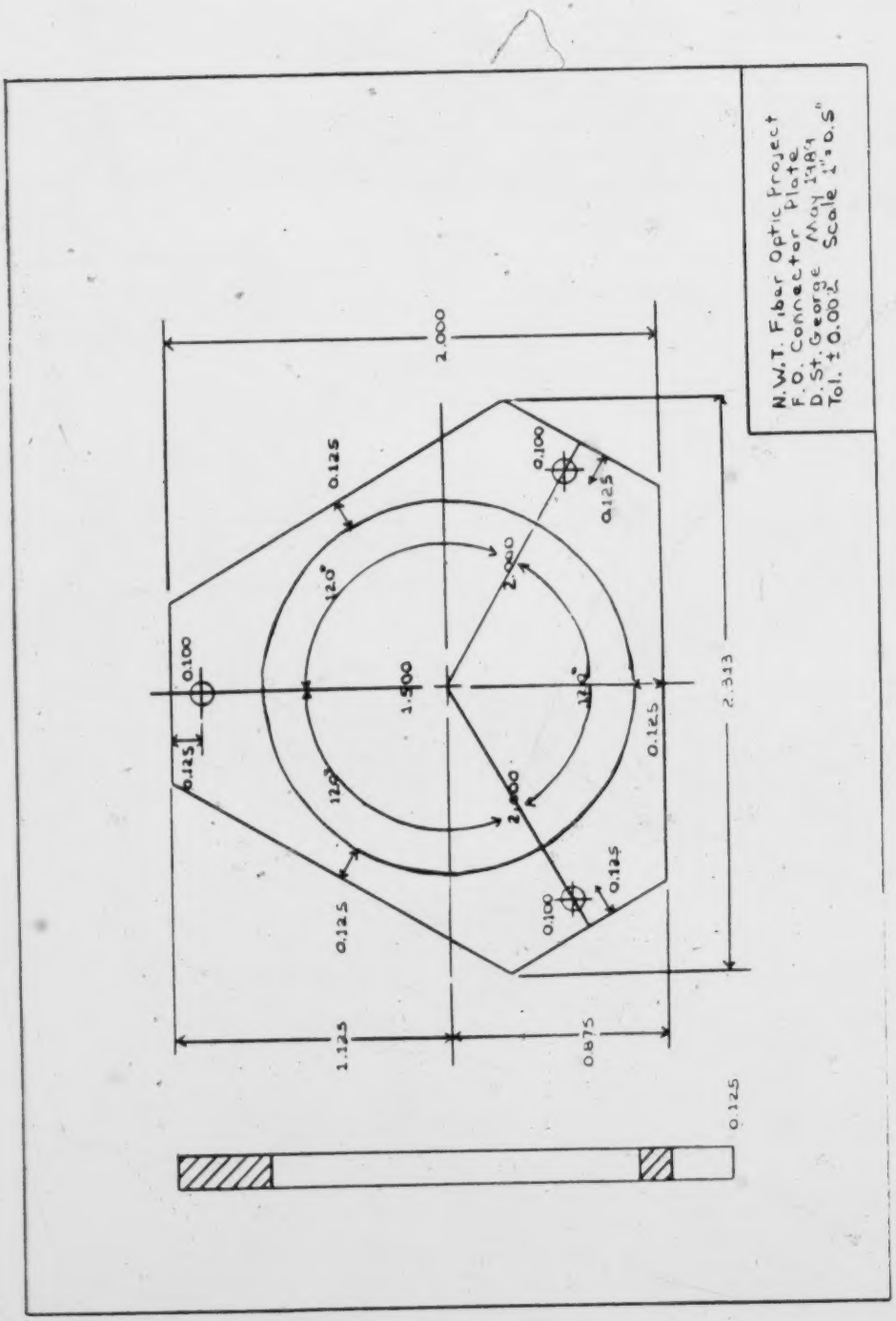
N.W.T. Fiber Optic Project
F.O. Connector Plate
D. St. George May 1989
Tol. ± 0.002" Scale 1" = 0.5"
2.000
0.125
0.100
0.125
120°
2.000
0.100
1.500
120°
0.125
2.313
120°
2.000
0.125
0.100
0.125
1.125
0.875
0.125

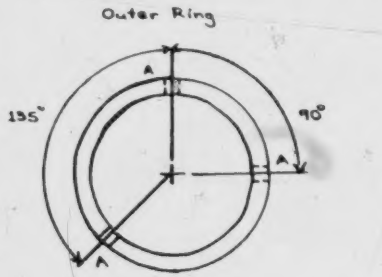

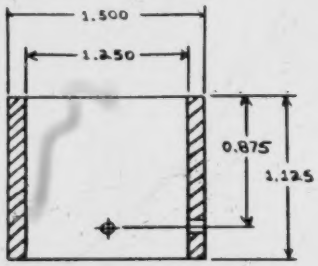

A No.3 56UNF 2B
Material Aluminum 6061

Machining Operations
1 Part Piece From Stock
2 Drill + Tap Holes

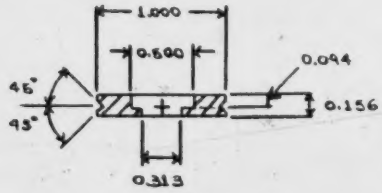

Material Aluminum 6061

Machining Operations
1 Cut Groove
2 Drill Thru Hole
3 Counterbore
4 Part Piece From Stock

N.W.T. Fiber Optic Project
F.O. Connector Rings
D. St. George May 1981
Tol. ±0.005 Scale 1" = 1"

APPENDIX E

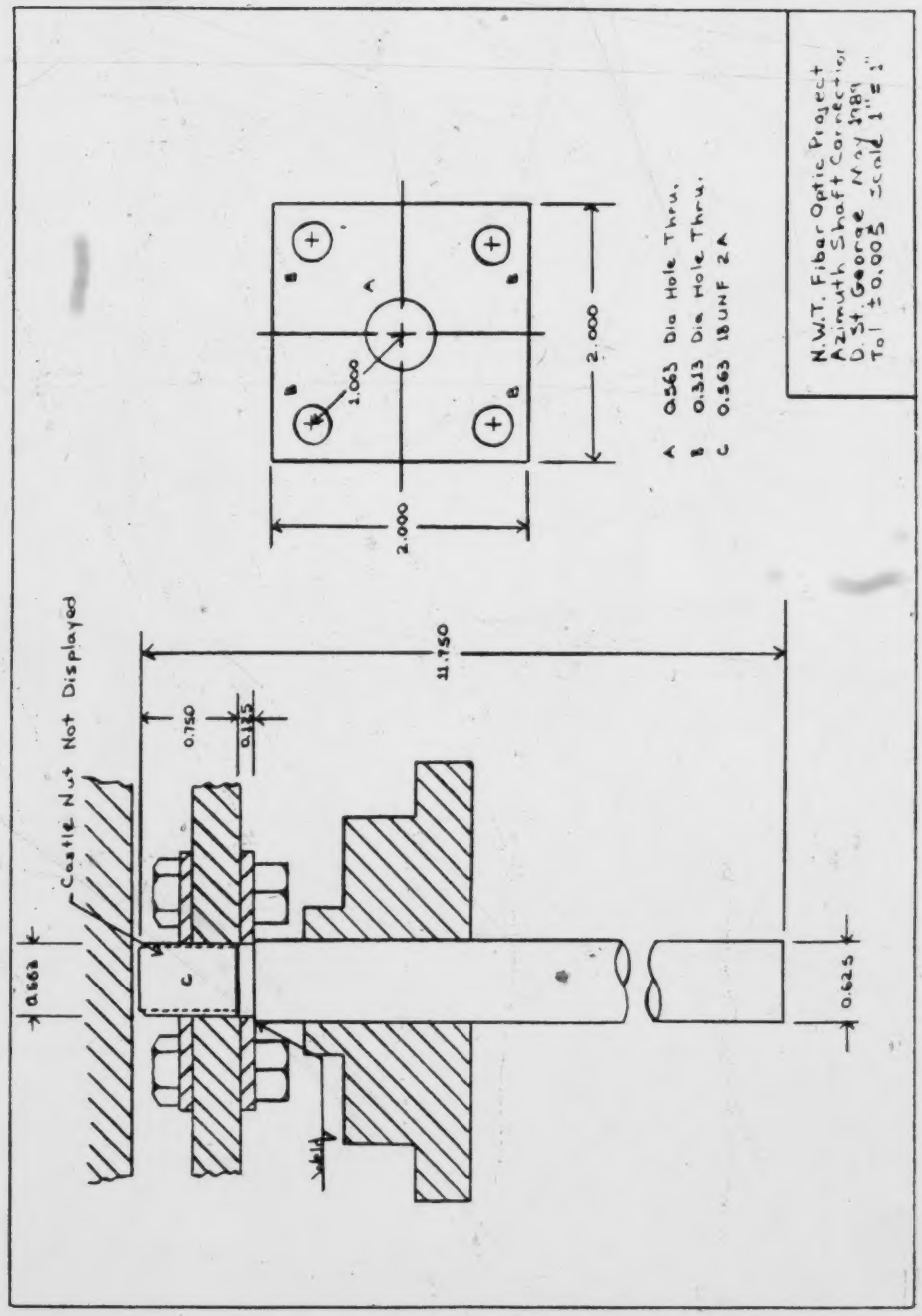
N.W.T. Fiber Optic Project
Azimuth Shaft Connector
D.St.George May 1989
Tol ±0.005 Scale 1" = 1"
A 0.563 Dia Hole Thru.
B 0.313 Dia Hole Thru.
C 0.563 18UNF 2A
2.000
2.000
1.000
11.750
0.750
0.125
Castle Nut Not Displayed
0.563
0.625

APPENDIX E

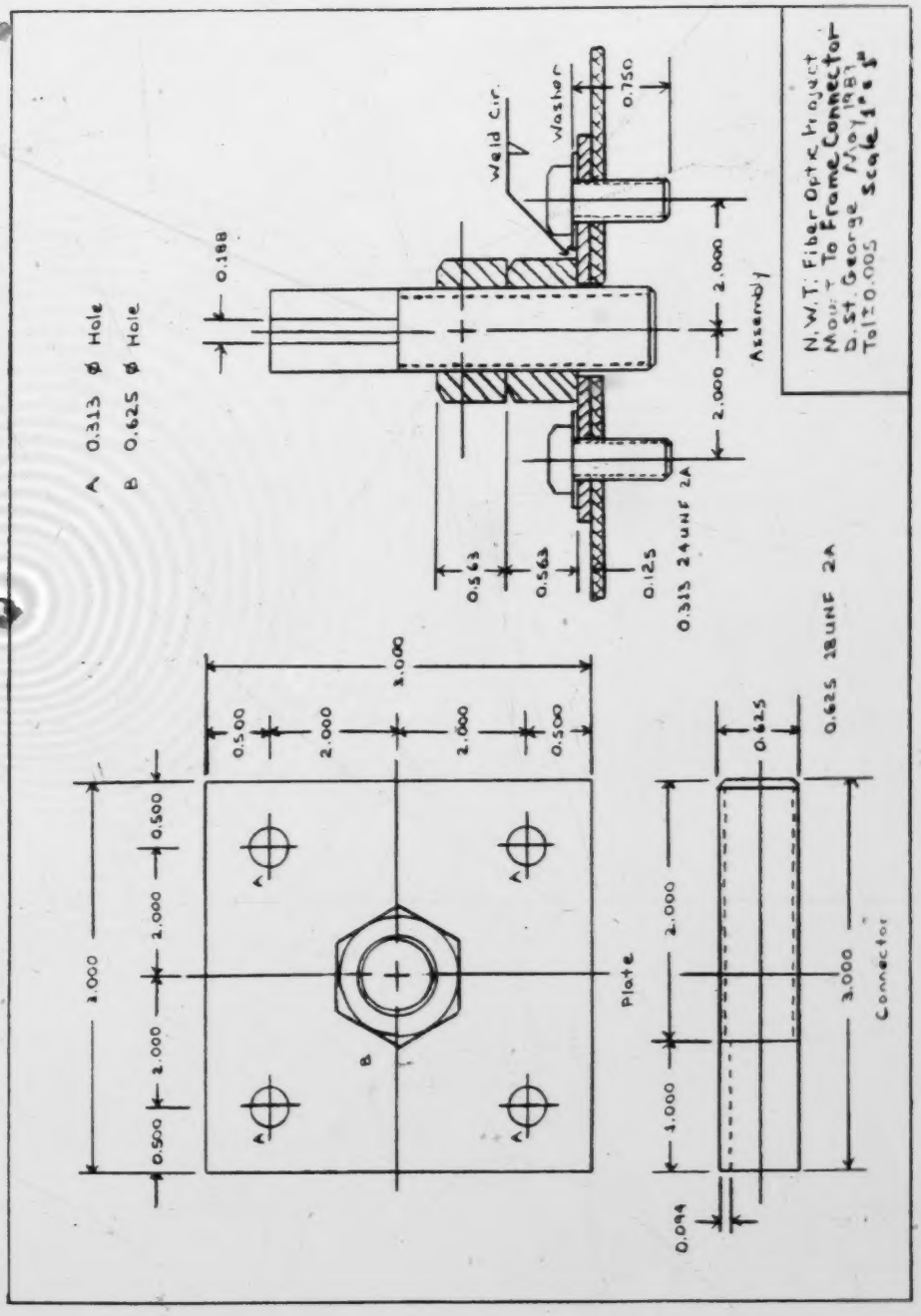
N.W.T. Fiber Optic Project
Mount To Frame Connector
D. St. George May 1981
Tol ± 0.005 Scale 1" = 5"
A 0.313 ø Hole
B 0.625 ø Hole
Weld Cir.
Washer
0.750
0.188
2.000
Assembly
2.000
0.563
0.563
0.125
0.313 24 UNF 2A
0.625 18 UNF 2A
3.000
0.500
2.000
2.000
0.500
Plate
0.625
2.000
3.000
1.000
Connector
0.094

APPENDIX E

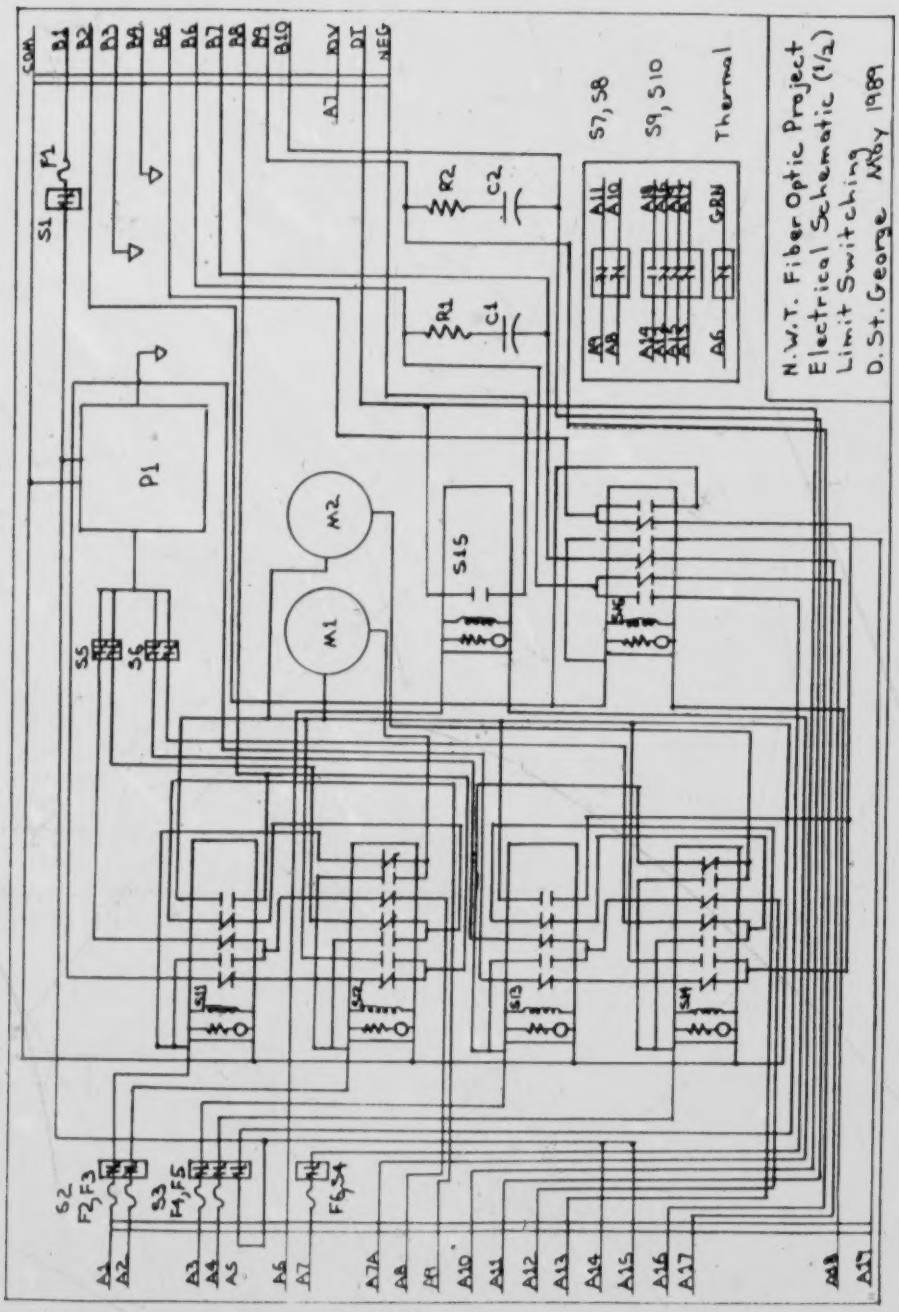
N.W.T. Fiber Optic Project
Electrical Schematic (1/2)
Limit Switching
D. St. George May 1989
S7, S8
S9, S10
Thermal
P1
M1
M2
S15
R1
C1
R2
C2
S1
S2
S3
S5
S6
F1
F2, F3
F4, F5
F6, F7
COM
NEG

A1 Elevation Up From Controller 110 V AC
A2 Elevation Down From Controller 110 V AC
A3 Azimuth Right From Controller 110 V AC
A4 Azimuth Left From Controller 110 V AC
A5 110 V AC To Power 360° Return
A6 110 V AC To Power DC Supply
A7 Manual From Pendant Switch 10 V DC
A8 Elevation Up To Limit Switch 110 V AC
A9 Elevation Down To Limit Switch 110 V AC
A10 Elevation Up From Limit Switch 110 V AC
A11 Elevation Down From Limit Switch 110 V AC
A12 Azimuth Right To Limit Switch 110 V AC
A13 Azimuth Left To Limit Switch 110 V AC
A14 110 V AC To Initiate 360° Return To L.S.
A15 110 V AC To Maintain 360° Return To L.S.
A16 Azimuth Right From Limit Switch 110 V AC
A17 Azimuth Left From Limit Switch 110 V AC
A18 110 V AC To Initiate 360° Return From L.S.
A19 110 V AC To Maintain 360° Return From L.S.
B1 Line 1 110 V AC
B2 Line 2 110 V AC
B3 Ground 110 V AC
B4 Gear Motor Ground
B5 Common To Azimuth Motor 110 V AC
B6 Azimuth Left To Azimuth Motor 110 V AC
B7 Azimuth Right To Azimuth Motor 110 V AC
B8 Common To Elevation Motor 110 V AC
B9 Elevation Down To Elevation Motor 110 V AC
B10 Elevation Up To Elevation Motor 110 V AC
B11 Synthetic Track From Sensor 10 V DC
B12 Synthetic Track To Controller 10 V DC
C1 Capacitor For Phase Shift Azimuth
C2 Capacitor For Phase Shift Elevation

F1 Fuse 110 V 1 AMP
F2 Fuse 110 V 1 AMP
F3 Fuse 110 V 1 AMP
F4 Fuse 110 V 1 AMP
F5 Fuse 110 V 1 AMP
F6 Fuse 10 V 1 AMP
M1 Elapse Time Meter For Elevation Motor
M2 Elapse Time Meter For Azimuth Motor
P1 DC Power Supply
R1 Resister For Phase Shift Azimuth
R2 Resister For Phase Shift Elevation
S1 Main Switch 110V AC Toggle
S2 Elevation Disable Switch Toggle
S3 Azimuth Disable Switch Toggle
S4 Manual Disable Switch Toggle
S5 Elevation Brake Disable Switch Toggle
S6 Azimuth Brake Disable Switch Toggle
S7 Elevation Down Limit Switch
S8 Elevation Up Limit Switch
S9 Initiate 360° Return, Azimuth Right L.S.
S10 Halt 360° Return, Azimuth Left L.S.
S11 Elevation Up Brake Disable Relay
S12 Elevation Down Brake Disable Relay
S13 Azimuth Right Brake Disable Relay
S14 Azimuth Left Brake Disable Relay
S15 Manual Interrupt 360° Return Relay
S16 Interrupt 360° Return Relay

N.W.T. Fiber Optic Project
Electrical Schematic (2/2)
Limit Switching + Braking
D. St. George May 1989

APPENDIX F

Regression Output:	Nov. 29/89
Constant	13.9063
Std Err of Y Est	15.8779
R Squared	0.17676
No. of Observations	828
Degrees of Freedom	826
X Coefficient(s)	0.03813
Std Err of Coef.	0.00286

Regression Output:	Dec. 3/89
Constant	1.59793
Std Err of Y Est	13.9588
R Squared	0.25255
No. of Observations	1228
Degrees of Freedom	1226
X Coefficient(s)	0.02829
Std Err of Coef.	0.00139

Regression Output:	Dec. 4/89
Constant	1.44222
Std Err of Y Est	10.4755
R Squared	0.10743
No. of Observations	1483
Degrees of Freedom	1481
X Coefficient(s)	0.01186
Std Err of Coef.	0.00088

Regression Output:	Feb. 28/90
Constant	1.619165
Std Err of Y Est	6.038375
R Squared	0.316251
No. of Observations	1275
Degrees of Freedom	1273
X Coefficient(s)	0.030462
Std Err of Coef.	0.001255

Regression Output:	Mar. 1/90
Constant	1.466379
Std Err of Y Est	29.25339
R Squared	0.324567
No. of Observations	963
Degrees of Freedom	961
X Coefficient(s)	0.095380
Std Err of Coef.	0.004438

Regression Output:	Mar. 2/90
Constant	3.55463
Std Err of Y Est	12.9547
R Squared	0.81613

APPENDIX F

No. of Observations	1542
Degrees of Freedom	1540
X Coefficient(s)	0.12172
Std Err of Coef.	0.00147

Regression Output:	Mar. 13/90
Constant	-610.64
Std Err of Y Est	39.1038
R Squared	0.28341
No. of Observations	1539
Degrees of Freedom	1537
X Coefficient(s)	0.92761
Std Err of Coef.	0.03762

Regression Output:	Mar. 14/90
Constant	-462.61
Std Err of Y Est	37.3728
R Squared	0.37471
No. of Observations	1454
Degrees of Freedom	1452
X Coefficient(s)	0.69271
Std Err of Coef.	0.02348

Regression Output:	Mar. 15/90
Constant	-78.043
Std Err of Y Est	31.3853
R Squared	0.19458
No. of Observations	1798
Degrees of Freedom	1796
X Coefficient(s)	0.23020
Std Err of Coef.	0.01105

Regression Output:	Mar. 16/90
Constant	5.53859
Std Err of Y Est	4.32772
R Squared	0.78371
No. of Observations	1251
Degrees of Freedom	1249
X Coefficient(s)	0.09149
Std Err of Coef.	0.00136
Regression Output:	Mar. 21/90
Constant	1.767333
Std Err of Y Est	11.27402
R Squared	0.485827
No. of Observations	762
Degrees of Freedom	760
X Coefficient(s)	0.041367
Std Err of Coef.	0.001543

CURRICULUM VITAE

DENNIS R. ST. GEORGE

Address	Box 6, Group 5, RR #1 Dugald, Manitoba, R0E 0K0
Birthdate	December 24, 1961

WORK EXPERIENCE

1) **Teaching Assistant, January 1988 To December 1989**
   Department of Agricultural Engineering,
   University of Alberta, Edmonton, Alberta

2) **Production Engineer, March 1985 To June 1987, (Promotion)**
   Motive Power and Car Equipment
   CN Rail, Montreal, Quebec

3) **Assistant Industrial Engineer, May 1984 To February 1985**
   Motive Power and Car Equipment
   CN Rail, Winnipeg, Manitoba

4) **Research Assistant, Summer 1983**
   Department of Agricultural Engineering,
   University of Manitoba, Winnipeg, Manitoba

EDUCATION

Master of Science **(Agricultural Engineering)** May 1990	University of Alberta Edmonton, Alberta GPA 7.20/9.00
Bachelor of Science **(Agricultural Engineering)** May 1984	University of Manitoba Winnipeg, Manitoba GPA 3.56/4.00

SCHOLASTIC HONOURS AND AWARDS

Natural Sciences and Engineering Research Council of Canada (NSERC)
Postgraduate Scholarship
Awarded 1987 And 1988, Value $13,500 per year

University of Alberta Graduate Faculty Fellowship
Awarded 1987 And 1988, Value $2000 per year

The J. MacGregor Smith Graduate Scholarship
Awarded 1989, Value $3000 per year